Effects of biocompatible encapsulations on the acoustic characteristics of CMUTs

Dissertation
zur Erlangung des Grades
des Doktors der Ingenieurswissenschaften
der Naturwissenschaftlich-Technischen Fakultät
der Universität des Saarlandes

von

Jorge Oevermann

Saarbrücken

2022

Tag des Kolloquiums: 01. April 2022

Dekan: Prof. Dr. J. Walter

Berichterstatter: Prof. Dr. H. Seidel
Prof. Dr. T. Stieglitz

Vorsitz: Prof. Dr. G. Frey

Akad. Mitarbeiter: Dr. F. Soldera

Abstract

Advances in modern medicine enable the use of medical implants for the treatment of an increasing number of diseases. If different implanted systems need to communicate with each other, data transmission using ultrasound is a promising solution. This requires a biocompatible encapsulation that allows efficient data transmission. In this dissertation, an encapsulation strategy, which allows the use of capacitive micromachined ultrasonic transducers (CMUTs) within conventional implant housings, was developed and evaluated for the first time.

The novel encapsulation approach consists of a silicone layer for coupling the CMUT to a layer of polyether ether ketone (PEEK) or titanium. Both materials are widely used for medical implant housings. Finite element simulations, complemented by measurements in air and in immersion as well as ex vivo experiments, have shown that effective data transmission over at least $6\,\text{cm}$ is possible with this encapsulation strategy. In the ex vivo experiments, the wide frequency bandwidths of the encapsulated CMUTs enable efficient data transmission, reaching data rates of minimum $0.8\,\text{Mbps}$. An additional experiment comparing with conventional encapsulations for CMUTs confirms the great potential of the novel encapsulation made of silicone and PEEK. Finally, starting points for increasing signal amplitude and data rate were identified and discussed.

Kurzzusammenfassung

Die Fortschritte in der modernen Medizin ermöglichen immer häufiger den Einsatz von medizinischen Implantaten zur Therapie. In Anwendungsfällen, die eine Kommunikation mehrerer implantierter Systeme untereinander erfordern, stellt die Datenübertragung mit Hilfe akustischer Wellen eine vielversprechende Lösung dar. Hierfür ist eine biokompatible Kapselung nötig, die eine effiziente Datenübertragung nicht verhindert. In dieser Arbeit wird erstmals eine Kapselungsstrategie entwickelt und evaluiert, die den Einsatz von kapazitiven mikromechanischen Ultraschallwandlern (CMUTs) innerhalb konventioneller Implantatgehäuse ermöglicht.

Die untersuchte neuartige Kapselung besteht aus einer Silikonschicht zur Ankopplung an eine Schicht aus Polyetheretherketon (PEEK) oder Titan, zwei weitverbreitete Materialien für die Kapselung medizinischer Implantate. Finite Elemente Simulationen, Messungen in Luft und Flüssigkeit sowie ex vivo Experimente haben gezeigt, dass mit dieser Kapselungsstrategie eine effektive Datenübertragung über mindestens 6 cm möglich ist. Die in ex vivo Experimenten ermittelten Frequenzbandbreiten der gekapselten CMUTs ermöglichen Datenraten von mindestens 0.8 Mbps. Ein zusätzlicher experimenteller Vergleich mit herkömmlichen Kapselungen für CMUTs bestätigt das große Potenzial der neuartigen Kapselung aus Silikon und PEEK.

Abschließend wurden zukünftige Ansatzpunkte zur Steigerung von Signalamplitude und Datenrate identifiziert und diskutiert.

Glossary

CMOS complementary metal-oxide-semiconductor.

CMUT capacitive micromachined ultrasonic transducer.

FDM finite difference method.

FEM Finite element method.

FFT fast Fourier transform.

FIT finite integration technique.

FVM finite volume method.

FWHM Full Width at Half Maximum.

KLM model of Krimholtz, Leedom and Matthaei.

LDV laser Doppler vibrometer.

LPCVD low-pressure chemical vapor deposition.

NDT non-destructive testing.

PDMS polydimethylsiloxane.

PECVD plasma-enhanced chemical vapor deposition.

PEEK polyether ether ketone.

PVDF polyvinylidene fluoride.

PZT lead zirconate titanate.

RMS root mean square.

RoHS Restriction of Hazardous Substances Directive of the European Union.

Si silicon.

Si$_3$N$_4$ silicon nitride.

SiO$_2$ silicon dioxide.

SNR signal-to-noise-ratio.

SOI silicon on insulator.

SU-8 SU-8, an epoxy-based negative photoresist.

TEOS tetraethyl orthosilicate.

WMTS Wireless Medical Telemetry Service.

Contents

vi

1 Introduction

Sound waves can be found everywhere on earth and are important for the interaction between humans. Acoustic waves with frequencies beyond the human audible range are referred to as ultrasound. Whereas some animals, such as bats, can naturally make use of ultrasound, humans have gradually opened up its applications with the advancement in technology. Nowadays, ultrasound is used extensively in medical imaging, non-destructive testing (NDT), and sonar applications [1]. This thesis targets onto a different field of its application: As a communication medium between medical implants.

Medical implants are one of the rapidly growing markets in the world. In February 2021, the market research company *Market Research Future (MRFR)* forecasted that until 2027 the average annual growth of the global medical implant market would be 7.5% [2]. Whereas some medical implants could work autonomously, there are many conceivable fields of application in which two or more implants need to communicate with each other in order to realize an optimal therapeutic success. An example given by Teshome *et al.* is an implanted insulin pump that communicates with an implanted glucose sensor to provide an optimized dose of insulin [3].

In present, technologies used for communication with and between medical implants are suffering from drawbacks, which is why ultrasound-based communication could become an interesting alternative (refer to Section 3.1). The challenge here is the biocompatible encapsulation of the ultrasonic transducers for a long-term use in the human body, as a conventional housing for medical implants would reflect a large part of the ultrasonic waves. This thesis therefore addresses the question of how ultrasonic transducers can be integrated into a conventional housing of a medical implant to enable an effective communication. The effects of such an encapsulation on the acoustic characteristics of the ultrasonic transducer were examined.

Since Pierre and Jacques Curie discovered the piezoelectric effect in 1880, the inverse piezoelectric effect became the fundament for generating ultrasonic waves [4]. By applying an alternating current to a piezoelectric material like lead zirconate titanate (PZT), the material oscillates in the same frequency as the alternating current. Thus, ultrasonic waves can be generated. Over the last decades, many efforts were made to improve the performance of piezoelectric transducers in terms of bandwidth or sensitivity, in transmit and receive mode. For adapting the transducers to specific applications, different piezo-electric materials, composite transducers or complex systems of matching and backing layers were invented. However, the physical principle for generating ultrasound remains the same.

In 1996, Matthew I. Haller and Butrus T. Khuri-Yakub developed a new type of ultrasonic transducer, with the original goal to realize airborne ultrasonic transducers in the megahertz range [5]. As this new type of transducer is based on miniaturized capacitors, the resulting transducers are named capacitive micromachined ultrasonic transducers (CMUTs). CMUTs offer advantages over piezoelectric ultrasonic transducers in terms of their high bandwidth or integrability on electronic circuits. Additionally, the materials used for CMUTs are compatible with the Restriction of Hazardous Substances Directive of the European Union (RoHS) [6]. Because of these advantages, CMUTs are the better substitute for piezoelectric ultrasonic transducers in the application of communication between medical implants and have been investigated in this thesis.

In general, this type of transducer is made of a multitude of very small parallel-plate capacitors where the ground electrode is fixed whereas the upper electrode is movable. By applying an alternating current, the upper electrode starts to swing and then generates ultrasonic waves.

In designing CMUTs, apart from the acoustic characteristics of the transducer itself, it is also important to consider the external environment at which the CMUTs will be applied. While encapsulation might not be necessary for some laboratory experiments, the medical use of CMUTs requires a biocompatible encapsulation to protect both, the patients and the CMUT. Due to the small dimensions of a CMUT cell in comparison to those of the encapsulation, such encapsulations have a major impact on the characteristics of the CMUT, like resonance frequency, sensitivity, or bandwidth. This makes the question on how to encapsulate CMUTs for the use within medical implants important.

Although the fabrication of CMUTs is cheap in batch production, the costs in money and time are relatively high for prototypes. It is therefore very important to precisely predict the behavior of specific CMUT geometries as accurately as possible, for which various analytical and numerical simulation tools are used. Finite element simulations play an important role in this work. Finite element method (FEM) tools and PZFlex in particular are described in details in Section 2.3.1.

The methods and devices used for verification of CMUT simulation results are described in Chapter 4. CMUTs are commonly driven with a combination of a large DC voltage and a smaller AC voltage (refer to Section 2.2.2). While this is state of the art, there is a gap in knowledge when it comes to the question which ratio of AC to DC should be applied and how different ratios influence the CMUT behavior. Based on a previously verified simulation model, one part of this work was to examine the influence of different ratios between the applied DC bias voltage and the AC excitation voltage (refer to Section 5.3).

The main part of this thesis focuses on the design and effects of an encapsulation of CMUTs for biomedical applications. The aim of integrating conventional CMUTs into

conventional housings of medical implants is achieved by using an acoustic window (refer to Section 4.4), a thinned part of the housing of the medical implant, at which the CMUT is attached via a silicone layer. This approach is a new way of encapsulating CMUTs. Until now, CMUTs have mainly been encapsulated using thin layers of parylene-C or polydimethylsiloxane (PDMS). Both two materials are not suitable for the long-term use in the human body (refer to Section 3.5).

The novel encapsulation approach is examined in FEM simulations, laser Doppler vibrometry in air, immersion experiments, and ex vivo experiments (refer to Section 5.4). Examined parameters are the oscillation behavior, sensitivities in transmit and receive, and the influence of the encapsulation on the frequency spectra of the CMUTs.

2 Fundamentals

This chapter provides the necessary fundamentals for this thesis. After a general intro-
duction to ultrasound, CMUTs are explained in terms of their basic operating principle.
Subsequently, an overview of the fabrication of CMUTs as well as the most important
analytical equations for describing their behavior will be given. A substantial part of this
thesis is comprised of simulations, which is why some important methods for simulation,
especially the FEM, are also presented in this chapter.

2.1 Ultrasound

Acoustic waves within the frequency range from $20\,\mathrm{kHz}$ up to $1\,\mathrm{GHz}$ to $10\,\mathrm{GHz}$ (de-
pending on the source) are referred to as ultrasonic waves [7][8]. The most important
way to generate or receive ultrasonic waves is based on the (inverse) piezoelectric ef-
fect. This effect is based on special piezoelectric materials, such as quartz, which have
an asymmetric lattice structure. When a voltage is applied to a piezoelectric material,
this leads to a change in its physical dimensions [7][9]. For the fabrication of ultrasonic
transducers, in most cases a piezoceramic material is used. In particular, lead zirconate
titanate (PZT) is a widely used material. Equipped with electrodes placed on top and
bottom of the piezoelectric material, an oscillation of the ceramic can be induced by
applying an alternating voltage signal, and thus ultrasound waves can be emitted. In
receiving mode, the deformation of the ceramic when ultrasonic waves arrive can be
detected (direct piezoelectric effect) in terms of a voltage signal. In contrast to this bulk
material oscillation of a piezoelectric ceramic, CMUTs are membrane oscillators. They
are not yet widely used in commercial products and are described in detail in Section 2.2.

Apart from the properties of ultrasonic waves, like frequency, amplitude and sound
pressure, the properties of the medium through which the acoustic wave propagates are
also important. Here, the speed of sound, the acoustic impedance and the damping of
the medium are to be mentioned. For the speed of sound, a distinction must be made
between longitudinal and transverse sound velocity, whereby transverse acoustic waves
only occur in solids. The speed of sound depends on the medium and the values of
some important media are shown in Table 2.1. The speed of sound of Fluorinert FC-72
(*3M*, St. Paul, USA), a non-conductive fluid used in initial transmit experiments, was
determined experimentally; values of human tissues are from Duck [10], and the other
values are extracted from Lerch *et al.* [1].

Table 2.1: Sound velocities of selected media.

Material	c_{long}	c_{trans}
Air @ 20 °C [1]	344 m/s	-
Water @ 20 °C [1]	1480 m/s	-
Fluorinert FC-72	512 m/s	-
Aluminum [1]	6420 m/s	3040 m/s
Silicon nitride [1]	11 000 m/s	6250 m/s
Human breast (avg.) [10]	1510 m/s	
Human skeletal muscle [10]	1580 m/s	
Human radius bone [10]	3406 m/s	

For liquids, the (longitudinal) speed of sound can be calculated as follows [1]:

$$c = \sqrt{\frac{1}{\chi \rho_0}} \tag{2.1}$$

where ρ_0 is the density of the medium and χ is its adiabatic compressibility, which is the reciprocal of the compression modulus. As the density is temperature-dependent, this is also true for the speed of sound.

For isotropic solids, the longitudinal and the transverse sound velocities can be determined from Young's modulus E and Poisson's ratio ν [1]:

$$c_l = \sqrt{\frac{E(1-\nu)}{\rho_0(1-\nu-2\nu^2)}} \tag{2.2}$$

$$c_t = \sqrt{\frac{E}{2\rho_0(1+\nu)}} \tag{2.3}$$

From the speed of sound (c) of the medium and the frequency (f) of the sound wave, the wavelength (λ), which means the smallest distance between two points of the same phase, can be determined as [1]:

$$\lambda = \frac{c}{f} \tag{2.4}$$

Important parameters of an ultrasonic probe are its resonance frequency, bandwidth (Full Width at Half Maximum (FWHM), see Figure 2.1) and sensitivity in transmit and receive. The design of CMUTs to a specific resonance frequency is described in Section 2.2.2. Imaging requires a large frequency bandwidth (FWHM) because it enables a high spatial resolution. A high bandwidth is also important for the application of this work because it is associated with a high data rate.
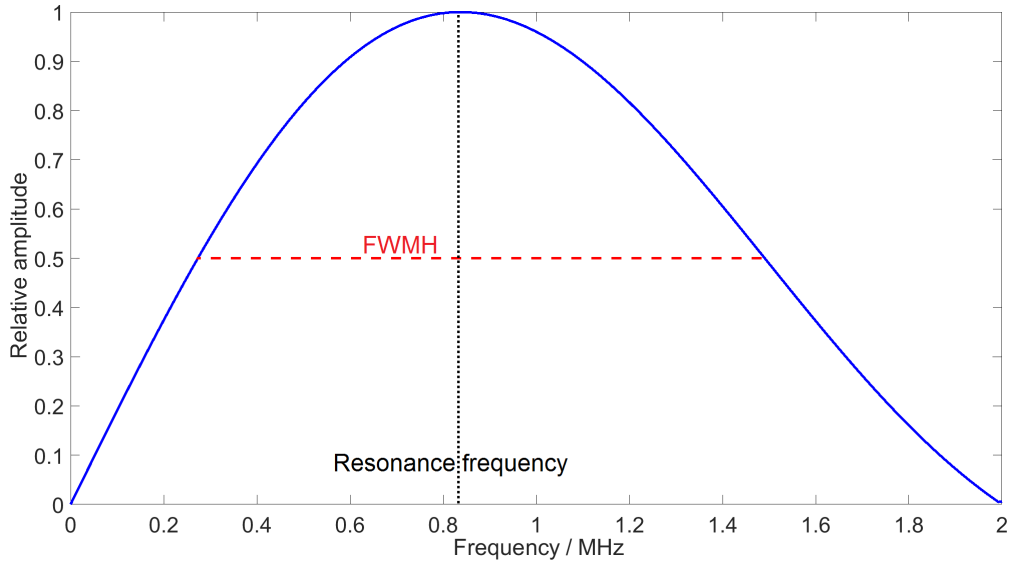
Figure 2.1: Frequency spectrum of a generic sine burst at $830\,\text{kHz}$.

2.1.1 Acoustic impedance

If an ultrasonic wave reaches the interface between two different media, the acoustic impedances of these media determine which portion of the energy is reflected and which is transmitted. Sutilov specifies the reflection coefficient, which corresponds to the reflected portion, regarding the acoustic pressure as [11]:

$$\Gamma = \frac{Z_2 - Z_1}{Z_2 + Z_1} \tag{2.5}$$

where Z_1 and Z_2 are the specific acoustic impedances of the two media. The specific acoustic impedance of a material is given by the product of its sound velocity (c) and its density (ρ):

$$Z = c \cdot \rho \tag{2.6}$$

Specific acoustic impedances of materials, which are important to this work, are shown in Table 2.2. The value for Fluorinert FC-72 (*3M*, St. Paul, USA) was determined experimentally, those for human breast and human skeletal muscle are from Duck ([10]), the others are referred to the book by Kino [9].

6

Table 2.2: Specific acoustic impedances of selected materials.

Material	Acoustic impedance
Air	$427 \, \text{kg/(m}^2\text{s)}$
Water	$1.483 \times 10^6 \, \text{kg/(m}^2\text{s)}$
Fluorinert FC-72	$0.860 \times 10^6 \, \text{kg/(m}^2\text{s)}$
Human breast	$1.54 \times 10^6 \, \text{kg/(m}^2\text{s)}$
Human skeletal muscle	$1.645 \times 10^6 \, \text{kg/(m}^2\text{s)}$
Aluminum	$17.33 \times 10^6 \, \text{kg/(m}^2\text{s)}$
Silicon nitride	$36.0 \times 10^6 \, \text{kg/(m}^2\text{s)}$
Titanium	$27.3 \times 10^6 \, \text{kg/(m}^2\text{s)}$
PZT	$\sim 34.0 \times 10^6 \, \text{kg/(m}^2\text{s)}$

Due to the large difference in specific acoustic impedance between PZT and water, air or human tissue, it is necessary to have one or more impedance matching layers in between, in order to prevent most of the energy from being reflected at the surface from the transducer to the medium. The usage of impedance matching layers is not necessary for CMUTs, as they are membrane oscillators having a lower mechanical impedance than piezoelectric transducers [12].

2.1.2 Near-field length

Ultrasonic transducers do not exhibit a homogeneous sound field in the area directly in front of the transducer aperture. Interferences between acoustic waves emitted at different positions on the transducer aperture are responsible for the fact that a small change in the position of the detector can lead to a big change in the received pressure. The near-field length is the distance between the transducer surface and the furthest local maximum in which local minima and maxima occur. It depends on the size of the sound-emitting aperture, the frequency and the propagation medium. According to Lerch *et al.*, the near field length N of a circular transducer can be calculated from the diameter D of the transducer and the wavelength λ as [1]:

$$N = \frac{D^2}{4\lambda} \tag{2.7}$$

Using Scalp, a simulation tool developed by the Fraunhofer IBMT for sound field calculation based on point source synthesis, the near field lengths for different frequencies in Fluorinert FC-72 and water, both liquids used in the transmit experiments, were estimated. Two sound pressure curves generated by a transducer on the acoustic axis that were simulated by Scalp and are shown in Figure 2.2. The underlying aperture has an area of $5 \, \text{mm} \times 5 \, \text{mm}$ and thus corresponds to the edge lengths of the CMUT chips used. In Figure 2.2, it should be noted that the calculation was performed without considering the damping effect of the medium.

The decrease of the acoustic pressure of the blue curve (1 MHz) beginning from about 1.8 cm is entirely due to geometric effects. In addition to the beam expansion, sound waves are gradually damped by friction when passing through a medium. The damping constant depends on the medium, and increases with the frequency of the acoustic wave. As a result, the red curve (5 MHz) is superimposed by a declining function in reality, so that the maximum sound pressure no longer occurs at approx. 8.3 cm but closer to the transducer. Both curves were also normalized to their own maximum. A direct comparison of the sound pressures at the two frequencies shown is therefore not possible. Nevertheless, the graph shows that at a separation of more than 8 cm between two CMUTs, the receiving spectrum is not distorted by near-field effects in Fluorinert FC-72 for acoustic waves with frequencies of 5 MHz or below.
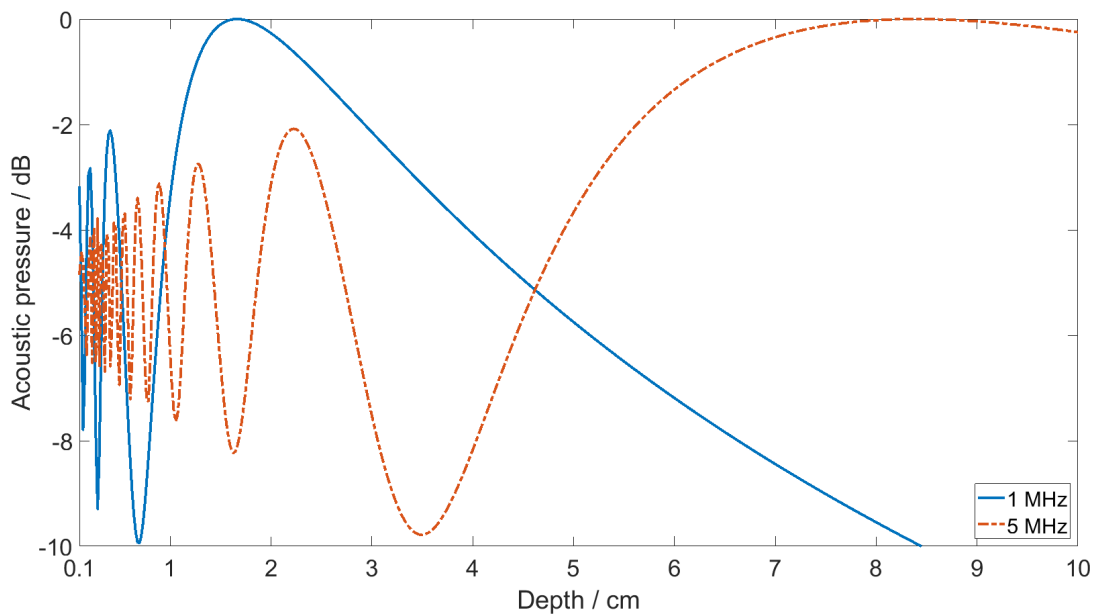

Figure 2.2: Simulated acoustic pressure on acoustic axis for a 5 mm × 5 mm transducer in Fluorinert FC-72.

The result of the same simulation using water instead of Fluorinert FC-72 as the propagation medium is shown in Figure 2.3. The near-field length at a frequency of 5 MHz is 2.85 cm, so that the measurements in water could be performed with a smaller separation between the transducers.
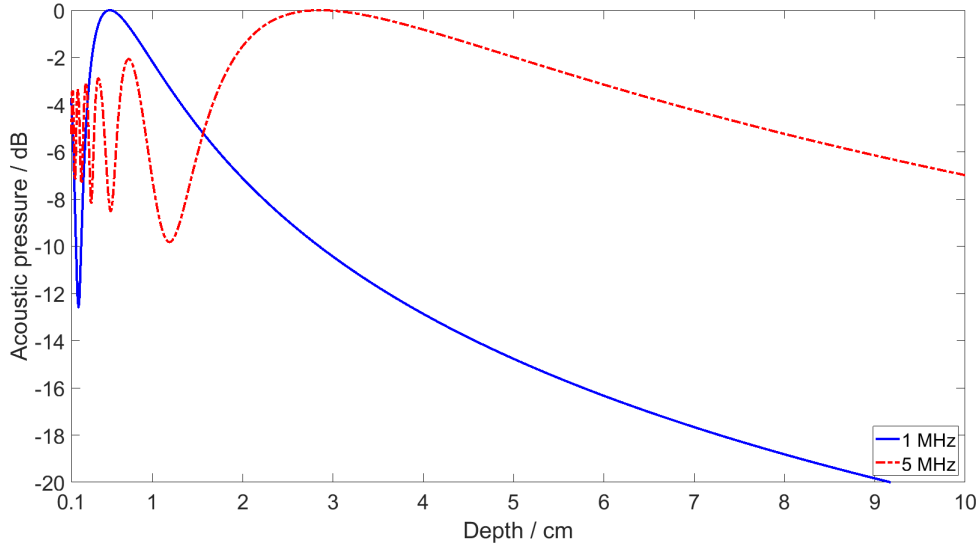
Figure 2.3: Simulated acoustic pressure on acoustic axis for a $5\,\text{mm} \times 5\,\text{mm}$ transducer in water.

2.1.3 Wave equations

To describe the propagation of ultrasonic signals, the corresponding wave equation must be solved. This can be done numerically by simulation tools (Section 2.3). The acoustic pressure in a gas or liquid can be described by the following wave equation [1]:

$$\frac{1}{c^2}\frac{\partial^2 p}{\partial t^2} - \Delta p = 0 \tag{2.8}$$

Here, p is the acoustic pressure, c is the sound velocity in the medium and t is the time. For sound propagation in a solid, the following wave equation applies in the linear one-dimensional case [1]:

$$\mu \Delta u + (\mu + \lambda)\frac{\partial}{\partial x}\left(\text{div}\vec{d}\right) = \rho_0 \frac{\partial^2 u}{\partial t^2} \tag{2.9}$$

where

$$\mu = G = \frac{E}{2(1+\nu)} \tag{2.10}$$

and

$$\lambda = \frac{E\nu}{(1+\nu)(1-2\nu)} \tag{2.11}$$

are Lamé constants and $\vec{d}$ is the displacement vector. For the three-dimensional case in an isotropic solid, the equation changes to [1]:

$$\mu \Delta \vec{d} + (\mu + \lambda)\,\text{grad div }\vec{d} = \rho_0 \frac{\partial^2 \vec{d}}{\partial t^2} \tag{2.12}$$

All three wave equations mentioned here can be solved analytically only for special cases such as a plane wave in a homogeneous media. Alternatively, as in this work, numerical methods can be used, which are presented in Section 2.3.

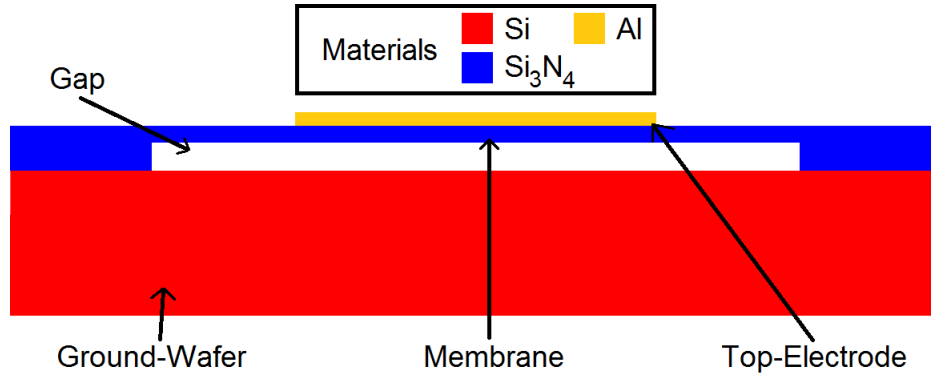## 2.2 Capacitive Micromachined Ultrasonic Transducers

Figure 2.4: Schematic view of a basic CMUT model.

Basically, a CMUT can be described as a parallel plate capacitor [5]. The general design of a CMUT can be seen in Figure 2.4. Typically, a doped, conductive wafer forms the ground electrode. On top of an evacuated gap or cavity, a thin layer of e.g. silicon nitride or silicon is acting as the top plate [13]. An additional electrode (e.g. made of aluminum) is placed on top of the top plate [5]. For manufacturing reasons but also for insulation in the case of a collapse of the membrane, CMUT designs usually include additional layers such as an insulation layer at the bottom of the cavity. By applying an AC voltage to this parallel plate capacitor, the electrostatic force induces an oscillation of the membrane, resulting in the emission of ultrasonic waves. In the receiving mode only a DC voltage is needed. The incoming ultrasonic wave causes the membrane to deflect, changing the capacitance of the capacitor and enabling a displacement current to be measured.

In the last decades, several research groups worked on the field of CMUTs [14]. While the first CMUTs were introduced by Haller and Khuri-Yakub in 1996 [5], the idea behind this technology is much older. One of the first scientific articles about electrostatic transducers was written by Kuhl in 1954 [15]. Such electrostatic transducers are preferable for many applications because of their good adaptation in the acoustic impedance to important media like air, water or human tissue [16]. After the first electrostatic transducers were invented, it took some decades until the micro-machining techniques were advanced enough to fabricate micromachined ultrasonic transducers, CMUTs, in a

reproducible and sufficient quality. Crucial to the competitiveness of CMUTs is a high manufacturing precision so that very narrow cavities can be realized, allowing electric fields on the order of 1×10^8 V/cm to be realized inside [17].

It is common to bias CMUTs by applying a DC voltage. In transmit mode, this is necessary for linear operation and for amplification; in receiving mode, the DC voltage enables the detection of a capacitance change when the membrane is deflected by incident ultrasonic waves [18]. This change in capacitance is measured as a current or voltage signal. The meaning of the bias voltage is explained further in Section 2.2.2 and a deflected CMUT membrane can be found in Figure 2.5.

Figure 2.5: Schematic: Bending of a CMUT membrane.

2.2.1 Fabrication

CMUTs can be classified into two types, depending on the materials used. Most CMUTs are silicon-based. The main materials used in their fabrication are silicon (Si), silicon nitride (Si_3N_4) and silicon dioxide (SiO_2) [6]. Another approach is to manufacture CMUTs from polymers. There are much less publications on this type than on the silicon-based so far. Polymer-CMUTs have been realized using SU-8, an epoxy-based negative photoresist (SU-8) or polyimide as membrane material [19][20]. In this work, only silicon-based CMUTs are used so the following description of the fabrication methods is limited to this type of CMUTs.

Although each research group or company has its own slightly adapted method, there are basically only two approaches to fabricate silicon-based CMUTs: *Wafer bonding* and *sacrificial release process*. Both technologies have advantages and disadvantages, with the result that both are still in use. Whereas the fabrication process itself makes no difference in general for simulating the CMUT cell, some side effects can occur that have to be considered. Baum *et al.*, for example, report that outgassing of water or plasma-enhanced chemical vapor deposition (PECVD) SiO_2 occurred during their wafer bonding process, leading to buckled membranes [21]. Other researchers report of large intrinsic stresses which can also lead to a bending of the membrane [22]. These effects require adaptions to the cell design, when using sacrificial release process as they strongly influence two crucial design parameters: Resonance frequency and pull-in voltage. Despite it is possible to include residual stresses in the simulation model when using PZFlex, such stresses themselves cannot be calculated within this tool and due to that cannot be taken into account in this work.

One of the major issues concerning residual stresses is to correctly measure them, which is important as the usage of erroneously estimated or measured values could worsen the accuracy of the simulation model. Both fabrication approaches will shortly be introduced in the following paragraphs.

Fabrication - Wafer Bonding

A schematic drawing of the basic wafer bonding process is shown in Figure 2.6 [23].
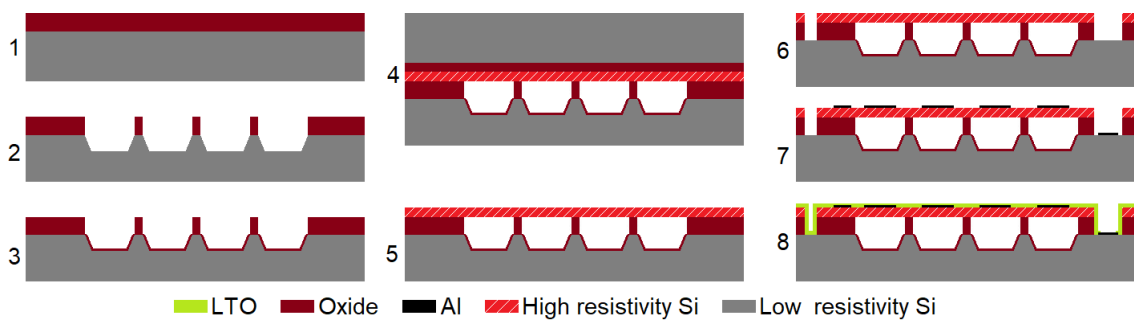

Figure 2.6: Wafer bonding process, adapted from [23].

The wafer bonding process usually starts with growing an oxide layer on top of a silicon wafer (Figure 2.6 (1)). Afterwards the cavities are etched either only into the oxide layer or, if a bigger cavity is necessary, also into the silicon wafer (2). For electrical isolation, a further (thermal) oxide layer is grown afterwards (3). In the next step (4) a silicon on insulator (SOI) wafer is bonded on top the cavity wafer. Box layer and handle wafer are ground and etched back afterwards so that only the device layer of the SOI wafer is remaining (5). This device layer is the membrane of the final CMUT. As last crucial steps, vias are etched through the top layer to contact the ground wafer acting as bottom electrode (6) and an electrode material (e.g. aluminum) is patterned (7) on top of the membrane as well as on the free surface of the ground wafer. Instead of using a high resistivity silicon as membrane material, some low resistivity material can be used so that no additional electrode material is needed. This reduces the amount of steps but also the degrees of freedom concerning the electrode design. E.g. Bozkurt *et al.* were able to show that patterning the top-electrode can be used to optimize the bandwidth of the transducer [24]. If a passivation is needed, e.g. a further oxide layer can be deposited, covering the whole surface (8).

This basic process is adapted by many research groups according to their devices and equipment. According to Huang *et al.* wafer-bonding with a single crystal silicon gives a membrane with less internal defects and lower internal mechanical loss than thin-film deposited silicon [25].

Fabrication - Sacrificial release process

Figure 2.7 schematically shows the sacrificial release fabrication process according to Jin *et al.* [26].
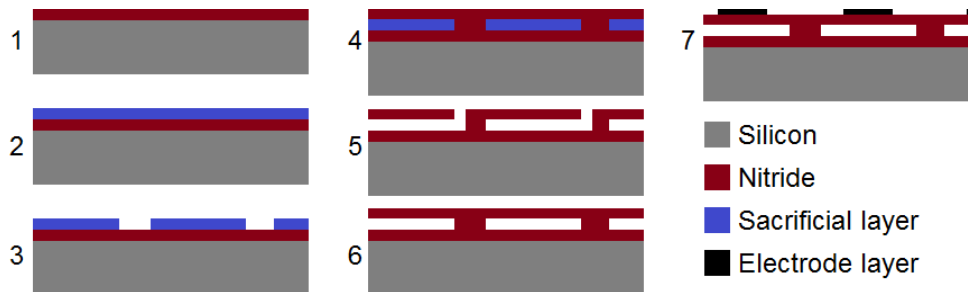

Figure 2.7: Sacrificial release process, adapted from [26].

CMUT fabrication based on a sacrificial release process usually starts with the deposition of a nitride layer (1) on top of a highly doped silicon wafer to work as an etch stop. Afterwards the sacrificial layer, e.g. amorphous silicon or tetraethyl orthosilicate (TEOS) (as for the CMUTs used in this work), is deposited (2) and structured (3). This sacrificial layer defines the later cavity of the CMUT cell. A further nitride layer is deposited, e.g. by low-pressure chemical vapor deposition (LPCVD), to form the membrane (4). Next, vias are dry etched and used to etch away the sacrificial layer (5). After the vias are vacuum-sealed with nitride (6) (by PECVD-Si$_3$N$_4$ for the CMUTs used in this work), electrode material (e.g. aluminum) is patterned on top of the membranes (7). The first CMUTs ever were produced by Haller and Khuri-Yakub using a sacrificial release process [5].

Comparison

Both manufacturing processes are still in use today by research groups and companies. The reasons for this are on the one hand the different weighting of the respective advantages and disadvantages, on the other hand the individual conditions regarding expertise and hardware of the manufacturers.

The difficulty of the sacrificial layer process is the exact adjustment of the cavity height and especially of the membrane thickness, which is much easier in the wafer bonding process [6]. In addition, the roughness of the silicon nitride membrane can change the effective gap height, so that the actual device performance may differ from the desired one. In comparison to the wafer bonding process, the sacrificial layer process benefits from the fact that it is relatively simple and reliable. Poor yields, as can occur due to imperfections (high demands on surface roughness and cleanliness) in wafer bonding, are not to be expected here. For complementary metal-oxide-semiconductor (CMOS) integration, the sacrificial release process offers the advantage that the process temperature can be limited to 250 °C [27].

The wafer bonding process, instead, offers the advantage of high accuracy in the adjustment of the membrane thickness, which is determined by the device layer of the SOI wafer used. The residual stress in the membrane is significantly reduced [28]. In addition, the fabrication time decreases.

Both, the higher accuracy of the membrane thickness and the reduced residual stress in the membrane, lead to the conclusion that the properties of CMUTs fabricated by wafer bonding are less complex to accurately predict or simulate. In the simulation program PZFlex, residual stress can be taken into account in an additional initial step to reduce the deviations between simulation and experiment. However, this requires an accurate prior measurement of the layer stresses, which is an additional source of error. Deviations in the membrane thickness could be taken into account by varying the thickness in simulation. The simulation of membranes of inhomogeneous thickness, however, is difficult.

The CMUTs examined within this work were fabricated using a sacrificial release process by microfab Service GmbH, Bremen, Germany.

2.2.2 Mathematical description of CMUTs

In order to estimate the basic behavior of CMUTs, simplifying analytical formulas can be used. This allows to find starting values for subsequent FEM simulations when designing a CMUT cell. Equations for two important parameters, resonance frequency and pull-in voltage, are discussed in this section. In addition, the purpose of the bias voltage is explained and a description of the spring softening effect, which leads to a shift in the resonance frequency depending on the applied bias voltage, is given.

Bias voltage

When using CMUTs as transmitters, a DC voltage is usually applied that is greater than or equal to the amplitude of the AC voltage. There are several reasons for this. The force acting on the top electrode of a capacitor (and thus approximately on the membrane of a CMUT) is proportional to the square of the applied electrical voltage (cf. Equation (2.13)) [29].

$$F_{\text{capacitor}}(t) = \frac{\epsilon A U(t)^2}{2\left(d_0 - x(t)\right)^2} \tag{2.13}$$

Here, $U(t)$ is the voltage applied between the capacitor plates, A is the area of the plates and d_0 is the distance between the capacitor plates. ϵ is the electric permittivity and $x(t)$ is the displacement of the capacitor plates relative to each other [29]. Since the total voltage applied is equal to the sum of the partial voltages $U_{DC} + U_{AC}$, $U(t)^2$ in

Equation (2.13) can be rewritten as follows:

$$
\begin{aligned}
U(t)^2 &= \left(U_{DC} + \hat{U}sin(\omega t)\right)^2 \\
&= U_{DC}^2 + 2U_{DC}\hat{U}sin(\omega t) + \hat{U}^2 sin^2(\omega t) \\
&= U_{DC}^2 + 2U_{DC}\hat{U}sin(\omega t) + \hat{U}^2 \left(1 - cos(2\omega t)\right)/2
\end{aligned}
\tag{2.14}
$$

The first term in Equation (2.14) results in an amplification. The second term, $2U_{DC}\hat{U}sin(\omega t)$, is the wanted signal which is amplified by the bias voltage. The third term, $\hat{U}^2 \left(1 - cos(2\omega t)\right)/2$, is a harmonic distortion. Thus, in transmit mode the bias voltage results in an amplification of the wanted signal. When operating without bias, the first two summands are omitted, making the force and thus the vibration of the membrane become proportional to twice the applied frequency.

In receive mode, the change of the capacitance of the capacitor results in a displacement current ($I(t)$) that can be measured.

$$
I(t) = U_{DC}\frac{dC}{dt}
\tag{2.15}
$$

According to Equation (2.15), the bias voltage is required in receive mode to be able to measure a displacement current. In both modes of operation, the bias voltage increases the sensitivity of the CMUT.

Pull-in voltage

A large applied voltage increases the deflection of the CMUT membrane. Due to the limited height of the cavity, however, there is a limit to this deflection. If the applied voltage rises above a certain value, the so-called *pull-in voltage*, the center of the membrane is moved to the ground of the cavity. If a CMUT is operated with a voltage that is at least equal to the pull-in voltage, it is referred to as operating in collapse mode. In this mode, the membrane no longer vibrates as a whole, but only the outer area, so that the acoustic properties change. Therefore, it is important to know the pull-in voltage for a CMUT design.
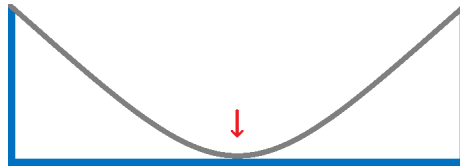

Figure 2.8: Schematic: Collapse of the membrane.

The pull-in voltage depends on the membrane parameters and the height of the cavity. The thinner and larger the membrane is, the more it bends with the same force applied, so the easier the pull-in state is reached. Different Young's-moduli of different membrane materials also mean different deflections with the same applied force. The exact calculation of the pull-in voltage is made more difficult by the fact that layer stresses can occur in the CMUT fabrication process during the deposition of the individual layers, which influence the behavior of the membrane, but are not taken into account in analytical calculations or most simulation models.

Wygant *et al.* provide theoretical background to analytically calculate the displacement of a circular CMUT membrane, approximated by a circular clamped plate [30]. They assume that the plate is deflected by atmospheric pressure P_{atm} and an electrical force F_{el}, resulting from an applied voltage.

$$P = P_{atm} + \frac{F_{el}}{\pi a^2} \tag{2.16}$$

Here, a is the radius of the plate. The electrostatic force is non-uniform as the membrane does not move downwards as a whole in the form of a rigid body movement (*piston-like motion*) if a voltage is applied, but is bent much stronger in the middle than at the edges (cf. Figure 2.8). Consequently, these differences in the effective distance between the two plates, depending on the position on the membrane, lead to the situation that the electrostatic force acting on the center of the membrane is bigger than that acting on the edge of the membrane. Based on basic plate theory, the deflection ω at the radial position r of the plate can be calculated as [30]:

$$\omega(r) = \frac{Pa^4}{64D} \left(1 - \frac{r^2}{a^2}\right)^2 \tag{2.17}$$

Here, D is the flexural rigidity of the plate material and can be calculated using Young's modulus E, Poisson ratio ν, and thickness h of the plate:

$$D = \frac{Eh^3}{12\left(1 - \nu^2\right)} \tag{2.18}$$

The maximum deflection of the plate ω_{pk}, occurring at its center ($r = 0$) can be calculated as:

$$\omega_{pk} = \frac{Pa^4}{64D} \tag{2.19}$$

The average deflection over the entire area of the plate equals one third of the deflection of the center:

$$\omega_{avg} = \frac{\int_0^a 2\pi r \omega(r) dr}{\pi a^2} = \frac{Pa^4}{192D} = \frac{\omega_{pk}}{3} \tag{2.20}$$

16

Applying $P = F/A$, the average plate displacement can be written as:

$$\omega_{avg} = \frac{Pa^4}{192D} = \frac{Fa^2}{192\pi D} = \frac{1}{k_1}F \tag{2.21}$$

Where k_1 is a linear spring constant:

$$k_1 = \frac{192\pi D}{a^2} \tag{2.22}$$

Assuming a high-frequency immersion device, large deflection forces and atmospheric pressure can be neglected. For this case, energetic considerations of Wygant *et al.* result in an equation for the displacement ω_{PI} at which the pull-in occurs:

$$\frac{\omega_{PI,pk}}{g_0} = 0.46 \tag{2.23}$$

Here, g_0 is the effective cavity height, which is calculated from the cavity height t_{cavity}, the thickness of the insulation layer $t_{insulator}$ underneath the cavity, and the relative permittivity $\epsilon_{r,insulator}$ of the insulation material:

$$g_0 = t_{cavity} + \frac{t_{insulator}}{\epsilon_{r,insulator}}. \tag{2.24}$$

According to Equation (2.23) and Equation (2.20), the maximum average deflection of the plate is 15% under the assumptions made. If a non-linear spring is assumed instead of a linear one, the average membrane deflection at which the pull-in occurs increases to $\omega_{PI,avg} = 24\%$ or correspondingly $\omega_{PI,pk} = 72\%$ in the center of the membrane [31].

Assuming a circular membrane, a linear spring constant k_1, and a high-frequency immersion device, the voltage V_{PI} at which the pull-in occurs was numerically found by Wygant *et al.* as [30]:

$$V_{PI} = 0.39\sqrt{\frac{g_0^3 k_1}{\pi a^2 \epsilon_0}} \tag{2.25}$$

The CMUT design used in this thesis is composed of a rectangular silicon nitride membrane on which an aluminum electrode with smaller edge lengths is applied. Consequently, the calculation of the pull-in voltage is significantly more complex and Equation (2.25) can only be used to provide an initial value for subsequent FEM simulations.

Resonance frequency

An important parameter of CMUTs is their resonance frequency. Similar to the pull-in voltage, the resonance frequency of a CMUT depends on the thickness, shape, diameter

(or edge lengths) and material of the membrane. According to Leissa, the resonance frequency for circular membranes can be estimated as follows [32]:

$$\omega = \frac{10.22}{a^2 \sqrt{\rho h / D}} \qquad (2.26)$$

Here, a is the radius of the membrane, h is its thickness, ρ is the density of the membrane material and D is the flexural rigidity (Equation (2.18)).

For rectangular membranes, the corresponding equation gets more complex. Depending on the boundary conditions and the mode observed, there are many formulations for the resonance frequency of rectangular plates [32]. For a plate with all four sides clamped, Leissa refers to a publication of Galin („On the Transverse Vibrations of Plates", 1947), written in Russian language, giving a resonance frequency of:

$$\omega = 12 \sqrt{\frac{7}{2} \left(\frac{1}{a^4} + \frac{4}{7} \frac{1}{a^2 b^2} + \frac{1}{b^4} \right)} \sqrt{\frac{D}{\rho h}} \qquad (2.27)$$

for a and b being the edge lengths of the rectangular plate.
The resonance frequency of a rectangular plate simply supported at all four sides is given as [32]:

$$\omega = \sqrt{\frac{D}{\rho h} \left[\left(\frac{\pi}{a} \right)^2 + \left(\frac{\pi}{b} \right)^2 \right]} \qquad (2.28)$$

Simply supported means that the deflection and the bending moment of the elements are zero at the edges of the rectangular plate [33]. An even more restrictive boundary condition is the case of a clamped membrane, where deflection and slope are zero.
According to Bellaredj *et al.*, the boundary conditions of CMUTs are between all clamped and simply supported [34]. Beside this, deviations from experimental values are to be expected, since residual stress in the membrane is neglected and in the case of the rectangular membranes used in this work the top-electrode with edge lengths smaller than the membrane is not considered. Furthermore, the surrounding medium is neglected in the formulas mentioned, which has an influence on the resonance frequency. Viscous damping and acoustic radiation reduce the vibrating energy of the membrane, altering the resonance frequency [35]. Hongbin *et al.* provide the following equation for the resonance frequency in a fluid depending on the virtual mass β added by the fluid [35]:

$$f_{fluid} = \frac{f_{vacuum}}{\sqrt{1 + \beta}} \qquad (2.29)$$

β can be calculated from the densities of membrane (ρ_{mem}) and liquid (ρ_{fluid}), thickness (h) and radius (a) of the membrane, dynamic viscosity (η) of the fluid and, if necessary, energy dissipation ξ:

$$\beta = 0.669 \frac{\rho_{fluid} \times a}{\rho_{mem} \times h}, \qquad \text{(Lamb's model, for } \eta \leq 10 \, \text{mPa s)} \qquad (2.30)$$

$$\beta = 0.6538 \frac{\rho_{fluid} \times a}{\rho_{mem} \times h} \times (1 + 1.082 \xi), \quad \text{(Kozlovsky's model, for } \eta > 10 \, \text{mPa s)} \qquad (2.31)$$

Spring softening effect

To describe the behavior of a CMUT, Brenner *et al.* approximate it by a parallel plate capacitor, which in turn is approximated by a mass-spring-damper system model [6]. The parallel plate capacitor is described by the spring constant k_p, the mass constant m_p, and the damping constant r_p. The acoustic medium is represented by a damping constant r_m and a mass m_m. According to them, the capacitance of the capacitor is [6]:

$$c(x) = \frac{A\epsilon_0\epsilon_r}{g_{eff} - x} \tag{2.32}$$

Here, x and A are the displacement and the area of the top plate of the capacitor, ϵ_0 and ϵ_r are the permittivity of vacuum and the relative permittivity of the materials used for the membrane and the insulation layer. g_{eff} is the effective gap height. The effective gap height can be calculated using the thicknesses of insulator (t_i) and membrane (t_m) and the initial gap distance g_0 as [6]:

$$g_{eff} = \frac{t_i + t_m}{\epsilon_r} + g_0 \tag{2.33}$$

According to Newton's second law, the CMUT dynamics could be described as follows [6]:

$$m_p\frac{d^2x}{dt^2} + r_p\frac{dx}{dt} + k_p x = f_{el} + f_{ac} - p_0 \tag{2.34}$$

Here, f_{el} and f_{ac} are the forces due to electrical and acoustic loading. The influence of the atmospheric pressure is included by p_o.

As the intrinsic viscoelastic damping of the top plate r_p is usually negligible according to Brenner *et al.*, they use the principle of minimum potential energy to calculate f_{el} and f_{ac} as [6]:

$$f_{el} = \frac{-\epsilon_0\epsilon_r AU(t)^2}{2\left(g_{eff} - x\right)^2} \tag{2.35}$$

$$f_{ac} = -p(t)A \tag{2.36}$$

with the acoustic pressure $p(t)$ an the applied voltage $U(t)$. Equation (2.35) shows that the force due to electrical loading is nonlinear in the plate displacement x.
The authors exploit the fact that CMUTs are usually driven by a high DC bias voltage in combination with a low AC signal voltage (transmit mode) or low acoustic pressures resulting in small AC voltages in receive mode. Based on this, they linearize the electrostatic force at U_{DC} and x_{DC}. The linearized equation of motion is obtained by using $x = x_{DC} + x_{AC}$ and $U = U_{DC} + U_{AC}$ and omitting the second order terms [6]:

$$(m_p + m_m)\frac{d^2x_{AC}}{dt^2} + r_m\frac{dx_{AC}}{dt} + (k_p + k_s)x_{AC} = \frac{-\epsilon_0\epsilon_r AU_{DC}U_{AC}(t)}{2\left(g_{eff} - x_{DC}\right)^2} \tag{2.37}$$

Here, k_s is the spring softening effect [6]:

$$k_s = \frac{\epsilon_0 \epsilon_r A U_{DC}^2}{(g_{eff} - x_{DC})^3} \tag{2.38}$$

This means, the effective spring constant is reduced if a higher bias voltage is applied. Applying a bigger DC bias voltage gives a bigger static displacement of the membrane, causing an increased electrostatic force. As a result, the same alternating voltage signal causes a greater deflection of the membrane, it becomes „softer". Simultaneously, this implies that the resonance frequency decreases for higher bias voltages, so that this is generally referred to as the spring-softening effect.

2.3 Simulation

To correctly predict the behavior of devices during operation is a very important part of product development. E.g. for safety in car industry one of the important properties is the deformation of the car during a crash. In the design development of a new aircraft the flow behavior plays a significant role, so flow experiments and simulations are done. When ultrasound probes in general are developed it is important to find out parameters like resonance frequency, bandwidth, emitted pressure or the shape of the acoustic field (radiation pattern) to optimize the transducer layout and materials regarding to the specific requirements. For ultrasound probes based on CMUT technology, additionally the pull-in (or collapse) voltage needs to be determined.

One way to achieve the needed parameters is to build prototypes and perform experiments. Calculations and simulations can be done before the experiments to reduce the amount of prototypes and, by that, reduce the amount of time and money needed.

Predicting the device behavior means solving the underlying equation systems. While some of these equations are relatively easy to solve, many others can not be solved analytically so numerical approaches are necessary. The large variety of applications is covered by many different simulation software applications that are based on diverse methods. Three important ones, Finite element method (FEM), finite difference method (FDM) and finite volume method (FVM) are introduced and discussed in this section. Special methods like the finite integration technique (FIT) or the widely used equivalent circuit models (Mason model, model of Krimholtz, Leedom and Matthaei (KLM) or Redwood) are only suitable for the calculation of some aspects, but cannot cover the complete, transient behavior of a CMUT and are therefore only mentioned here for completeness.

2.3.1 Finite Element Method

The simulations in this thesis are based on a finite element approach, which is why this method is discussed in more detail.

Already over 2000 years ago, polymathes such as Aristotle (384–322 BC) introduced the idea of breaking macroscopic objects down into very small elements. However, it was not until the 1940s that Hrenikoff (1941) and McHenry (1943) published the first scientific papers that exploited the idea of breaking an object down into many small elements in order to solve the corresponding equation systems numerically [36]. As these discretizations suffered from some restrictions (only rectangular mesh structures), a later work of Turner, Clough, Martin and Topp, published in 1956, is commonly seen as the start of the finite element method [37]. Their aim was to speed up the design process for new aircrafts and to achieve more accurate results when calculating e.g. dynamic loads. Therefore they developed a method that makes use of the processing power of recent computers. Their „original" finite element approach is as follows [37]:

- The (complex) structure is replaced by many finite elements, connected at so called node points. The stiffness matrix must be known for each of these simplified elements.

- The global stiffness matrix is developed by holding all nodes fixed while displacing a single one and calculating forces and reactions.

- Support conditions can be specified by eliminating columns and corresponding rows in the stiffness matrix, which reduces its order and makes it non-singular.

- Matrix calculations are applied to the stiffness matrix for any external forces at the nodes, to calculate all components of the node displacements as well as external reactions.

- In a final step, forces in the internal members can be determined by applying the corresponding force-deflection relations.

An essential feature of the FEM is, that for each element a solution can be set up first which is then used to assemble the solution for the whole structure. So the complex problem is divided into many smaller partial problems that are easier to solve [38]. While the solvers used to calculate these matrices have changed since the first steps of the FEM, the basic idea remains still the same. When using a finite element method the setup is subdivided into small elements with usually 3-4 nodes (triangles or rectangles) in case of 2D and eight nodes (cuboids) in 3D models [39]. The commercial software package PZFlex (Glasgow, UK), which was mainly used for this work, is based on the finite element method [39]. More precisely PZFlex uses explicit algorithms and works in time-domain.

For the case of a 2D model with elements consisting of three nodes each, a rough sketch can be found in Figure 2.9.
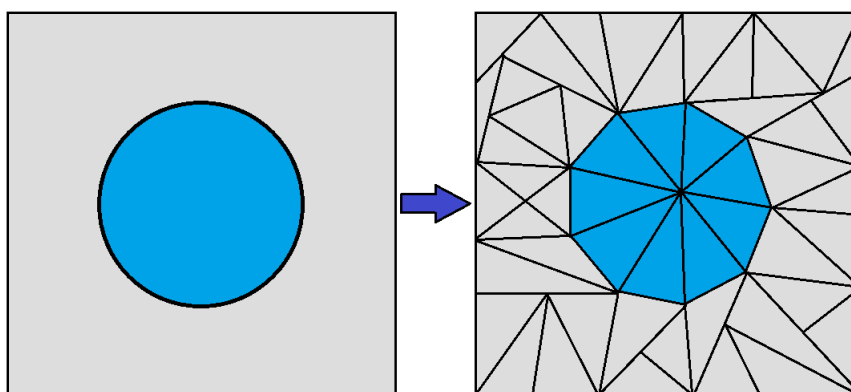
Figure 2.9: Exemplary meshing of a circle inside of a square using triangles.

To solve the underlying differential equations, assumptions are made about the time behavior of the electromechanical characteristics [40]. *Harmonic* analyses take place in the frequency-domain. Under the assumption that the temporal behavior can be completely described by sine or cosine functions, time is eliminated as an independent variable. Harmonic analyses are often used to determine the resonance frequency of a system, since the calculation time is usually shorter than with transient analyses.

Instead, *transient* calculations take place in the time-domain and provide the complete temporal behavior of the system. In the case of CMUTs, for example, this means that the result of the calculation ideally shows not only the resonance frequency but also the deflection at different points on the membrane at different times. This allows the transient response or the pull-in voltage to be determined

Explicit - Implicit

The different approaches for solving the partial differential equations for transient analyses using the finite element method can be divided into two categories: Implicit and explicit procedures [40]. For implicit methods, the solution vector of time step n is coupled. These methods are named implicit because the solution at time t_{n+1} depends on the solution at time t_n but also on the solution at time t_{n+1} itself.

First, a preliminary solution for the time step t_{n+1} is calculated. Based on this, a recalculation back to the time step t_n is done and the deviation is analyzed.

If the deviation is above the previously defined convergence criterion, the calculation of the solution for the time step t_{n+1} is repeated with slightly different parameters. Depending on the selected convergence criterion, a large number of iterations may be necessary.

Explicit methods yield the solution of the approximation at time t_{n+1} explicitly in terms of the solution calculated at time t_n [41]. So the equation for a certain grid point at time

t_{n+1} is fully decoupled from the other grid points and can be computed independently from them.

According to Wojcik *et al.*, implicit algorithms are preferable for steady state oscillations and linear static problems while explicit algorithms should be prefered for transient calculations [40]. While implicit methods have the advantage of being unconditionally stable regarding the time step, they suffer from the big amount of calculations that need to be done for each time step.

Explicit approaches are only conditionally stable, e.g. the time step needs to be small enough to effectively decouple the nodes. On the other hand, the calculation effort per time step is significantly lower for explicit methods compared to implicit ones.

For stability, explicit algorithms need a sufficiently small time step [42]. Here, the Courant-Friedrichs-Levi condition (CFL condition) is used as stability criterion. According to Schäfer, the CFL condition for time step Δt, grid spacing Δx and sound velocity v is [43]:

$$\Delta t < \frac{\Delta x}{v} \tag{2.39}$$

For the simulation of sound waves, fulfilling the CFL condition therefore means that a sound wave cannot propagate further than to the next nodal point within a single time step. With PZFlex, the maximum possible time step is calculated automatically. The user only has the possibility to select a time step below this maximum to increase the stability. Most of the simulations in the course of this work were done with a time step of 90% of the maximum possible time step.

Boundary conditions

The behavior of a device always depends on its environment. In the case of ultrasonic transducers it makes a difference which materials are in contact to the surfaces of the transducer. For example, if the environment on its backside is evacuated, no energy can be emitted there in the form of acoustic waves. As a result, more energy is released to the front than it would have been the case if the area behind the transducer had been filled with water. For this work, CMUTs coated with silicone and a polyether ether ketone (PEEK) or titanium foil were simulated. Since the models would otherwise have become very big, which would have increased the computational effort and thus the calculation time enormously, only single cells were simulated. The effects of this limitation on the oscillation behavior of the single CMUT membrane are small. Basically only effects due to cross-coupling are not considered. Regarding the PEEK or titanium foil, however, it could make a difference whether it has the size of a single CMUT cell or, as in the experimental setup, is larger than the entire CMUT chip. To consider such dependencies, boundary conditions are defined in the simulation model.

The simulation models for this thesis use three different types of boundary conditions: *symmetry, absorbing* and *fixation.*

A *symmetric* boundary condition is often used at *xmin* ($x = 0$) and *ymin* ($y = 0$). Instead of simulating the whole (round or rectangular) membrane, e.g., only a quarter of the membrane is calculated and the result is converted for the whole cell. A disadvantage of exploiting existing symmetries is that unsymmetrical modes can no longer be considered. For a simulated evaluation of the symmetry boundary condition see also Section 4.1.2.

The active structure of a CMUT is usually small compared to the surrounding media. Instead of unnecessarily inflating the size of the simulation model, the water or air load can also be simulated with a smaller thickness. In order to prevent reflections on the upper side of the sonicated medium, an *absorbing* boundary condition is applied there. This is often referred to as a perfectly matched layer (PML) in other simulation tools. Sound waves are always partially reflected when they hit a material with a different acoustic impedance. The absorbing boundary condition in PZFlex (or the PML in other tools) prevents such reflections by assuming a material with the same acoustic impedance outside the actual model in the corresponding direction. Figuratively speaking, such a boundary condition ensures that the material located at the corresponding edge of the simulation model is continued infinitely outside the model.

In the case of the *fixating* boundary condition, all (or selected) degrees of freedom of the affected elements are fixed. This type of boundary condition is used in this work to avoid having to model the ground wafer to its full thickness. In reality, the CMUT is built on a ground wafer whose thickness is significantly larger than that of the other layers. This physically ensures that only the membrane is excited to oscillate, but not the part below the cavity. In the simulation model, a realistic implementation would lead to an enormously large quantity of additional finite elements and thus to a large increase in the computational effort. Therefore, only a thin ground layer is modeled here instead, which is then stabilized by the fixing boundary condition.

In addition to PZFlex, important tools for the simulation of ultrasonic transducers that are based on FEM are Ansys (Canonsburg, USA) and COMSOL (Stockholm, Sweden).

Note:

During the preparation of this thesis a major update of the software PZFlex was released. Basically two things have changed: The calculations of the simulation models are no longer performed locally, on the own hardware, but online in the AWS (Amazon Web Services, Seattle, USA) cloud. In addition, the name has been changed from PZFlex to OnScale (Glasgow, UK). Since neither the basic handling of the program nor the method of calculation have changed, within this thesis the software is always referred to as PZFlex, even if the later simulations were done with OnScale.

2.3.2 Finite Difference Method

The FDM is based on the work of Richardson from 1910 [38]. It can be used successfully for many problems, especially if a regular square mesh can be used to generate the grid points. For geometrically more complicated areas, however, the FDM can become very complex.

From the fundamental point of view one of the main differences between FDM and FEM is that the FEM uses the original mathematical equations on the elements in which the model is divided. Consequently the approximations are only physical, not mathematical. The FDM instead approximates the mathematical equations of the actual physical system by converting the differential equations into difference equations.

In contrast to finite element applications, tools for calculation using the finite difference method are usually programmed in-house and are comparatively rarely available commercially.

A commercially available tool for calculating the propagation of sound waves based on the finite difference method is Wave2000[1].

2.3.3 Finite Volume Method

Especially for solving problems in fluid mechanics numerically, finite volume methods gained some popularity since they were introduced in the 1970s by McDonald, MacCormack, and Paullay [43].

If the problem domain is subdivided into cells and the field equations are written in integral form on these cells, the approach is called finite volume method [44]. Usually the FVM includes five steps [43]:

- Fragmentation of the target volume into a finite number of subvolumes,

- Formulating integral balance equations for each of these volumes,

- Numerical integration to approximate the integrals,

- Interpolation with nodal values to approximate function values and derivatives,

- Composition and solution of the discrete algebraic system.

A tool for calculations based on the finite volume method is Ansys FLUENT [45].

---

[1]www.cyberlogic.org/wave2000.html

3 State of the art

In this chapter, the state of the art for this thesis will be discussed. First, an insight into the communication with medical implants is given. This is followed by a general description of the current state of CMUT technology as well as on the simulation of CMUTs. Some CMUT applications are given as examples, especially with regard to applications inside the human body. The chapter concludes with the state of the art in the coating or encapsulation of CMUTs.

3.1 Communication with medical implants

Communication with medical implants is necessary in two different scenarios. Firstly, communication from the outside (by the treating physician) with the implant inside the patient can be needed for control, monitoring or adjustment of functions. Another frequently used reason for the connection from the outside to the implant is powering the implant.
Secondly, different implants within a patient can interact with each other, for example to improve therapy success or to transmit data measured by a sensor to another implant. For example, Teshome *et al.* mention an implanted insulin pump, which communicates with an implanted glucose sensor to provide insulin exactly when it is needed [3].

According to Khanna, communication with medical implants as well as power supply for them can be realized by percutaneous wires or by wireless technologies [46]. Wired methods have the disadvantages of an increased risk of infection, low acceptance by the patient, and restrictions on mobility. For these reasons, wireless methods are preferred and the possibility of wired transmission is mentioned here for completeness.

The main options for wireless communication with medical implants are as follows: inductive coupling, antenna-enabled RF communication, galvanically and capacitively coupled intrabody communications (IBC), optical IBCs, and ultrasound [3].

According to Teshome *et al.*, **inductive coupling** is often used for short distances [3]. Here, the current in a transmitter coil induces a magnetic flux, which in turn induces a current in a receiving coil. Teshome *et al.* list muscle stimulators, retinal implants, cochlear implants and pacemakers as examples of applications for communication with implants via inductive coupling. Communication via inductive coupling has the disadvantage of a short range (Teshome *et al.* states a range of: $<4\,\mathrm{cm}$ [3]). Tomlinson *et al.* mention interference with other magnetic fields as a potential disadvantage [47].

26

According to Wang *et al.*, inductive links have very limited coupling efficiencies at distances greater than the diameter of the coils, so larger coil diameters or larger electrical signals are needed for longer distances [48].

According to Tomlinson *et al.*, the most commonly used technology for intra-body communication is based on **radio frequency waves** [47]. There are several standards for RF-based data transmission. Wireless Medical Telemetry Service (WMTS) includes three frequency bands: 608 MHz to 614 MHz, 1395 MHz to 1400 MHz, and 1429 MHz to 1432 MHz. According to Tomlinson *et al.*, WMTS is primarily used for remote patient monitoring. MedRadio (formerly Medical Implant Communications Service MICS) covers the frequency range from 401 MHz to 406 MHz (bandwidths between 100 kHz and 6 MHz) and is mainly used for on-body and embedded sensor communications. In addition, there are other frequency bands, such as the millimeter wave (5G) range of 30 GHz to 300 GHz, whose use for communication with medical implants is currently being researched. Tomlinson *et al.* see RF's biggest drawback as its high attenuation, which requires greater transmit power while also heating the tissue being traversed. Wang *et al.* report data rates in tissue of up to 500 Mbps (range: 3.6 cm, frequency range: 3.1 GHz to 7 GHz) for the antenna-based RF technology [48]. For the MedRadio frequency range, Tomlinson *et al.* report a range of 20 cm and achievable data rates of 80 kbps [47]. In the frequency range of 3.1 GHz to 10.6 GHz (ultra wideband), transmission distances of 12 cm and data rates of 500 Mbps are reported as possible.

Another technology for wireless communication is based on **galvanically or capacitively coupling**. The human body has a common electric field with its environment. For capacitive coupling, this is used to induce a current flow between transmitter and receiver [47]. One electrode of the transmitter and one from the receiver is attached to the body while the others are floating. Teshome *et al.* mention data rates of 2 Mbps for 100 kHz signals [3]. Tomlinson *et al.* also report a maximum possible 2 Mbps, here for frequencies from 1 MHz to 200 MHz [47]. In first experiments even data rates of up to 60 Mbps were realized by multi-level coded transmission schemes. According to Tomlinson *et al.*, a major disadvantage of capacitively coupled communication is that the signals significantly extend beyond the body and external interference leads to increased noise. According to Teshome *et al.*, this problem can be avoided by using galvanically coupled communication instead [3]. Unlike capacitive coupling, in galvanic coupling the AC signal is coupled inside the body and not between body and environment [47]. A voltage is applied between two transmitter electrodes, alternating current propagates through the body based on its ion content and is measured differentially at the receiver electrodes. Tomlinson *et al.* specify the frequency range for galvanically coupled communication as 10 kHz to 100 MHz and cite another publication in which data rates of 1.23 Mbps were realized over distances of up to 15 cm at a frequency of 200 kHz [47]. According to Tomlinson *et al.* and Teshome *et al.*, communication based on galvanic coupling in particular is yet to be explored extensively [47][3].

Optical IBCs: Teshome *et al.* mention data transmission by laser diodes emitting infrared signals as another possibility for communication with medical implants [3]. The state of the art is frequencies from 300 GHz to 430 THz. Data rates of 115.2 kbps at 348.596 GHz over a distance of 24 mm have been demonstrated so far. The feasible transmission distances are probably the biggest disadvantage of infrared-based communication, limiting effective communication to the millimeter range. As a result, optical communication methods are only suitable for communication with superficial implants (transcutaneous or subcutaneous). Especially for subcutaneous implants (distances of less than 4 mm), high data rates of up to 50 Mbps are reported to be possible.

According to Tomlinson *et al.*, **ultrasound** is the standard technology for underwater communication [47]. Because of the water-like acoustic properties of human tissue, it seems reasonable to use ultrasound for communication with or between medical implants in the human body as well. Jafaar *et al.* state that ultrasound has a great capability for the intrabody communication between different implants [49]. Compared to RF-based methods, ultrasound has the advantage of significantly lower attenuation in the body [47]. A larger bandwidth corresponds to a larger achievable data rate. The bandwidth but also the attenuation in the body increase with increasing frequency of the ultrasound signal. This necessitates a compromise between the highest possible bandwidth and the lowest possible attenuation when selecting the carrier frequency. Wang *et al.* specify the optimum frequency for data transmission in the human body over a distance of 15 cm to be 2 MHz [48]. The achievable data rates would be a maximum of 10 Mbps for distances of 10 cm and more. However, the information on achievable data rates varies significantly. While Tomlinson *et al.* quote publications with values between 700 kbps and 28.12 Mbps (the latter only for synthetic phantoms), Teshome *et al.* quote data rates of only 50 kbps [47] [3]. Wang *et al.* also cite a publication in which data rates of 30 Mbps were achieved at a distance of 5.86 cm thanks to quadrature amplitude modulation [48]. According to Wang *et al.*, data rates of 10 Mbps are possible at distances of 10 cm using orthogonal frequency division multiplexing (OFDM). The authors point out that most of the values mentioned were achieved on phantoms under laboratory conditions. The feasibility of achieving comparable data rates with miniaturized transducers integrated into implants would still need to be investigated.

The work published so far on communication in the human body using ultrasonic waves is based on piezoelectric ultrasonic transducers. The author is not aware of any publications on acoustic communication using CMUTs at the time of submission of this thesis.

3.2 CMUTs in general

The general structure of CMUTs and the standard manufacturing processes are described in Section 2.2. The membranes of CMUTs are typically made of silicon or silicon nitride, but there are also first CMUTs with polymer membranes [6]. Using different materials and especially membrane geometries, a very wide frequency range has already been ac-

cessed with CMUTs. In the low frequency range, Wygant *et al.* fabricated CMUTs with a resonance frequency of 50 kHz (membrane diameter: 4 mm) [50]. In the high-frequency range, Zhuang *et al.* fabricated CMUTs with a resonance frequency of 50 MHz [51].

In recent years, research on CMUTs has been strongly stimulated by both, university research groups as well as industrial companies. In the university context, Khuri-Yakub et al. at Stanford University are particularly noteworthy. The group not only pioneered the CMUT technology but also made significant progress in manufacturing as well as in the expansion of potential applications of CMUTs [5][6]. Other important centers of academic research on CMUTs are the research groups of Giosue Caliano (Roma Tre University, Italy), Ömer Oralkan (North Carolina State University, USA), Levent Degertekin (Georgia Institute of Technology, USA), and Erik V. Thomsen (Technical University of Denmark, DTU, Denmark) [52][53][27][54]. Of these, two professors, Degertekin and Oralkan, graduated at Stanford University in Khuri-Yakub's group.

The first commercially available ultrasound device based on CMUTs was not released in Europe until late 2019, when the US company Butterfly Network inc. (Guilford, USA) started offering a transducer based on a 2D CMUT array with 9000 cells for medical imaging [6].

Figure 3.1: First CMUT probe available in Europe: Butterfly iQ+ [55]

In contrast to conventional ultrasound devices, no additional hardware is required here, as the acquisition, processing and display of the measurement data is done on a standard smartphone.

An important company offering ultrasound transducers based on CMUTs is Kolo Medical Inc. (Suzhou, China) [51]. Other industrial companies that already offer a wide range of piezoelectric ultrasonic transducers and have published at least initial results of their research on CMUTs are Koninklijke Philips N.V. (Eindhoven, Netherlands, [56]), Esaote (Genoa, Italy, [57]) and Vermon SA (Tours, France, [58]). However, it is not clear from the product sheets available online whether these companies already sell CMUT probes commercially.

Regardless, it is possible to have CMUTs designed and manufactured by several companies, such as Philips Innovation Services or Fraunhofer IPMS [6]. During the period of preparation of this thesis, Fraunhofer IBMT also started CMUT development. Within the scope of several research projects, processes for manufacturing were tested and feasibility studies were carried out.
Considering the advantages of CMUTs in terms of low-cost mass production, it is remarkable that the big commercial breakthrough has not yet occurred.
To get an overview of the patent situation, the patent search *Espacenet* of the European Patent Office was used[1]. At the time of the query on 04.05.2021, it found 92 patents containing *CMUT* and 70 containing *capacitive micromachined ultrasonic transducer* in the title. The patents focus mainly on manufacturing processes, special CMUT designs and applications (e.g. gas or temperature sensing). For the latter see section 3.4. Several patents listed by the search engine of the European Patent Office are held by universities. The Chinese Xi'An Jiaotong University and the Georgia Institute of Technology in the USA are particularly well represented. While the first focuses on applications such as the use of CMUTs as temperature or pressure sensors, the patents of the latter university mainly concern manufacturing methods. Stanford University, which is home of Prof. Khuri-Yakub, one of the pioneers of CMUT technology, holds six patents primarily related to the design of CMUT arrays, according to this patent search on *Espacenet*.
Koninklijke Philips N.V. holds the majority of the patents held by companies (23 patents). Other companies with several entries in the list of found patents are Kolo Medical Inc., Texas Instruments Incorporated and Olympus Medical Systems. Encapsulation of CMUTs is only a minor issue in the patents found. For example, Koninklijke Philips N.V. has patented a CMUT array with an acoustic window layer in which a polymeric material is applied directly on the membrane for encapsulation (patent no.: US2018021813A1).

The patent search conducted did not reveal any patent that conflicts with the approach developed within this thesis.

3.3 Simulation of CMUTs

A common way to reduce costs for fabrication is to optimize the cell design, e.g. in terms of membrane diameter and thickness, in advance by analytical calculations and

---

[1] https://worldwide.espacenet.com/

computer-based simulation models (see section 2.3). The aim is to reduce the amount of prototypes needed which means a reduction in fabrication time and costs. For simple cell designs, analytical calculations (see Section 2.2.2) are able to predict the basic behavior of the CMUT with high accuracy [59]. For a hexagonal shaped CMUT cell, Sharma *et al.* reported a relative deviation between analytic calculations and Ansys simulations of only 1.69% [60]. For a circular membrane, Havreland *et al.* were able to analytically predict the pull-in voltage with a relative error between -5% and 20% [61].

As analytical calculations can only be used to get some basic information for simple CMUT cell designs, making use of FEM-Tools, mainly Ansys and to a smaller part also PZFlex, is very common in the CMUT research community. Maity *et al.* reported a very high agreement between PZFlex results and analytical calculations in terms of membrane displacement, impedance, coupling factor and pull-in voltage [62]. Engholm used PZFlex to successfully investigate cross-coupling between neighboring CMUT cells [63]. In a comparison between experimentally derived data and PZFlex results, he found a deviation of less than 3% with respect to the resonance frequency. Regarding the acoustic output, Eames showed a very high agreement of the signal amplitude with a deviation of only 4.1% or a cross-correlation coefficient of 0.92 in the comparison between data simulated with PZFlex and measured data [64].

More widely used for the simulation of CMUTs is Ansys. The main purpose is the design of CMUTs cells with regard to resonance frequency and pull-in voltage. Lee *et al.* report deviations of less than 6% with respect to resonance frequency [65]. Chee *et al.* report for two different cell designs accuracies of up to 95% with respect to resonance frequency and very good agreement between Ansys simulation and experimental results with respect to pull-in voltage [66]. Bellaredj *et al.* report the deviation between (with Ansys) simulated and experimentally determined resonance frequency for four different cell designs with a deviation of 3% for the smallest membrane radius (r $=50\,\mu$m) [34].

In summary, the selection of publications shows that it is possible to predict the behavior of CMUTs with high accuracy using standard FEM tools like Ansys or PZFlex.

3.4 Applications of CMUTs

In principle, most areas of ultrasound are open for CMUTs. A large field of application is medical imaging. In particular, the companies Butterfly Network Inc. and Kolo Medical Inc. should be mentioned here [67][51]. In the university sector, Gerardo *et al.* recently published their results on the potential of polymer-based CMUTs for medical imaging [68]. In addition, Maadi *et al.* published results of a dual-frequency CMUT array for multi-band imaging in 2021 [69]. The use of CMUT designs with two different resonance frequencies (2 MHz and 9 MHz) on the same chip enables high bandwidth and the possibility for multi-resolution imaging.

Figure 3.2: CMUT probe L62-38 by Kolo Medical Inc. [51]

CMUT based probes can also be used for therapeutic HIFU (high intensity focused ultrasound) applications. N'Djin *et al.* presented the possibility to induce thermal ablation by driving CMUTs in collapse-snapback operation [70]. Jang *et al.* were able to show that dual-mode CMUT arrays are possible, which can be used both to generate the high-intensity ultrasound waves for therapy and to generate the diagnostic ultrasound of lower intensity that can be used to monitor therapy [71]. In 2021, Seok *et al.* presented a CMUT based phased array system enabling electronic focusing of the sound waves for the use in neuromodulation [72]

3.4.1 CMUTs inside the human body

At the time of publication of this thesis, there were no publications on the use of CMUTs as part of medical implants. Instead, some research groups have looked at the use of CMUTs in endoscopy. Nikoozadeh *et al.* report on a CMUT ring array designed for use in endoscopy [73]. This consists of four rings with 128 elements each, which in turn consist of 12-20 CMUT cells each. The four rings have resonance frequencies between 6.5 MHz and 16 MHz. The inner diameter of the transducer is 5 mm, the outer diameter 10.1 mm. The encapsulation of the CMUTs, which have a silicon membrane, is done by 100 nm PECVD silicon nitride as passivation and protective layer as well as by Sylgard 160 (a silicone elastomer) [74]. Yildiz *et al.* have also investigated various CMUT-based ring and linear arrays for use in an endoscope [75]. They also use silicon membranes and realize frequencies between 2 MHz and 20 MHz by varying the membrane diameter. To protect them from dust and other contaminants, a 20 nm thick SiO_2 layer is applied on the membrane [76].

Apart from the presented work on CMUT assisted endoscopy, another approach to the use of CMUTs in the human body is described in the literature: the design of an ingestible capsule equipped with CMUTs on the outside [77]. This capsule is intended to take tissue images as it passes through the gastrointestinal tract. Although this device is still in the research phase, it should be mentioned here because it is the only published application of CMUTs in the human body besides the endoscope approaches. In this context, Wang

et al. are working on an ingestible capsule that contains the necessary electronics, power supply and a module for wireless transmission of the images inside [77]. A linear array of 128 individual elements, each separated by a strip of PDMS to provide the necessary bendability, is applied to the outside of the cylindrical capsule. As it passes through the gastrointestinal tract, this CMUT linear array continuously scans the tissue being traversed. The CMUT is designed for a center frequency of 5 MHz and a pull-in voltage of 40 V. A -3 dB bandwidth of more than 81 % and a surface pressure above 700 kPa could be realized. However, integration as well as assembly in the form of a bio-compatible capsule is still pending. No details are given on the intended encapsulation of the CMUT.

3.5 Encapsulation of CMUTs

Three reasons for coatings on CMUTs are reported in the literature. In addition to mechanical protection of the membrane, this is primarily its electrical insulation. A third reason frequently mentioned is functionalization to be able to use the CMUT for gas sensing [78]. Here, the membrane of a CMUT is covered with a functional layer which is exposed to the gas to be sensed. This functional layer binds the gas particles of interest and by this its weight increases. Consequently, the weight of the combination of membrane and functional layer increases, which shifts the resonance frequency. The magnitude of this frequency shift can then be converted into the quantity of the respective particle in the gas mixture. Park *et al.* tested different polymers using thicknesses between 20 nm and 50 nm as functionalization layer, Lee *et al.* tested another polymer (DKAP, a poly(dimethylsiloxane) derivative) with a thickness of 50 nm [78][79]. In each case, the functionalization layer is kept very thin to minimize the effects on the CMUT characteristics. Consequently, Lee *et al.* state the change in resonance frequency due to the coating as only 0.65%.

This thesis deals with the two other reasons why CMUTs are operated behind additional layers: The protection of the CMUT from the environment and vice versa. External applications of CMUTs on humans require a protection layer to protect the patient from the high voltages in case of a malfunction. A protective layer may also be necessary to ensure electrical insulation to guarantee the functionality of the CMUT. The CMUT design used in this work includes a top electrode that is exposed on the membrane. This makes the direct use in water impossible, as short circuits would occur. In the academic literature, only two materials are presented for these encapsulations: PDMS and parylene-C.

Zhuang *et al.* directly compared the two materials and published the results of their work in 2007 [80]. They chose a layer thickness of 2 μm for parylene-C and a thickness of 5 μm for PDMS. This resulted in increased cross-talk and a reduction of the membrane displacement by 18% (parylene-C) and 7% (PDMS). While no value is given for PDMS, the parylene coating electrically isolated the chip in water for 14 days.

Hsu *et al.* have coated chips with a parylene coating (thickness: 2 μm) [81]. He *et al.*

used a parylene-c coating of $5\,\mu m$ thickness and reported a shift in the capacitance due to the coating [82]. While the capacitance increased by $460\,pF$ when increasing the bias voltage from $0\,V$ to $40\,V$ before coating, the same setup gave an increase of the capacitance by only $402\,pF$ after coating.

Moini *et al.* ($100\,\mu m$), Jang *et al.* ($150\,\mu m$), Nikoozadeh *et al.* ($180\,\mu m$), Chen *et al.* ($350\,\mu m$) and La Cour *et al.* ($900\,\mu m$) published results for CMUT-chips coated with layers of PDMS with different thicknesses [83][84][85][86][54]. These groups used different PDMS materials (Sylgard 160, Sylgard 170 and Sylgard 184). While the other researchers mentioned above do not go into detail about the differences that result from the application of the coating, Chen *et al.* and La Cour *et al.* provide more information. Chen *et al.* (Sylgard 184) describe an increase of the resonance frequency from $3.1\,MHz$ to $5.7\,MHz$, an increase in bandwidth of 11 percentage points, and an 80% loss of receiving voltage due to the coating. They explain these effects as being due to the difference in acoustic impedance between PDMS and the medium [86]. La Cour *et al.* (Sylgard 170) describe different effects of coating depending on the transmitting or receiving mode [54]. The transmit signal decreases by 27% due to the coating and the receive signal by 35%. The center frequency decreases from $4.5\,MHz$ to $4.1\,MHz$ in transmit mode from $4.4\,MHz$ to $3.9\,MHz$ in receive mode. The reason for this is the added mass on the membrane. It is interesting to note that the relative bandwidth increases by 9% when transmitting, while it decreases by 15% when receiving. La Cour *et al.* explain the increased bandwidth during transmission with an increased damping in the membrane. In the receiving mode, the additional mass predominates, which thus leads to a reduced bandwidth.

Based on the studies mentioned above, parylene and especially PDMS can therefore be considered as good materials for encapsulating CMUTs for applications on patients. At least for a limited period of time, both materials provide sufficient isolation of the transducer from its environment.

A different approach for encapsulating CMUTs was suggested by Saeidi *et al.* [87]. Using motor oil or rapeseed oil, they coupled their CMUT chip to an encapsulation layer made of 'aluminum, ceramic, Teflon, or polycarbonate' ([87]). The authors describe the transmission losses due to the encapsulation to be between $0.37\,dB$ and $5.03\,dB$ depending on the setup.

Encapsulation providing a long-term insulation becomes even more important when CMUTs are used inside the patient's body. As with medical implants, a biocompatible encapsulation, often made of titanium, is compulsory. In cases where it is crucial that the chosen material ensures the isolation of the CMUT from its environment even after a long period of time, neither parylene nor PDMS are a valid option. Consequently, finding a suitable alternative is necessary for such cases.

Zhou and Greenbaum mention titanium as a material that can be used for biocompatible encapsulation of medical implants [88]. So titanium was examined in this work as an encapsulation material for CMUTs because of its proven encapsulation abilities. Nevertheless, titanium has the disadvantage of a large elastic modulus (E=114.17 GPa [89]). Additionally, a second encapsulation material, PEEK, was investigated in this thesis. PEEK is biocompatible and is used e.g. for orthopedic, trauma, and spinal implants [90].

According to Kurtz *et al.*, PEEK shows a great mechanical strength and a smaller elastic modulus (E = 4.21 GPa [91]) than titanium, facilitating the transfer of oscillations to the surrounding medium because of a reduced flexural rigidity (see Equation (2.18)) [90]. In comparison with titanium, a lighter PEEK film is sufficient for the same mechanical strength, which makes the material an interesting option for CMUT encapsulation. Publications on the operation of CMUTs behind an encapsulation of titanium or PEEK are not known to the author at the time of writing this thesis.

4 Materials and methods

This chapter describes the FEM model that was used for the simulation-assisted design of a customized CMUT cell, the optimization of the encapsulation strategy and the investigation of the effects of different encapsulations. Additionally, an introduction to the methods that were used to experimentally characterize the CMUTs with and without encapsulation is provided.

4.1 Development of a comprehensive FEM model

These sections describe the development of several comprehensive simulation models making use of the finite element tool PZFlex. According to the geometry of the CMUTs to be simulated, 2D and 3D models were created. 2D models exploit the existence of rotational symmetry. Consequently, the model consists of less finite elements resulting in less computing time. 2D models are suitable for CMUTs with circular membranes only. For the simulation of CMUTs with rectangular membranes, 3D models need to be developed. In order to reduce the number of finite elements to be modeled and thus calculation time and hardware requirements, up to two symmetry planes can be used, so that only a quarter of the CMUT is actually designed. Section 4.1.2 discusses the different symmetric boundary conditions and their effects in more detail.

The FEM simulations in this work make use of different excitation signals depending on the behavior to be investigated. Besides the excitation with a continuous sinusoidal signal, sinusoidal cycles with one, ten and 20 oscillating periods and Blackman-Harris pulses were applied. A Blackman-Harris pulse is the second derivative of the Blackman-Harris window [89]. Its frequency spectrum corresponds to a Gaussian distribution centered around the pre-defined center frequency. The pulse consists of three half-waves, has a duration of $t_d = 1.55/f_{center}$ and is exemplarily shown for a frequency of $2\,\mathrm{MHz}$ and an amplitude of $10\,\mathrm{V}$ in Figure 4.1.

The time step parameter, which is important in explicit FEM simulations (Section 2.3.1), varies between the different models. In this work, it was on the order of $9\,\mathrm{ps}$ for the simulations. A list of the material parameters used in the simulation models is provided in Chapter 8.
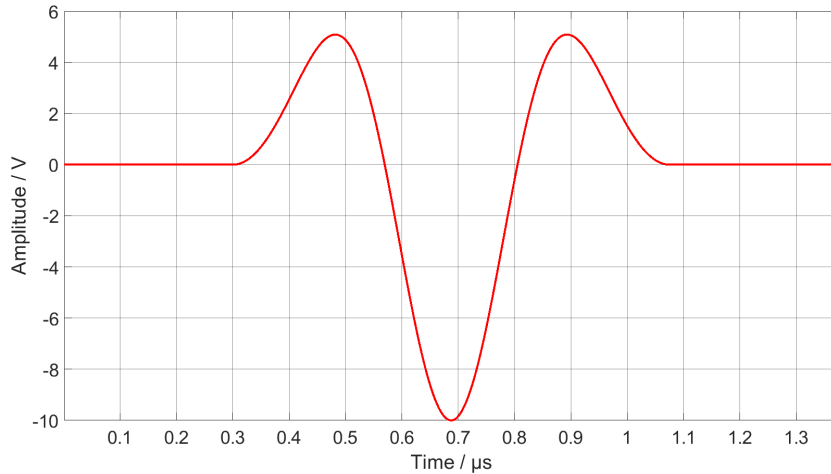
Figure 4.1: Signal course of a 10 V Blackman-Harris wavelet at 2 MHz.

4.1.1 Multi-phase procedure

When the cavity of the CMUTs is evacuated, the atmospheric pressure pushes the membrane downwards (towards the bottom of the cavity). Thus, the membrane is already pre-deflected without applying an electrical voltage. The amount of this deflection depends on the material, its density, and its dimensions and needs to be determined in PZFlex before starting the dynamic simulation. In order to prevent the membrane from vibrating due to a big gradient of the pressure on the membrane, the atmospheric pressure is increased over several time steps. In addition, an artificial strong damping is added, helping to reach the state of equilibrium faster.

Subsequently, the same procedure is applied to the electrical bias voltage. This procedure is demonstrated exemplarily in Figure 4.2, which shows the time course of the displacement of the membrane center on the left y-axis (blue, solid) and the corresponding applied voltage on the right y-axis (red, dashed). The calculation starts with the purple marked area where the atmospheric pressure is slowly raised over a period of 1 μs. Afterwards there is a 1 μs pause (gray background), allowing the membrane to reach its equilibrium state. While this break could be shortened for this particular model, it is especially important for the coated CMUT models, because the membrane reacts more slowly to external forces due to the additional mass. In the green-shaded section, the electrical bias voltage is increased from 0 V to 60 V over a period of 1 μs. This is followed by a pause of 3 μs, again highlighted in gray. This period itself can be subdivided into two areas: First, the artificial strong damping is still switched on (2 μs, light gray section), which serves to reach the state of equilibrium faster.
It is then switched off and calculations continue for some more time steps (1 μs, dark gray area) until any response to switching off the artificial damping has decayed and the membrane has reached its biased steady state.
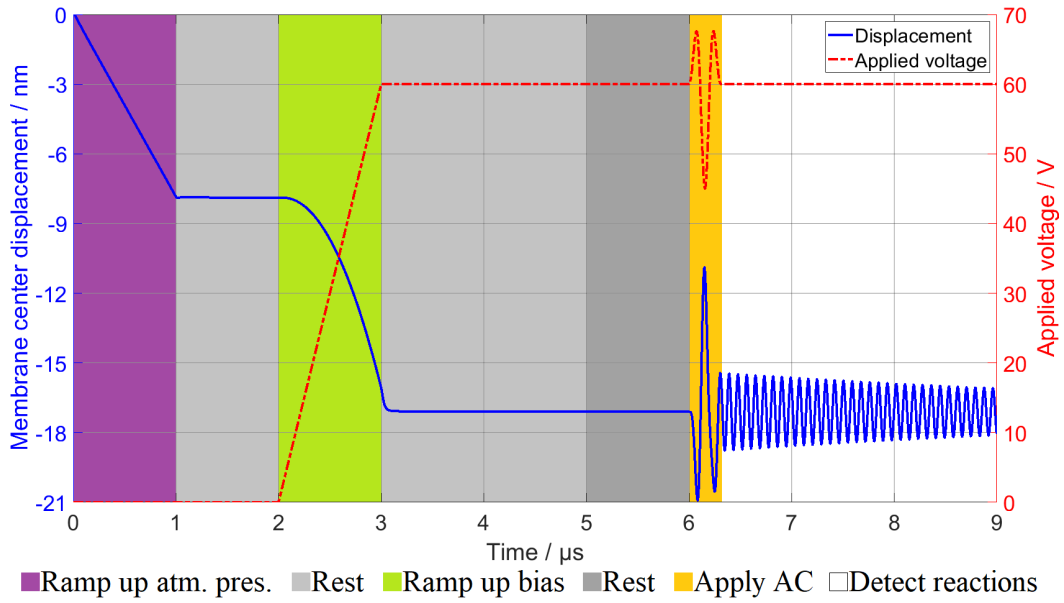
Figure 4.2: Exemplary representation of membrane deflection over time.

Afterwards, the AC voltage signal (Blackman-Harris wavelet, 15 V, 15 MHz) is applied in the orange area. Finally, the simulation continues for some time (white area, 2.8 µs) in order to observe possible post-oscillation and to enable the emitted sound waves to transmit through the medium in front of the membrane. In the example shown here, the damping is so low that the membrane remains oscillating. After the end of the actual excitation signal, the oscillation frequency is 11.7 MHz, which is the resonance frequency of the examined design.

The lengths of the individual sections must be adapted to the respective model so that the AC signal is not applied until the biased steady state is reached and the phases before applying the AC signal are as short as possible to minimize computing time.

A closer look at Figure 4.2 shows that the deflection of the membrane is linear in the purple area, while it increases quadratically in the green area, although both biases (atmospheric and electrical) increase linearly. This is a result of the fact that the electrostatic force (and thus also the membrane displacement) is proportional to the square of the applied voltage (see Section 2.2.2).

Meshing

For simulations with PZFlex, the meshing, the size of the finite elements, must be adjusted individually for each model. It is common for a single finite element in PZFlex to have a maximum size of one twelfth of the smallest resulting wavelength. Based on this initial value, the meshing is made finer until a stable result is achieved.

This is true if a small change in the meshing causes only small changes of the result. Figure 4.3 shows how the course of the displacement of the membrane center changes for different meshings for the 2D model from Section 4.1.2 (cavity height: 500 nm, Si membrane with 2 μm thickness and a diameter of 80 μm). The difference in the curves between the membrane composed of a single row of finite elements (blue) and the one composed of two rows (red) is very large. As the meshing becomes finer, however, the difference to the next coarser meshing gets smaller and smaller. With an increasing number of elements, the computing time increases enormously. For the model shown here, one would therefore perform further simulations with a meshing of 3 to 5 elements along the membrane thickness. The results obtained in this way can be described as stable since a finer meshing would only provide minor advantages in terms of the accuracy achieved.
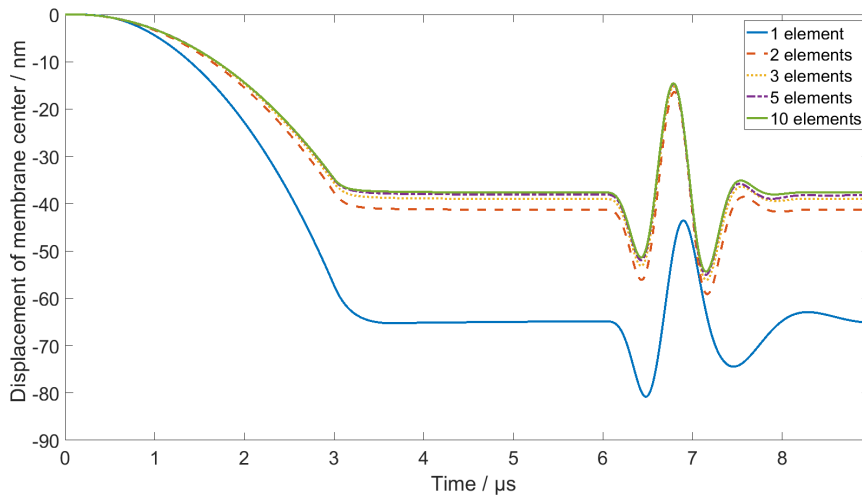
Figure 4.3: Displacement of the membrane center for different numbers of finite elements along membrane thickness. Voltages: $97.5\,\mathrm{V_{DC}}$, $32.5\,\mathrm{V_{AC}}$, Blackman-Harris pulse at $1.2\,\mathrm{MHz}$.

The typical initial meshing for piezoelectric bulk transducers of 12 elements per wavelength (λ) is not sufficient for CMUTs due to their very small dimensions. For example, a frequency of $2\,\mathrm{MHz}$ results for Si_3N_4 (membrane) in a value for $\lambda/12$ of $458.3\,\mathrm{μm}$ ($\lambda = 5.5\,\mathrm{mm}$) and for aluminum (top-electrode) of $262.75\,\mathrm{μm}$ ($\lambda = 3.15\,\mathrm{mm}$). In the final CMUT design, the Si_3N_4 membrane has a thickness of only $600\,\mathrm{nm}$, while the aluminum electrode is even thinner, with a thickness of $250\,\mathrm{nm}$. Thus, with a meshing of 12 elements per wavelength, both layers would be composed of only a single element in thickness, which is not sufficient to properly predict the behavior of the layer as can be seen in Figure 4.3. Therefore, much smaller elements are used for CMUT simulations, the sizes of which are based on the dimensions of the CMUT cell instead of the wavelength. In addition to the general finite element size that applies to the entire model, the min-

imum number of finite elements along each spatial dimension can be specified for each layer. This ensures that very thin layers, such as the top electrode made of aluminum, are composed of enough elements without the need to make the global size of the finite elements so small that their total number becomes extremely high. For the models within this work, a minimum number of four elements per layer was determined to be sufficient. With a thickness of the top electrode of 250 nm, this results in a minimum edge length of the finite elements of 62.5 nm, which corresponds to a resolution of 50,448 elements per wavelength. For comparison: In models of piezoelectric ultrasonic transducers, a meshing of 12-20 elements per wavelength is usually sufficient. Whereas the minimum number of elements per spatial direction in each layer was four for all models, the global size of the finite elements was optimized individually for each model. Here, it is important to choose the size of the finite elements as small as necessary and as large as possible, so that sufficient result accuracy is achieved within as little computation time as possible. The additional condition that each dimension of each layer must be built out of at least four finite elements leads to the fact that the simulation model is composed of elements of different sizes. In the thick layers of the model (for example, in the ground wafer), where the element size is not manipulated by the specification of a minimum number of elements, the dimensions of the finite elements are of the order of $(0.4\,\mu m)^3$.

Evaluation capabilities

The FEM simulations performed are transient simulations (Section 2.3.1). This has the consequence that the resulting parameters of interest can be analyzed directly over time. For example, it is possible to observe the membrane displacement, its acceleration, the voltage response on the electrodes or the sound pressure at an arbitrary depth in front of the membrane for different voltages and excitation frequencies. Due to the very fine meshing, in comparison to typical piezoelectric models (see Section 4.1.1), the propagation medium in the model must be kept as small as possible to save computation time. Therefore, only a few micrometers of the propagation medium are simulated. If the sound pressure or the sound field is to be evaluated at a greater depth, PZFlex offers the possibility to estimate the desired values based on Kirchhoff's extrapolation. For such sound field extrapolations, it is also possible to extrapolate the result of a large number of CMUT cells from the result of the FEM simulated single cell.

4.1.2 Exploiting symmetries

Simulations always require a compromise between computing time and result accuracy. When setting up a CMUT model, some simplifications have to be made. In reality, for example, hundreds or thousands of CMUT-cells are connected in parallel in order to increase the output pressure and thus the signal-to-noise-ratio (SNR).

As even an FEM model of a single cell can take hours to be calculated, simulating hundreds of cells is not a viable option. Instead, single cell models are used in this

work. By doing so, the general behavior of the cell can be examined for different setups in short time. As a drawback of such a single cell model, cell to cell interactions and cross-coupling-effects cannot be determined. For FEM simulations it is not the number of simulated CMUT cells but the size of the model in terms of the number of finite elements to be calculated that is decisive for the computing time required. One consequence is to use as few nodes as possible without crucially affecting the results.

A very important way to reduce the size of the model is to make use of symmetric boundary conditions. Symmetric conditions are usually exploited whenever it is possible. A general disadvantage that has to be kept in mind if doing so, is that asymmetric behaviors are no longer taken into account and thus cannot be detected. This is a general problem when examining the cell behavior to its full extent. However, from a practical point of view, those effects are negligible, as the CMUTs will be used in symmetric modes only. Asymmetric modes would disturb the sound field. Concerning the symmetric results, differences caused by making use of different symmetric boundary conditions are depending on the specific tool that is used as well as on its way to implement these boundary conditions. For this work, the commercial software PZFlex was used. So before developing and optimizing more complex CMUT models, its included symmetric boundary conditions were tested for a basic model.
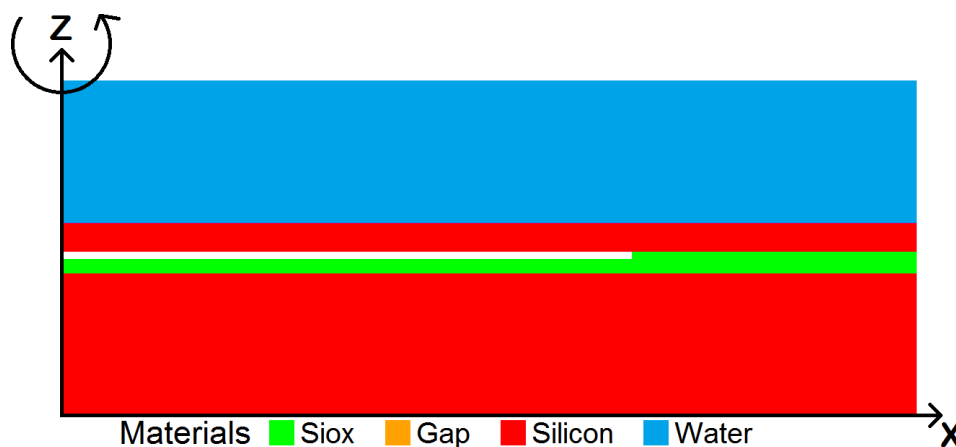
Figure 4.4: 2D model (radially symmetric).

The most options to exploit symmetric boundaries are available in PZFlex when simulating a single CMUT cell with a circular membrane. The simplest and fastest way to receive some results is to set up a 2D radially symmetric model as can be seen in Figure 4.4. As the model makes use of rotational invariance, the y-dimension is not entered directly, but rather added automatically according to the values entered for the x-dimension.

A more sophisticated option is to set up a 3D axisymmetric model. This is for example

necessary for simulating cells with a rectangular membrane. Instead of developing only a single slice of the CMUT, a quarter of the entire cell is built in this case. See Figure 4.5 for a schematic drawing. For a better understanding, all layers above the cavity are excluded here.
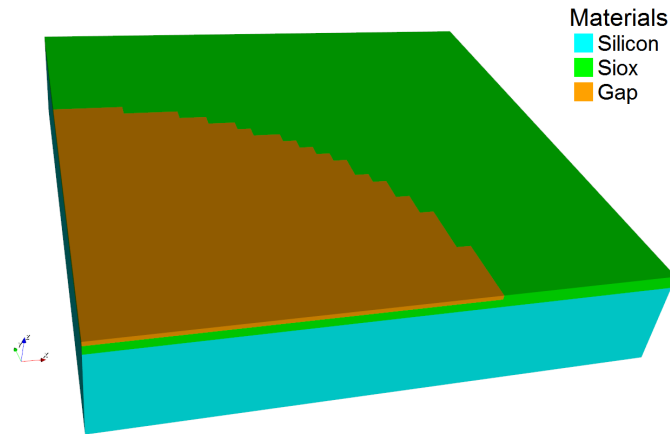
Figure 4.5: 3D model (two symmetry axes are used).

To simulate even more complex geometries or to examine effects that cannot be examined in a model making use of two symmetric axes, it is also possible to set up a model with only one (see Figure 4.6) or even without any symmetric axis. Due to the larger number of finite elements that needs to be calculated for such cases, as many symmetric axes as possible should be used.
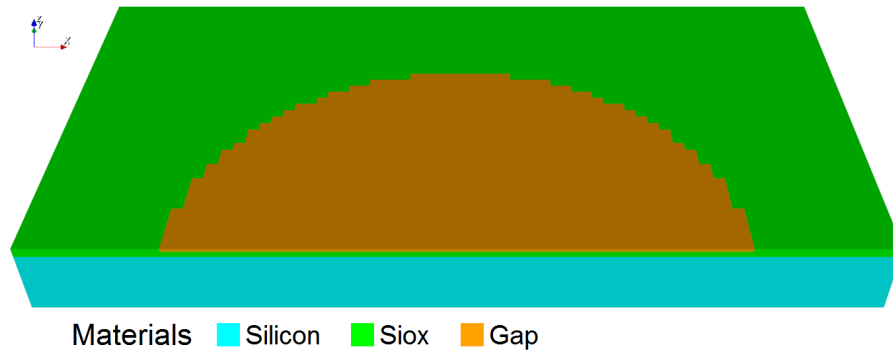
Figure 4.6: 3D model (one symmetric axis used).

In order to check the effects of the different symmetry conditions, all four models (2D, two symmetric boundaries, one symmetric boundary, full 3D model) were constructed and the results in terms of membrane displacement and generated sound pressure were compared. The CMUT design for this study is adapted from a design developed at

Fraunhofer IBMT for communication between implants [92].

All models consist of a ground wafer made out of silicon with a thickness that was reduced to 10 μm for a faster simulation. To better match with the much thicker ground wafers used in fabrication, the bottom surface of this layer is fixed artificially. On top of it, a silicon oxide layer with a thickness of 1 μm is used for insulation and as material beside the cavity. The height of the cavity is 500 nm and the diameter is 80 μm.
The whole model, as it can be seen in Figure 4.5, is covered with a 2 μm silicon layer representing the membrane. The surrounding area is filled with water (10 μm). Time for calculation ('runtime') and number of elements for the four different models can be found in Table 4.1.

Table 4.1: Specifications of the simulation models used for testing different boundary conditions.

Model	runtime	elements	total elements
2D model	6 min	$39 \times 1 \times 21$	819
2 symmetric boundaries	777 min	$39 \times 39 \times 21$	31,941
1 symmetric boundary	1.197 min	$77 \times 39 \times 21$	63,063
Full 3D model	1.213 min	$77 \times 77 \times 21$	124,509

While the number of elements in Table 4.1 is reproducible, the runtime in minutes varies depending on the computer used and on other software running on it at the same time. This is one reason why the full 3D model only needs slightly more time than the one with one symmetric boundary.
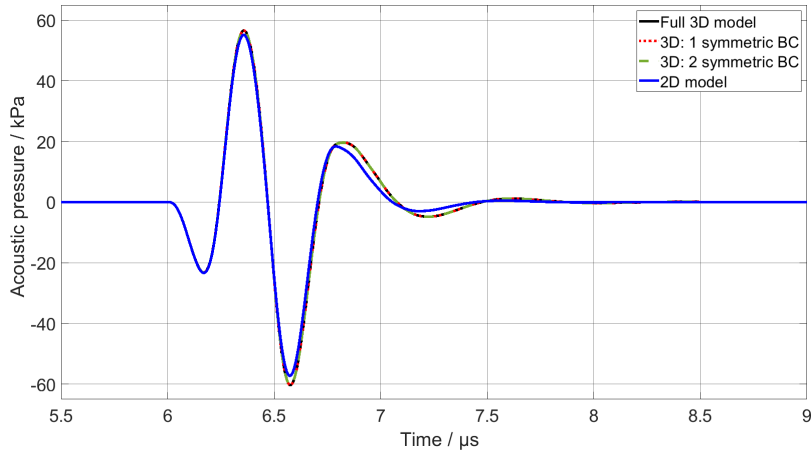
Figure 4.7: Acoustic pressure in 7 μm depth, bias: 97.5 V, ac signal: 2 MHz Blackman-Harris pulse with an amplitude of 32.5 V.

Having a look at Figure 4.7, the resulting acoustic pressure signal for applying a bias voltage of $V_{DC} = 97.5\,\mathrm{V}$ and a $32.5\,\mathrm{V}$-Blackman-Harris pulse at $2\,\mathrm{MHz}$ looks completely identically for all 3D models but slightly different for the 2D model. Concerning the membrane displacement, the differences between 2D and 3D models become a bit larger (see Figure 4.8). The main difference is the bigger static displacement of the membrane

Table 4.2: Results for the test of symmetric BCs.

Model	pressure amplitude	membrane displacement
2D model	$112.3894\,\mathrm{kPa}$	$25.6321\,\mathrm{nm}$
2 symmetric boundaries	$116.9114\,\mathrm{kPa}$	$26.2842\,\mathrm{nm}$
1 symmetric boundary	$116.9110\,\mathrm{kPa}$	$26.2841\,\mathrm{nm}$
Full 3D model	$116.9130\,\mathrm{kPa}$	$26.2834\,\mathrm{nm}$
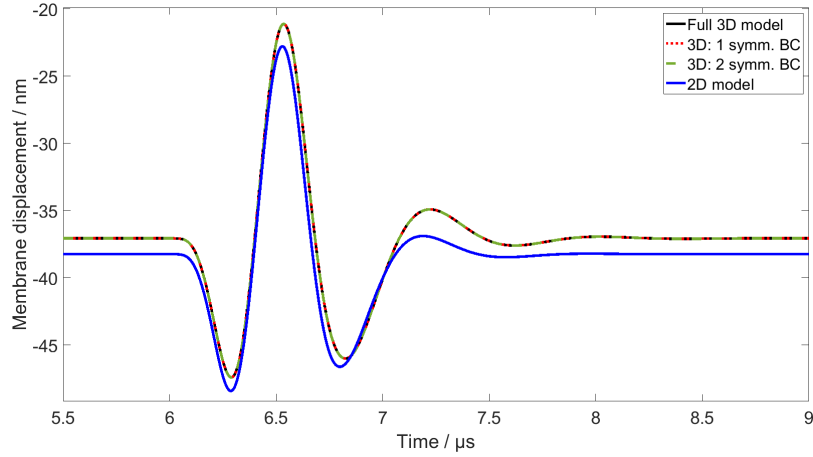
Figure 4.8: Membrane displacement for different symmetric BCs, bias: $97.5\,\mathrm{V}$, ac signal: $2\,\mathrm{MHz}$ Blackman-Harris pulse with an amplitude of $32.5\,\mathrm{V}$.

in the 2D model. The differences concerning the amplitude of membrane displacement and acoustic pressure wave generated can be found in Table 4.2.

The differences between the full 3D model and a 3D model exploiting two symmetric boundaries are very small concerning the resulting generated pressure ($\approx 0.001\%$) and membrane displacement ($\approx 0.003\%$). Differences only occur from the third decimal place. Since the deviations to be expected between the simulated results and the reality are significantly larger, for example due to deviating material parameters or tolerances in fabrication, the differences caused by using two symmetric boundary conditions can be neglected. As the number of finite elements that need to be calculated goes down by a factor of ≈ 3.9 while the runtime is reduced by $\approx \frac{1}{3}$, the following simulations for this thesis make use of two symmetric boundaries.

4.2 Basic 3D FEM Model

An essential step in FEM simulation is the verification of the simulated results by experimental data. To enable such verification, CMUT chips (design 'LA5') were provided by microfab Service GmbH (Bremen, Germany). The simulation model was adapted to this design. The cell design of these CMUT chips consists of a rectangular membrane made of Si$_3$N$_4$ (thickness 650 nm) with an overlying top electrode made of aluminum (thickness: 450 nm). The edge lengths of the evacuated cavity (height 250 nm) are 33 µm × 28 µm. The dimensions of the aluminum electrode are 23 µm × 20 µm. Following several optimization steps of the model and the subsequent successful verification of the same, this was used as a starting point to develop a custom CMUT design (named 'R2') according to the specifications established for the intended application. The parameters for the old and the new design are listed in Table 4.3.

Table 4.3: Dimensions of both CMUT designs.

Parameter	LA5	R2
Cavity length along x	33 µm	80 µm
Cavity length along y	28 µm	40 µm
Cavity height	300 nm	200 nm
Membrane thickness	650 nm	600 nm
Electrode length along x	23 µm	56 µm
Electrode length along y	20 µm	28 µm
Electrode thickness	450 nm	250 nm

The basic layer structure was left unchanged and is as follows for both designs:
The CMUTs used within this thesis rest on a 400 µm thick ground wafer. This layer is intended to ensure that the excited oscillation is conducted completely through the membrane while the ground electrode does not resonate but remains rigid. In comparison to the other layer thicknesses, this layer is very thick and is correspondingly structured by a large number of finite elements in the simulation model. To save computing time, its thickness was reduced to 4 µm in the simulation model.
The resulting reduced stiffness of the CMUT bottom side is compensated by a boundary condition that keeps the elements on the bottom side of the model fixed.

For manufacturing reasons (e.g. layer stresses) a silicon oxide layer ($t_{Siox} = 1.05$ µm), a silicon nitride layer ($t_{SiN} = 600$ nm) and a silicon layer ($t_{Si} = 550$ nm) are deposited on the ground wafer. This silicon layer is used as ground electrode. To prevent short circuits in case of contact of the membrane with the bottom of the cavity, the Si layer is coated with a 50 nm thin layer of silicon nitride. This insulating layer is 80% thinner than the aluminum top electrode (250 nm), the second thinnest layer. Therefore, it has a considerable influence on the meshing and the time step of the FEM model. Comparative simulations have shown that this Si$_3$N$_4$-layer has no significant influence on the

results from simulation. Therefore, it was decided not to include this layer in the FEM model, which increases the maximum possible time step from about 1 ps to approx. 9 ps. As a consequence, the required computing time decreases by a factor of 9.

The next layer is structured silicon nitride ($t_{gap} = 200$ nm), which forms the edge of the evacuated cavity. This is followed by another layer of silicon nitride ($t_{mem} = 650$ nm), forming the membrane of the CMUT together with the overlying aluminum electrode ($t_{alum} = 450$ nm). This top electrode is also rectangular. An image of the final FEM model is shown in Figure 4.9.
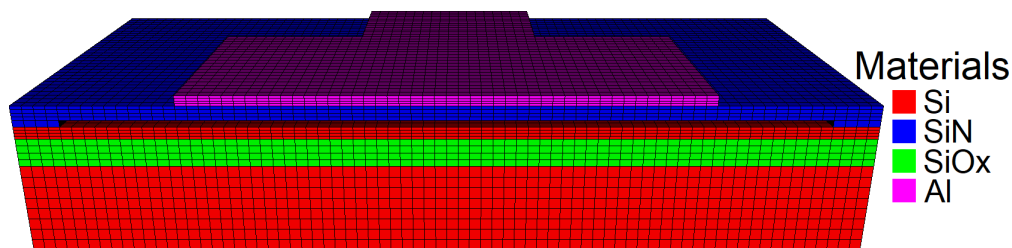
Figure 4.9: Final FEM model, design LA5.

Here and in Table 4.3, it can be seen that the edge lengths of the top electrode are smaller than the edge lengths of the cavity and thus of the membrane.

This has several advantages. Bozkurt *et al.* state that by reducing the electrode size to 40-50% of the membrane size, the bandwidth in immersion could be increased by 100% for a round cell compared to a full-size electrode [24]. In addition, an optimized top electrode size reduces parasitic capacitances and increases transduction efficiency [93]. The electrode size needs to be optimized for each cell design.

4.2.1 Verification

The FEM model for the LA5 design was verified with measurements and optimized in particular with regard to meshing in order to precisely predict the behavior of the CMUT. For this purpose, vibrometry measurements and analyses of the impedance response were acquired in air and compared with the simulation results.

Vibrometry-Measurements

Using a Polytec (Waldbronn, Germany) UHF-120 vibrometry system, the oscillation characteristics of several CMUT cells of design LA5 were investigated. Fast Fourier transform (FFT) scans were performed for a bias voltage of 40 V and an excitation with a single sinusoidal cycle at 13 MHz with an amplitude of 15 V. The results from three cells at different positions on the chip is shown in Figure 4.10. The CMUT design has a very narrow bandwidth in air and has an average resonant frequency at 11.7 MHz. The standard deviation is 0.1 MHz. The result of this simulation is shown in Figure 4.10 as a

black curve on the right Y-axis. The simulation model results in a resonance frequency of 11.8 MHz, which is within the range of variation between different cells on the CMUT chip.
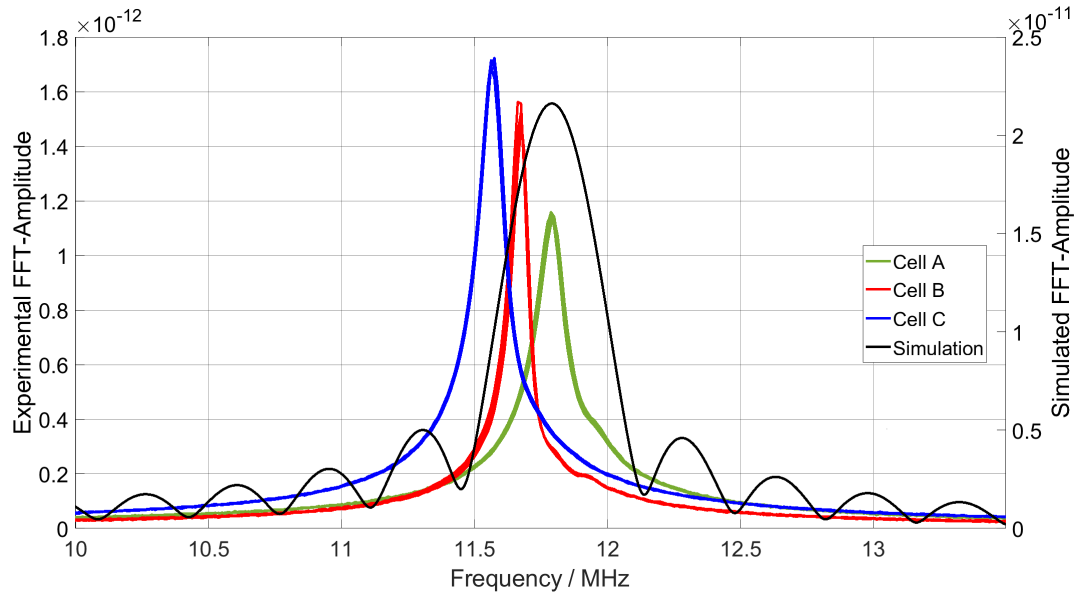
Figure 4.10: Vibrometry FFT-scan, $40\,\mathrm{V_{DC}}$, $15\,\mathrm{V_{AC}}$, excitation pulse at $13\,\mathrm{MHz}$.

In addition to the main maximum at 11.8 MHz, the simulated curve exhibits many small maxima in the frequency range shown. These are numerical artefacts resulting from the input signal for the FFT, the displacement of the center of the membrane, not having decayed to zero, which causes a discontinuity. It is noticeable that a significantly larger amplitude is achieved in the simulation than in the measurement (approx. by a factor of 13). This is partly due to the fact that the displacement was calculated exactly in the center of the membrane in the simulation, whereas this is not guaranteed with the vibrometer setup used. In addition, deviations are to be expected due to manufacturing tolerances, differing material parameters between the real and the simulated CMUT, release stresses in the layers as a result of the fabrication, and mainly charging effects. In the latter case, charge carriers accumulate in the insulating layer between the two electrodes, generating a counter-field to the applied bias voltage and thus reducing the effective applied bias voltage. The occurrence of such charging effects is described in more detail for the customized CMUT design *R2* in Section 5.2.2.

Impedance-Measurements

Using an impedance analyzer E4990A from Keysight (Santa Rosa, USA), the impedance response of the chip with the LA5 cell design was recorded for bias voltages between $0\,\mathrm{V}$

and 40 V (maximum voltage available). Unlike the previous vibrometer measurements, the behavior of an entire chip with 1200 parallel-driven CMUT cells is measured here instead of individual cells. Figure 4.11 and Figure 4.12 show the average values of magnitude and phase for experiment and simulation at 40 V bias. The magnitude minimum is at 11.6 MHz in both cases. The differences in the shape and magnitude of the curves are mainly due to the fact that the simulation describes the behavior of a single cell, while the experiment represents the parallel connection of 1200 cells.
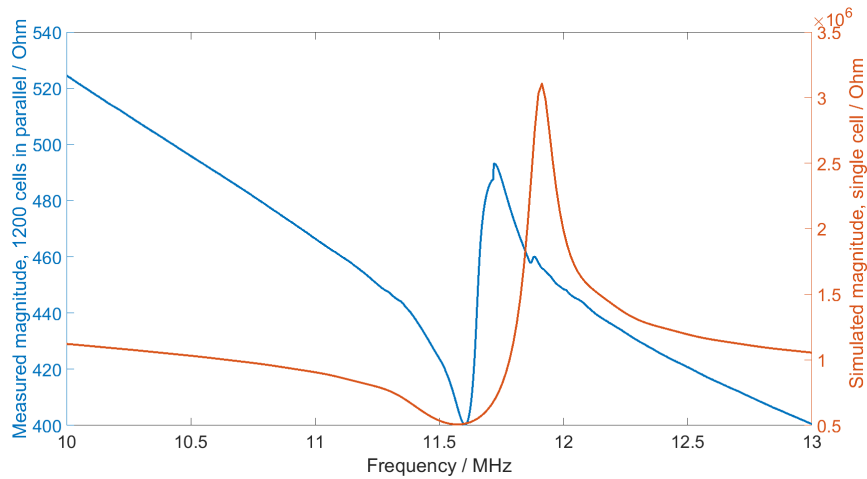
Figure 4.11: Magnitude of the impedance spectrum, measured vs. simulated.
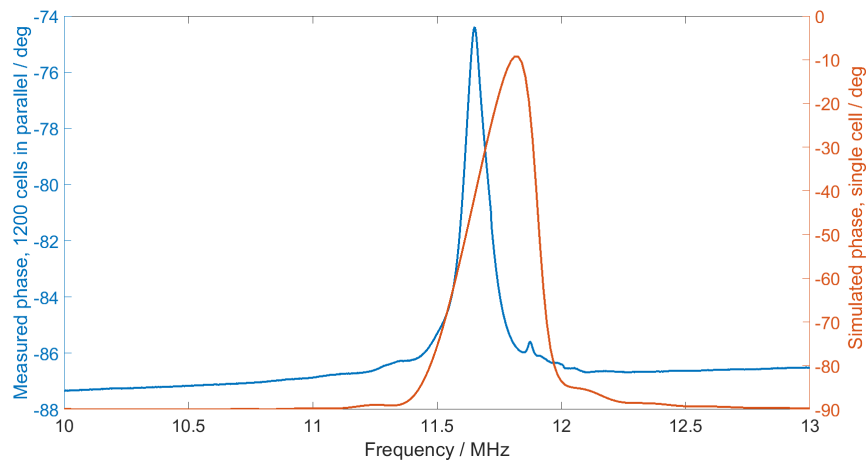
Figure 4.12: Phase of the impedance spectrum, measured vs. simulated.

4.2.2 Limits and capabilities of the model

The experiments with vibrometer and impedance analyzer have shown that the FEM model is a suitable tool for predicting the behavior of the CMUT geometry studied. Notably on the investigated parameters, resonance characteristics of the membrane displacement and impedance response, the exploitation of two symmetry axes and the omission of the $50\,\mu m$ Si_3N_4 layer on the bottom of the cavity have no significant influence. The model is therefore considered to be a good starting point for the preparation of a custom cell design, which was developed in this thesis using appropriate specifications (see Section 5.1.1).

4.3 CMUT characterization

After designing and fabricating CMUTs, a proper characterization and evaluation is crucial. For this work, three different methods were used for characterization, which are introduced in this section.

4.3.1 Laser Doppler vibrometer

An effective way for examining the vibration behavior of oscillating components in general and CMUTs in particular are laser Doppler vibrometers (LDVs). This method measures the velocity of the membrane, which can then be converted into its displacement. Laser Doppler vibrometry is based on the Doppler effect, a change of the frequency of a wave depending on the relative velocity between source and observer of the wave [1]. This frequency shift is:

$$\Delta f = \frac{2v}{\lambda}$$

Here, v is the velocity of the membrane and λ is the wavelength of the laser beam used. The setup of a laser Doppler vibrometry system is presented in Figure 4.13. The laser beam is split up (Beamsplitter 1, BS1) into a measurement beam pointing on the membrane of the CMUT and a reference beam. The measurement beam passes BS2 and is focused on the surface of the membrane. The reflected beam is deflected by BS2 and via BS4 interfered with the reference beam on the detector. As the optical path of the reference beam remains constant while the optical path of the measurement beam changes over time due to the vibrating object, an interference pattern is generated on the detector. The modulation frequency of this pattern is measured and can directly be converted into the velocity of the membrane. As the modulation frequency is independent of whether the membrane moves towards or away from the laser beam, an additional step is required to determine the direction of the movement. This step is a modulation of the reference beam. The reference beam passes a Bragg cell, shifting its frequency by typically $40\,MHz$.
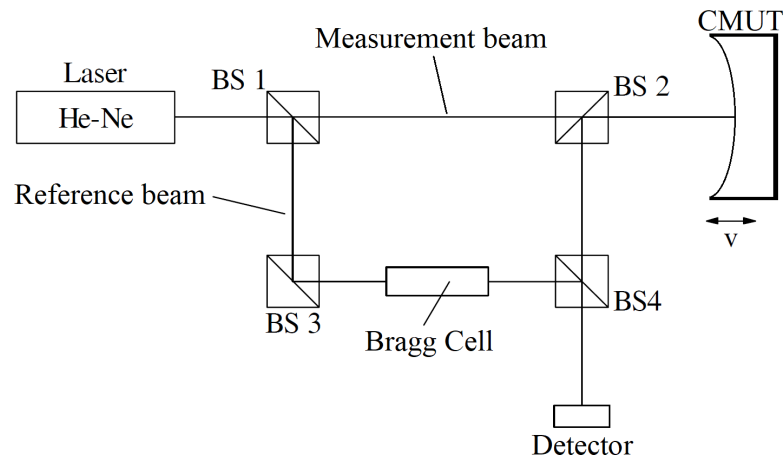
Figure 4.13: Principle of laser Doppler vibrometry, adapted from [1].

This results in a modulation frequency of less than 40 MHz when the membrane moves towards the laser beam and one of more than 40 MHz when it moves away from it. The modulation frequency is finally converted into the displacement of the membrane. Laser Doppler vibrometry provides the measurement data of a single point by default. To observe the vibration behavior of a CMUT membrane, a large number of such measurement points is distributed over the membrane surface (see Figure 4.14).
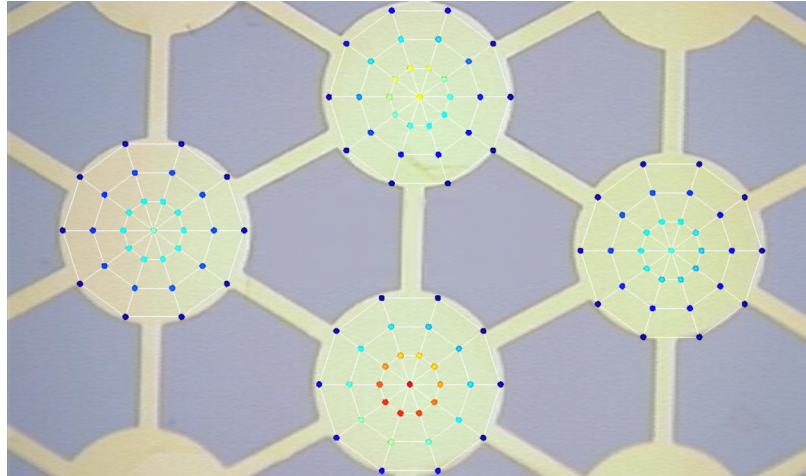
Figure 4.14: Exemplary representation of the measuring point distribution on CMUT membranes.

By examining the vibration behavior of a CMUT membrane for different bias voltages, it is possible to detect the pull-in voltage, at which the center of the membrane touches the ground. At this voltage, the maximum displacement of all examined points along the

membrane is no longer in the center of the membrane but in the outer area. While the steady state behavior of the CMUT is examined by applying continuous wave signals, the frequency behavior can be examined by applying a short pulse.

If the damping of the membrane is low enough, the CMUT membrane continues to oscillate after the end of the excitation signal. In this post oscillation interval, the CMUT always falls into its eigenfrequency or resonance frequency. Alternatively, an FFT scan can be performed. Here, the received signal is Fourier transformed and the resulting frequency spectrum is evaluated. Since even when using a short and therefore broadband excitation pulse, the proportions of the frequencies in the excitation spectrum differ significantly, it is necessary to compensate the received spectrum by the excitation spectrum for correct evaluation. Additionally, the FFT scan should be done at an excitation frequency in the order of the expected resonance frequency of the CMUT to ensure that the frequency range of interest is appropriately excited. A Polytech UHF-120 (Waldbronn, Germany) was available at Fraunhofer IBMT for such measurements.

4.3.2 Impedance analyzer

Another important and fast method for the characterization of CMUTs is impedance spectroscopy. While scanning many points of a CMUT membrane with a LDV takes at least 30 min, the impedance spectrum can be analyzed within a minute. For the determination of the impedance spectrum, a Keysight E4990A impedance analyzer (Santa Rosa, USA) was used in this work.

The electrical impedance is 'defined as the total opposition a device or circuit offers to the flow of an alternating current (AC) at a given frequency' ([94], p. 1-01). Electrical impedance is a complex value, consisting of real and imaginary part (resistance and reactance) or magnitude and phase angle. The Keysight impedance analyzer E4990A directly measures real and imaginary parts of the impedance vector and calculates all desired parameters from this measurement.

CMUTs are capacitive transducers and therefore show similar impedance characteristics as capacitors. The impedance (Z) of a capacitor can be calculated depending on frequency f and capacitance C as

$$Z = \frac{1}{2\pi f C} \tag{4.1}$$

Accordingly, impedance is bigger for lower frequencies. As CMUTs are more complex devices than pure capacitors, some local minima and maxima occur in the spectrum in addition to the global (capacitor-like) impedance spectrum. As the minima in magnitude occur for resonant excitation, an impedance measurement for different frequencies provides an information about the resonance frequencies of the CMUT.

The impedance analyzer used provides bias voltages of up to 40 V. The resonance frequency of a CMUT changes for different bias voltages due to the spring softening effect (cf. Section 2.2.2). This makes it necessary to also save the bias voltage when performing impedance measurements. As long as the CMUT is in conventional mode and as long as

the membrane is not in contact with the ground, a higher bias voltage leads to a larger bending of the membrane, causing a smaller effective cavity height. For a smaller cavity, the vibration of the membrane is bigger for the same AC voltage signal. As a result, the resonances in the impedance spectrum become more apparent the higher the applied bias voltage is (as long as the membrane does not collapse). Therefore, the bias voltage for impedance measurements should be close to the bias voltage used for later operation of the CMUT. The impedance measurements within this project were therefore performed using the maximum bias voltage available (40 V) as the CMUTs used are planned to be driven with 60 V in later applications.

4.3.3 nanofocus μsurf

A nanofocus μsurf system (Oberhausen, Germany) was used to evaluate the surface profile of the encapsulated CMUT chips. The system is based on confocal microscopy [95].
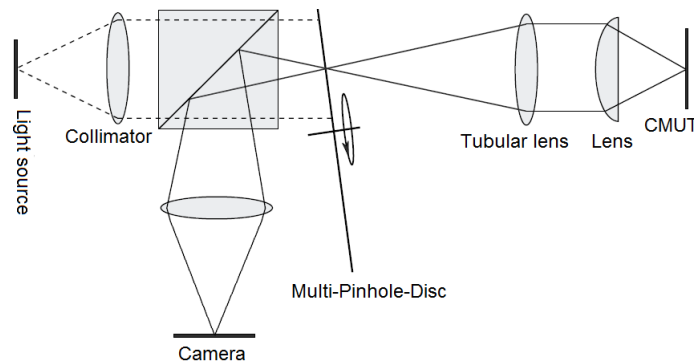
Figure 4.15: Operating principle of confocal microscope nanofocus μsurf [96]

A LED light source is focused through a multi-pinhole disc and an objective lens on the surface to be examined. The part of the reflected light that is in focus is recorded with a camera, the remaining light is blocked by the multi-pinhole disc. By moving the objective lens and repeating the measurement 200 to 400 times in different depths, a 3D height image can be calculated.

4.3.4 Transmit-Receive experiments

In many applications, ultrasonic transducers, such as CMUTs, are used for both, transmitting and receiving ultrasonic waves. While the measurements on the impedance analyzer only provide information about the electrical properties of the CMUT, the laser vibrometer can only measure the vibration behavior during transmission. To determine the transmitting and receiving characteristics of the fabricated CMUTs, transmit-receive experiments were performed. These were made in two different liquids, Fluorinert FC-72 and water.

Fluorinert FC-72

The CMUT design presented in Section 4.2 includes an exposed top-electrode. This makes it impossible to do immersion experiments with the uncoated CMUTs in water, as it would produce short circuits. Tests in distilled water have shown that the conductivity in distilled water is still too high. Consequently, a more insulating liquid was needed for the immersion experiments of the uncoated CMUT chips. It has been shown that Fluorinert FC-72 (*3M*, St. Paul, USA) meets this requirement. Fluorinert FC-72 (C_6F_{14}) is a non-conductive liquid used for electronic testing. The liquid is colorless and evaporates without residue within seconds. The density of Fluorinert FC-72 is specified as $\rho = 1680\,\mathrm{kg/m^3}$ [97]. Boiling point @ 1 atm is 56 °C, electrical resistivity (ASTM D-257) is specified as $1.0 \times 10^{15}\,\Omega\,\mathrm{cm}$. The sound velocity was determined to be $\mathrm{v}_l = 512\,\mathrm{m/s}$.

Hydrophone

To determine the acoustic pressure generated by a CMUT at a certain location in the sound field for a given excitation signal, the use of a calibrated transducer as receiver is necessary. In this work, a piezoelectric polyvinylidene fluoride (PVDF) foil hydrophone (type s, size of pressure-sensitive area: 1 mm) from *RP acoustics* (Leutenbach, Germany) was used for this purpose.

The hydrophone is delivered with a calibration report (Figure 4.16), which specifies the received voltage in mV for each frequency, which results from an acoustic pressure of 1 kPa. This allows a direct conversion of the received voltage into sound pressure.
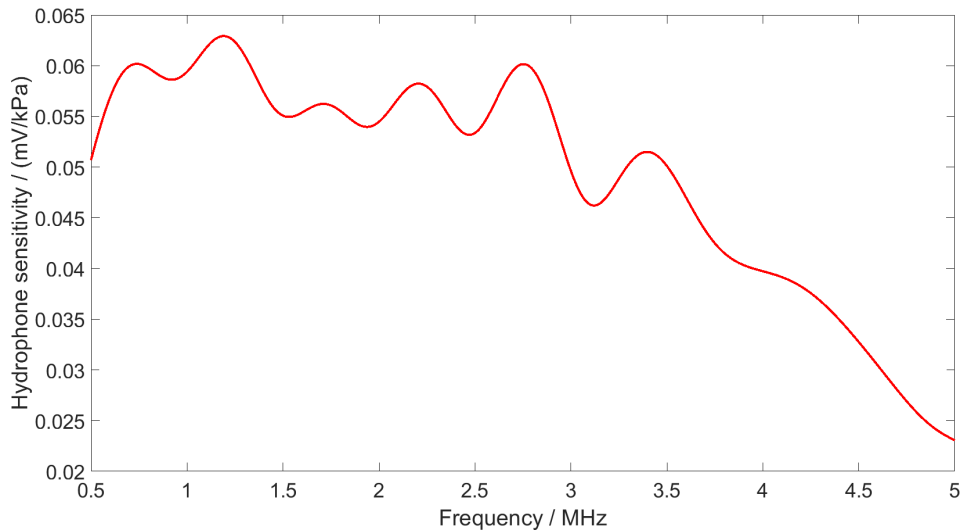
Figure 4.16: Calibration curve for hydrophone RP 52s in water.

The hydrophone is calibrated for operation in water whereas the first measurements were done in Fluorinert FC-72 (see Section 4.3.4). However, based on its mode of operation, a PVDF foil hydrophone that directly determines pressure via the piezoelectric effect, should also work properly in other liquids. To validate this statement, measurements were initially done in water and then in Fluorinert FC-72 to determine sensitivity differences. Based on the formula for acoustic pressure (Equation (4.2)), the hydrophone was thereby calibrated for use in Fluorinert FC-72.

$$p = \rho c \omega y \tag{4.2}$$

Here, p is the acoustic pressure, ρ and c are the density and the sound velocity of the medium, ω is the frequency and y is the particle displacement. For $c_{H_2O} = 1500\,\mathrm{m/s}$, $c_{\mathrm{Fluorinert}} = 512\,\mathrm{m/s}$, $\rho_{H_2O} = 1000\,\mathrm{kg/m^3}$ and $\rho_{\mathrm{Fluorinert}} = 1680\,\mathrm{kg/m^3}$ this results for the condition of equal acoustic pressure ($p_{\mathrm{Fluorinert}} = p_{H_2O}$) in both liquids in:

$$y_{\mathrm{Fluorinert}} = 1.74 y_{H_2O}$$

An identical acoustic pressure in Fluorinert and water corresponds to a particle displacement measured with the vibrometer which is larger by a factor of 1.74 in Fluorinert than in water. To calibrate the hydrophone, the displacement on the surface of the liquid was initially determined with the vibrometer for a piezoelectric transducer in a water-filled container using a signal voltage of $10\,\mathrm{V_{AC}}$. Subsequently, using the identical setup, the water was replaced by Fluorinert and the signal voltage applied to the transmitting transducer was varied in such a way that the particle displacement determined by the vibrometer on the surface of the liquid corresponds to 1.74 times the amplitude of the measurement in water. The signal voltage required for this was determined to be $9.3\,\mathrm{V_{AC}}$.

In the final step, the hydrophone was placed at the same position and the received signal was recorded for both liquids. The average of 20 measurements for the measurement in Fluorinert resulted in an amplitude of the received signal of $(2.42 \pm 0.13)\,\mathrm{mV}$ compared to $(2.26 \pm 0.11)\,\mathrm{mV}$ in water. When using the hydrophone in Fluorinert instead of in water, the measured values are therefore 7% too large. All experimental data recorded in Fluorinert are consequently reduced by 7%.

Setup of the transmission experiment

A schematic drawing of the setup used for transmit-receive experiments is shown in Figure 4.17. Two Rohde & Schwarz (Munich, Germany) DC Power Supplies NGL 35 are used to individually bias two CMUTs facing each other. Considering Section 2.1.2, the distance between the CMUTs was set to 83 mm for the measurements in Fluorinert FC-72 and 35 mm in water (unless otherwise specified).

In Figure 4.17, the transmitting CMUT is dotted, the receiving one is striped. The transmitting CMUT is additionally supplied with an AC voltage signal by a Rohde & Schwarz (Munich, Germany) AFGU function generator.
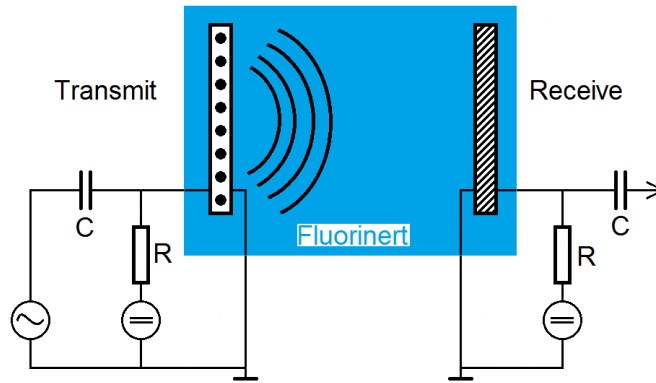
Figure 4.17: Schematic setup for transmit-receive experiments.

The signal at the receiving CMUT is displayed and stored via a Keysight (Santa Rosa, USA) DSOX4024A oscilloscope. To protect the function generator and the oscilloscope from the high DC voltage, a coupling capacitor (C=150 nF) is connected in series to each instrument. Similarly, the DC voltage sources are each protected from the AC voltage by a high-impedance resistor (100 kΩ). All measurements were performed without any additional signal amplifiers. To improve the SNR, a 16-fold averaging was applied.

4.4 Encapsulation

The aim of this work is to create a better understanding of the behavior of CMUTs behind relatively thick coatings or encapsulations (compared to the thickness of the CMUT-membrane). The investigated coatings have a total thickness in the order of tens of micrometers, whereas the membrane thickness is in the range of several hundred nanometers. The encapsulation approach investigated here aims to integrate CMUT chips into conventional housings of medical implants, which are usually made of titanium or PEEK (see Section 3.5). In order to increase the sensitivity of the CMUT in both, receive and transmit mode, the wall thickness of the implant in the area to be transmitted is reduced from a conventional 500 µm to a few tens of micrometers to form an acoustic window. A silicone layer is used for coupling the membrane with the wall of the implant housing. A schematic sketch of a CMUT chip integrated this way into an implant housing is shown in Figure 4.18.

For experimental evaluation of this encapsulation approach, CMUT chips were encapsulated with a silicone layer and an overlying foil of PEEK or titanium as follows:

First, the PEEK foil was plasma activated to ensure sufficient adhesion to the silicone. The titanium foil had a good adhesion without plasma activation, so that this step was not necessary here.
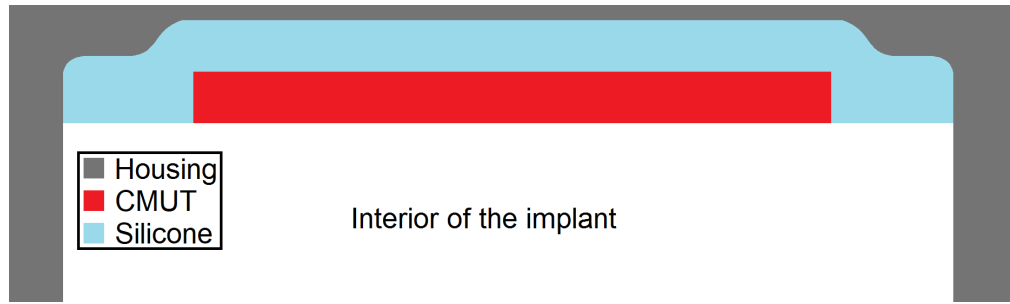
Figure 4.18: Schematic drawing of a CMUT integrated into the housing of a medical implant.

Then, the cavity of the fixture in which the CMUT chips were bonded, was filled with silicone (Wacker Elastosil E43, Munich, Germany) and the foil (made of titanium or PEEK, OSYPKA AG, Rheinfelden, Germany) was applied on top. Using a glass carrier, the excess silicone was pressed out to the sides. Finally, the setup was left aside at room temperature for 24 hours so that the silicone could cure (cf. Figure 4.19). During this curing process, the silicone shrinks, causing the foil to slightly sag downwards. The setup itself, but especially the shrinkage of the silicone, makes it difficult to precisely set the final layer thickness of the cured silicone. Due to the limited number of CMUT chips available, this meant that the layer thicknesses found to be optimal (see Section 5.4.1) in the simulation could not be realized exactly in experiment. The limited number of CMUT chips available in combination with the malfunction of some chips after encapsulation, only allowed to realize a small number of encapsulation setups.

To compare this new type of encapsulation with the literature standard, additional CMUT chips were coated with 150 µm thick silicone as well as with 5.5 µm thick parylene-C.

Figure 4.19: Schematic drawing of the experimental encapsulation setup.

5 Results

The objective of this thesis is to enable acoustic communication between medical implants using CMUTs. The essential point here is the development of encapsulation strategies for CMUTs for long-term use in the human body. The results of this study are presented in this chapter.

5.1 Development of a customized CMUT-design

5.1.1 Specifications

Prior to developing a customized CMUT design, specifications were elaborated that must be fulfilled for the planned application.

Frequency

As described in Section 2.1, the attenuation of an ultrasonic signal in the human body increases for an increasing frequency. In parallel, the signal length decreases so that more data can be transmitted in the same time. For a constant membrane thickness, the diameter of a CMUT membrane increases as the frequency decreases. Since CMUT-based ultrasonic transducers are made up of hundreds to thousands of CMUT cells operating in parallel, a lower resonance frequency does not necessarily lead to a larger transducer. Instead, there are fewer cells in the same area. For the application of acoustic communication in the human body, a target frequency of 2 MHz was found. This is a compromise between minimal attenuation (i.e. the lowest possible frequency) and minimal pulse length (the highest possible frequency). The decision to select a target frequency of 2 MHz is supported by a publication of Wang *et al.* who refer to 2 MHz as the optimal frequency for data transmission over distances of 15 cm (see Section 3.1)[48]. For a sound velocity of 1500 m/s the wavelength of a 2 MHz oscillation is 750 μm.

Bandwidth

The frequency spectrum of a signal is obtained by the FFT of its time course. A short pulse leads to a broadband frequency spectrum and a continuous sinusoidal oscillation leads to a line spectrum. So a high bandwidth of the ultrasonic transducer is given by the ability to generate short signals without any significant post-oscillation. The higher the bandwidth of a transducer, the larger the frequency range available for data transmission. Thus, a high bandwidth enables high data rates.

A $-6\,\mathrm{dB}$-bandwidth (FWHM) of 100% is accepted in signal processing as easily large enough and was therefore specified here as target for an efficient data transmission.

Electrical excitation

According to DIN VDE 0100-410, protection against direct contact with active parts under normal operating conditions is necessary if voltages of $25\,\mathrm{V_{AC}}$ or $60\,\mathrm{V_{DC}}$ are exceeded. In order to ensure safe operation, in the laboratory and in the later application, the developed CMUT design should therefore work properly with these voltages.

Transmission path

The transmission distance that must be covered depends on the medical application. Acoustic waves do not end abruptly in homogeneous media. In the far field (beyond the last local maximum on the acoustic axis), the signal decreases continuously due to attenuation. Accordingly, the transmission distance depends on the transmit and receive sensitivity of the CMUTs as well as the capability of any subsequent signal processing. For this work, a minimum value of $6\,\mathrm{cm}$ was set for the distance between the transmitter and receiver that must be transmitted acoustically. Because this is in the order of magnitude of the width or the thickness of spleen or kidney.

Customization of the CMUT design

Based on these specifications, the CMUT design presented in Section 4.2 was adapted. For this purpose, the manufacturer specified the parameter space described in Table 5.1. In addition to the basic cell design, the effects of various joints between the top-electrodes were also investigated. To drive all cells, connections between the individual top electrodes are necessary. There are three possibilities for this purpose, which were evaluated during the development of the cell design: The connecting links between the different top electrodes can be located on the long sides, on the short sides or on all four sides of the membrane.

Figure 5.1 shows the displacement of the membrane for the three investigated options if excited with a Blackman-Harris pulse of $1\,\mathrm{MHz}$, a DC voltage of $60\,\mathrm{V}$ and an AC voltage of $40\,\mathrm{V}$. As expected, the design option with electrode joints on all four sides has the smallest total displacement, since the membrane becomes stiffer. The other two variants show that electrode junctions on the long sides result in significantly greater total membrane deflections at the same voltage. As a larger deflection at the same voltage means that it is possible to work with lower voltages, positioning the electrode joints on the long sides is preferable. In addition to the amplitude of oscillation, the frequency dependence of its particle velocity, which corresponds to the generated acoustic

pressure, was also investigated.
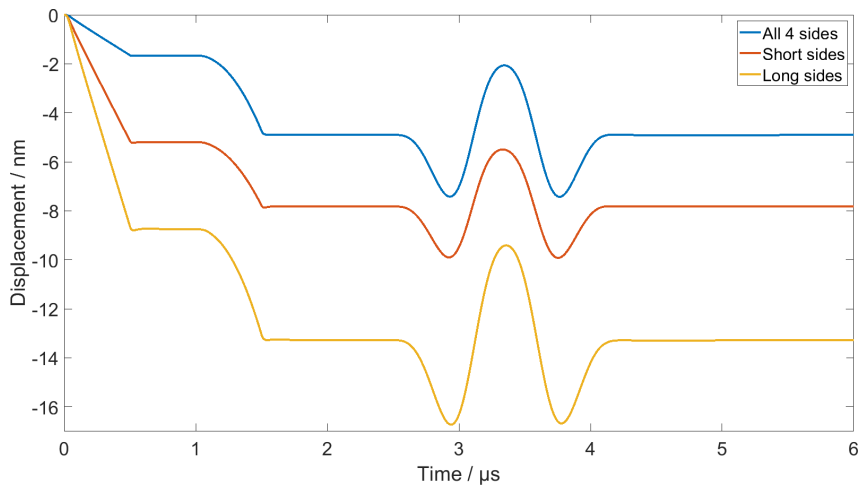
Figure 5.1: Simulation: Membrane displacement for electrode joints on different sides. Cell design LA5, excitation: $60\,\mathrm{V_{DC}}$, $40\,\mathrm{V_{AC}}$, Blackman-Harris wavelet.

For this purpose, the FFT of the time course of the velocity (Figure 5.2) was calculated for all three variants and presented in Figure 5.3. It has been shown that the position of the electrode joints has no influence on the bandwidth, which is $850\,\mathrm{kHz}$ in the investigated model. Based on the difference in oscillation amplitude, it was therefore decided to provide the electrode connections on the long sides.
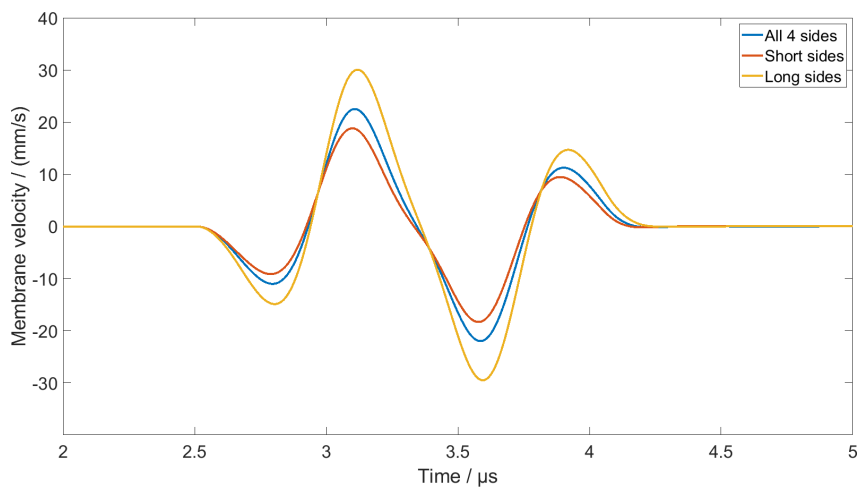
Figure 5.2: Simulation: Membrane velocity for electrode joints on different sides. Cell design LA5, excitation: $60\,\mathrm{V_{DC}}$, $40\,\mathrm{V_{AC}}$, Blackman-Harris wavelet.
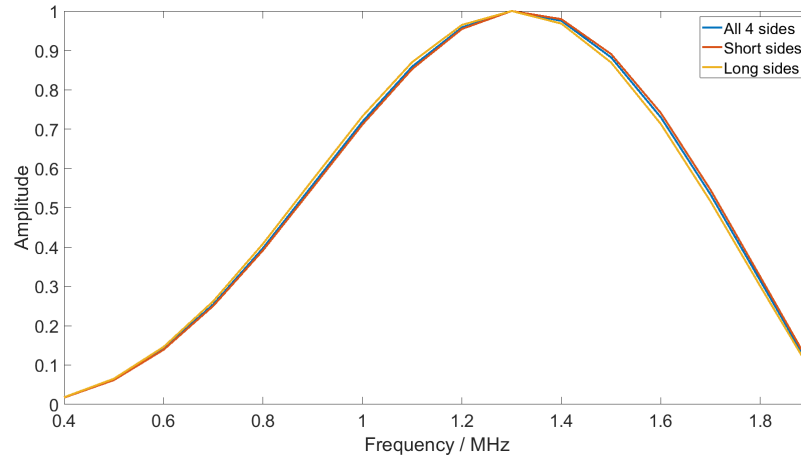
Figure 5.3: Simulation: Amplitude of FFT of membrane velocity for different electrode joint positions. Cell design LA5, excitation: $60\,V_{DC}$, $40\,V_{AC}$, Blackman-Harris wavelet.

Table 5.1: Available parameter space given by microfab Service GmbH for customized CMUT design.

Parameter	Minimum value	Maximum value
Cavity edge length	$20\,\mu m$	$400\,\mu m$
Cavity height	$200\,nm$	$500\,nm$
Thickness of Si_3N_4 membrane	$500\,nm$	$1000\,nm$
Thickness of aluminum top electrode	$250\,nm$	$1000\,nm$
Coverage by aluminum top electrode	50%	100%

Subsequently, the edge lengths and the thicknesses of membrane and top electrode, as well as the height of the cavity, were varied within the feasible parameter space (Table 5.1) to adapt the cell design to the specifications.

A successive variation of the parameters in the simulation model resulted in the following design that is shown in Figure 5.4:

- ALUMINUM TOP ELECTRODE: *Thickness:* $250\,nm$, *edge lengths:* $56\,\mu m \times 28\,\mu m$,

- Si_3N_4 MEMBRANE: *Thickness:* $600\,nm$, *edge lengths:* $80\,\mu m \times 40\,\mu m$,

- CAVITY HEIGHT: $200\,nm$.

After completing the optimization of the design of the single CMUT cell, the next step is

the design of the CMUT chip. A single cell is not able to realize the necessary pressures, so transducers based on CMUTs are composed of a large number of single cells connected in parallel. For a given cell size, the sound emitting area, the aperture of the CMUT chip, increases with each additional cell. However, a larger aperture is accompanied by a smaller opening angle of the sound field.
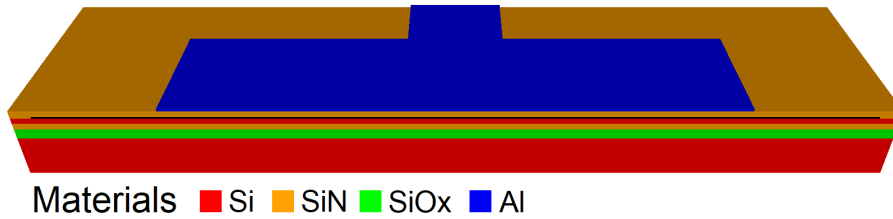
Figure 5.4: Final FEM model, design R2.

Using the software tool Scalp developed at Fraunhofer IBMT, which is based on point source synthesis, the opening angles ($-3\,$dB) for different edge lengths of square shaped chips were simulated for radiation in water at a frequency of $2\,$MHz (see Figure 5.5).
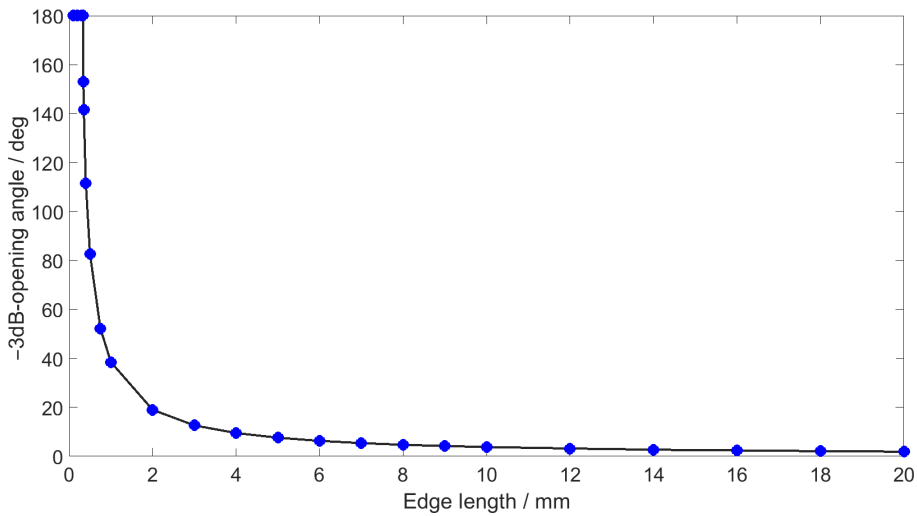
Figure 5.5: Simulation: Opening angle of a squared aperture at $2\,$MHz, v_{medium}=1500 m/s for different edge lengths of the aperture.

Because of etch channels but also to ensure a solid support of the membrane between two adjacent cavities, a minimum distance of $10\,\mu$m (between two long sides) or of $16\,\mu$m (between two short sides) separating two CMUT cells is necessary. While the edge lengths of the cavity are $80\,\mu$m $\times\,40\,\mu$m, those of the unit cell (cavity including frame) are $96\,\mu$m $\times\,50\,\mu$m.

To enable data transmission over 10 cm, larger chips were fabricated than it would have been optimal in terms of the opening angle. The realized chip size is 5 mm × 5 mm, with an area without CMUTs on the outside for better handling, so that the actual size of the sound emitting area is slightly smaller at 4.39 mm × 4.47 mm. This corresponds to opening angles of 8.64° and 8.48°.

The use of this chip size allows the opening angle to be increased at a later stage by shading the outer cells if the required sound pressures can also be achieved with less cells. For redundancy reasons, there are two contact pads each on the chip for contacting the top and the bottom electrodes. In addition, recesses are provided on two opposite sides of the chip for handling. The remaining area is filled with a total of 3416 CMUT cells. A microscopic image as well as a photography of the CMUT chip are presented in Figure 5.6 and Figure 5.7.
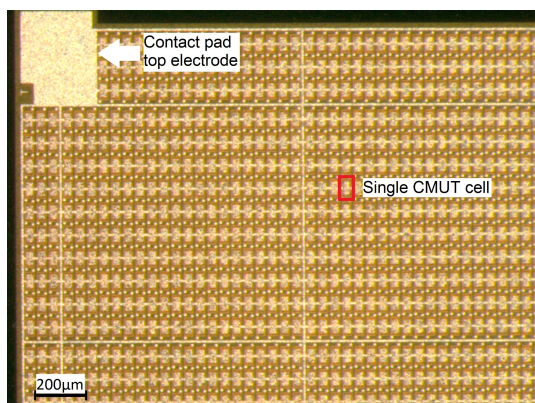
Figure 5.6: Microscopic image of the CMUT chip.
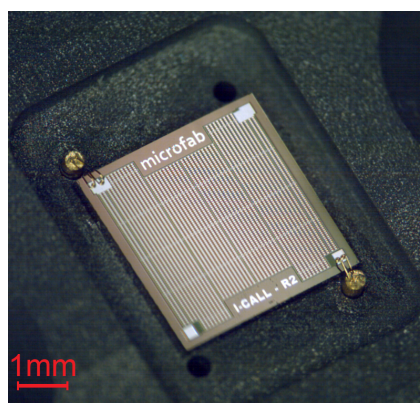
Figure 5.7: Macroscopic image of the CMUT chip.

5.2 Experimental characterization

After fabrication, the CMUT chips were attached into polyurethane frames and contacted by wire bonding. The design of the polyurethane frame is shown in Figure 5.8. The edge lengths are 15 mm × 27 mm. Two holes are provided on the outside for fixation to the experimental setup by screws. The CMUT chip is glued into a recess of 550 µm depth with edge lengths of 11 mm × 7 mm. This recess is in the center of the frame. Wire-bonded gold wires for contacting the chip can be led through four holes directly next to the corners of the CMUT chip to the back of the carrier, where slots enable the contacting wires to be led out to the side.
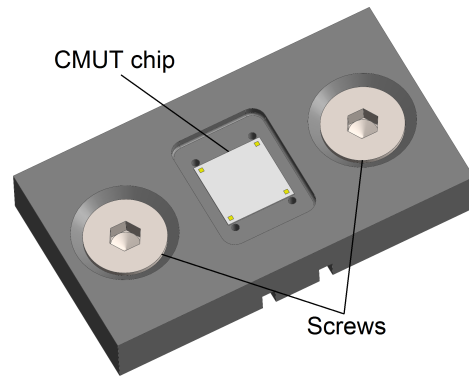
Figure 5.8: Polyurethane frame for handling the CMUT chips. $5\,mm \times 5\,mm$ CMUT chip in light gray, screws for fixation in medium gray, carrier in dark gray.

5.2.1 Laser Doppler vibrometry in air

To characterize the oscillation behavior of the fabricated CMUTs, measurements in air were performed using a laser Doppler vibrometer, UHF-120 from Polytec GmbH (Waldbronn, Germany).

The cell design of the CMUTs is customized for a center frequency of 2 MHz for operation in water. According to Section 2.2.2, the resonance frequency in air is expected to be higher than in water because of less damping. Also, the additional load on the CMUT caused by the water results in a wider bandwidth. To verify the simulation model with the vibrometry measurements, it was adapted and executed using air instead of water as propagation medium.

In the experiment, with a bias voltage of 60 V and a signal voltage of 10 V at a frequency of 10 MHz (single sinusoidal cycle), three different resonance frequencies occur for three cells at different positions on the chip (cf. Figure 5.9). Cell 1 shows its main resonance at about 9.6 MHz, cell 2 at 14.2 MHz and cell 3 at 9.4 MHz. The resonance frequencies of the examined cells on the same chip consequently vary between 9.4 MHz and 14.2 MHz. A reason for this is to be found in manufacturing tolerances.

Microfab Service GmbH (Bremen, Germany) specifies for example the thickness of the Si_3N_4 membrane as 600 nm $\pm$ 10 nm. The thickness error of the TEOS layer, which defines the cavity, is 10%. In addition to tolerances in the dimensions of the individual layers that make up the CMUT, layer stresses that occur during the deposition of the various layers play a crucial role. The combination of these factors leads to an increase in the variance between different cells on a chip and to a change in the resonance frequency. The simulation results in a resonance frequency of 8.51 MHz for a bias voltage of $60\,V_{DC}$ and a signal voltage of $10\,V_{AC}$ (see Figure 5.9). Thus, the simulation model slightly underestimates the resonance frequency in air. Differences between simulation and reality are due to the fact that neither layer stresses nor manufacturing tolerances were taken into account in the simulation.
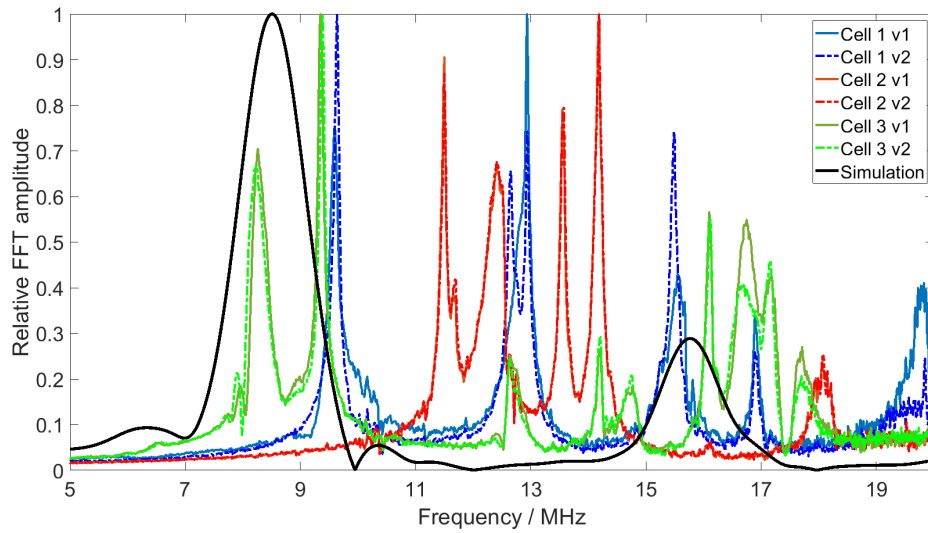
Figure 5.9: FFT-scan of three different CMUT cells on the same chip using a laser Doppler vibrometer. Bias voltage: $60\,\mathrm{V_{DC}}$, signal: Single sinusoidal cycle, $10\,\mathrm{V_{AC}}$, $10\,\mathrm{MHz}$.

In Figure 5.9, several resonances can be found for each cell. This is a result of different vibration modes of the membrane. As an example, the oscillation behavior of a single CMUT cell is examined in more detail. The frequency spectrum recorded by the laser Doppler vibrometer is shown in Figure 5.10.
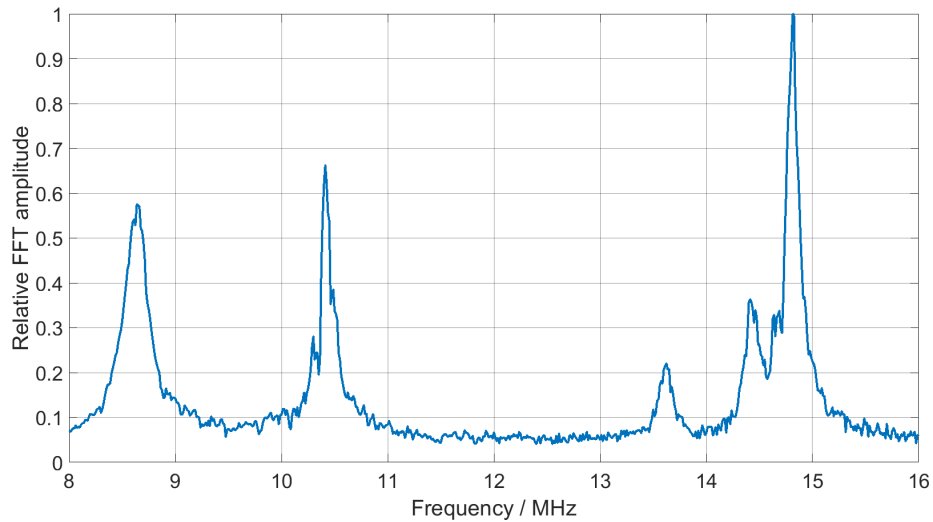
Figure 5.10: FFT-Scan of a single CMUT cell using a laser Doppler vibrometer. Bias voltage: $60\,\mathrm{V_{DC}}$, signal: Single sinusoidal cycle, $10\,\mathrm{V_{AC}}$, $10\,\mathrm{MHz}$.

The frequency spectrum shows characteristic peaks at 8.65 MHz, 10.41 MHz, 13.6 MHz, and 14.81 MHz. Consequently, the mode of vibration was analyzed for each of these frequencies.
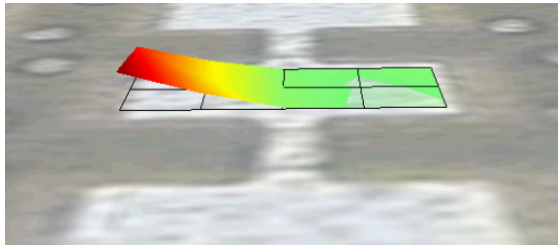
Figure 5.11: Vibration at f = 8.65 MHz.
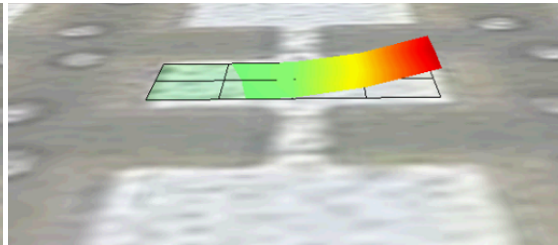
Figure 5.12: Vibration at f = 10.41 MHz
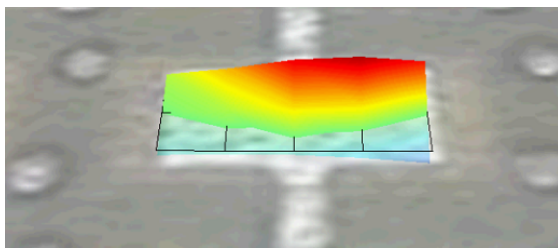
Figure 5.13: Vibration at f = 13.60 MHz.
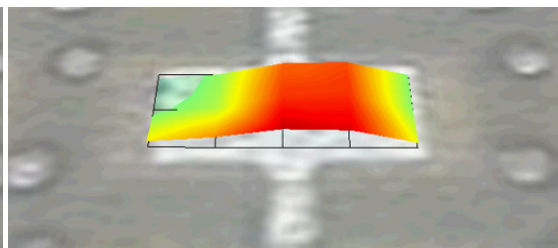
Figure 5.14: Vibration at f = 14.81 MHz.

Figures 5.11 to 5.14 show the displacement profile of a single CMUT membrane for the four resonance frequencies found. As these displacement profiles result from an FFT-scan, where the CMUT is excited with a single sinusoidal cycle at 10 MHz, the magnitudes of the displacement profiles are not accurate which is why the color scale is intentionally excluded. However, a red color corresponds to large displacements while a green color corresponds to negligible displacements of the membrane.

It can be seen that only the left half of the membrane oscillates at a frequency of 8.65 MHz (Figure 5.11) while the right half remains in its idle state. The maximum displacement is found at the left edge of the membrane. For a frequency of 10.41 MHz, the situation is mirror inverted (Figure 5.12). Now the left half of the membrane remains in its idle state while the right half oscillates.

A different mode of vibration is found for a frequency of 13.6 MHz (Figure 5.13). Here, the membrane is segmented along the longitudinal axis. Its upper half is oscillating upwards and downwards while the lower half remains in rest position. Finally, the CMUT membrane shows a typical membrane displacement at a frequency of 14.81 MHz (Figure 5.14). The left and the right edge of the membrane remain in rest position, the remaining membrane is deflected with a maximum displacement at the center of the

membrane.

Due to manufacturing tolerances and layer stresses, these modes of vibration can be found at different frequencies for the other membranes of the CMUT. This results in a frequency spectrum of the whole CMUT chip with resonance peaks at many different frequencies.

5.2.2 Transmit experiments - dielectric charging

When a DC voltage is applied, a strong electric field is formed between the two electrodes. In long time applications, this causes charge carriers to be trapped in the insulating layers which are located between the two electrodes to prevent a short circuit in the case of a collapse of the membrane [98]. These charge carriers generate an opposing field to the applied bias voltage, so that the DC voltage effectively applied is reduced. This effect increases with a higher bias voltage. It can be reduced by optimizing the deposition process of the insulation layers or could be used for pre-charging the CMUTs so that they can operate without DC voltage [99].
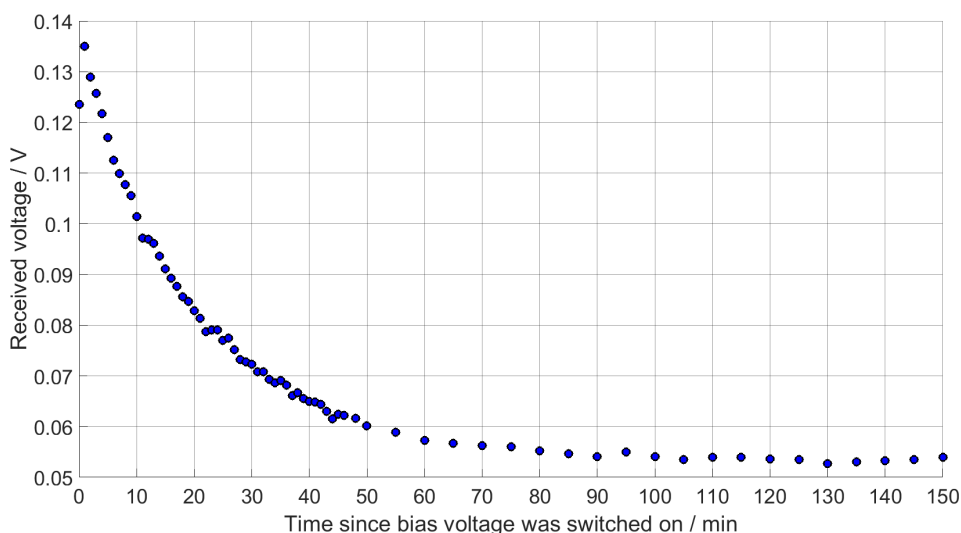
Figure 5.15: Received voltage amplitude within 150 minutes after switching on the bias voltage. $60\,\mathrm{V_{DC}}$, $15\,\mathrm{V_{AC}}$, $5\,\mathrm{MHz}$, Fluorinert FC-72, $35\,\mathrm{mm}$ distance.

In this work, frequency spectra were recorded for both the measurements in Fluorinert FC-72 and in water by manually sweeping the excitation frequency from $500\,\mathrm{kHz}$ to $5\,\mathrm{MHz}$ and determining the received signal amplitude for each frequency. Since such a measurement cycle takes between $20\,\mathrm{min}$ and $45\,\mathrm{min}$, depending on the size of the frequency step used, it was necessary to check first whether there was also a significant charge effect in the CMUTs that could superimpose the measurement result.

For this purpose, two CMUTs were mounted opposite each other at a distance of 35 mm. The setup was immersed in Fluorinert FC-72 and a bias voltage of 60 V was applied at the beginning of the measurement. In addition, an AC signal of 15 V was continuously applied (10 sinusoidal cycles at 5 MHz). Figure 5.15 shows the amplitude of the received signal for the first 150 min starting from switching on the bias voltage. It can be seen that the CMUTs exhibit strong charging behavior. The amplitude of the received signal decreases exponentially to 40% of the initial value within the first 150 min after switching on the bias voltage.

Without taking this effect into account, the actual measurements would measure only 61% after 20 min and only 46% after 45 min of the signal amplitude that is present immediately after the bias voltage is switched on. The measurements started at the lowest frequency (500 kHz) and ended at the highest frequency (5 MHz). Thus, the high frequencies would yield significantly lower values. To prevent such a distortion of the frequency spectra, each CMUT chip was biased with 60 V for at least 60 min before starting a measurement. Test measurements with start at 5 MHz and end at 500 kHz have confirmed that thereby the order or the time of the measurement of a certain frequency have no more any influence on the result. The charging of the insulation layers leads to the fact that the transmitted sound pressures are about 60% lower than the maximum possible values with the selected setup.

5.2.3 Transmit experiment in Fluorinert FC-72

Before encapsulation, the CMUT chips cannot operate in water due to the exposed aluminum top electrode, as this would lead to short circuits. Tests with distilled water showed that the conductivity of this medium is still too high to prevent a short circuit. Fluorinert FC-72 was therefore used (see also Section 4.3.4). Using the hydrophone (RP acoustics, type s) calibrated for operation in Fluorinert (see Section 4.3.4), the acoustic pressure was recorded at a distance of 83 mm in front of the CMUT, with $60\,V_{DC}$ and $10\,V_{AC}$. 20 sinusoidal cycles were used as excitation signal with a frequency varied in 25 kHz steps from 500 kHz to 5 MHz.

The acquired frequency spectra are shown in Figure 5.16. The small dots indicate the different measured values, the large dots represent the average value over all five measurements. It can be seen that the result accuracy decreases for frequencies above 2.5 MHz as the deviations between the different measurements (small dots) increase. This is caused by the decreasing sensitivity of the hydrophone for high frequencies (see Section 4.3.4). It can be seen that the resonance frequency is higher than predicted by simulation. The maximum pressure was generated at a frequency of 3.15 MHz (7.4581 kPa). The center frequency is 3.28 MHz (-6 dB from 1.75 MHz to 4.8 MHz). This is consistent with the fact that the resonance frequency was also higher in the vibrometer measurements in air than predicted by simulation (cf. Section 5.2.1). The recorded frequency spectra show local maxima at 950 kHz, 1.55 MHz, 2.6 MHz, 3.15 MHz and 4.7 MHz. Manufacturing tolerances and layer stresses lead to this behavior in the superposition of the different
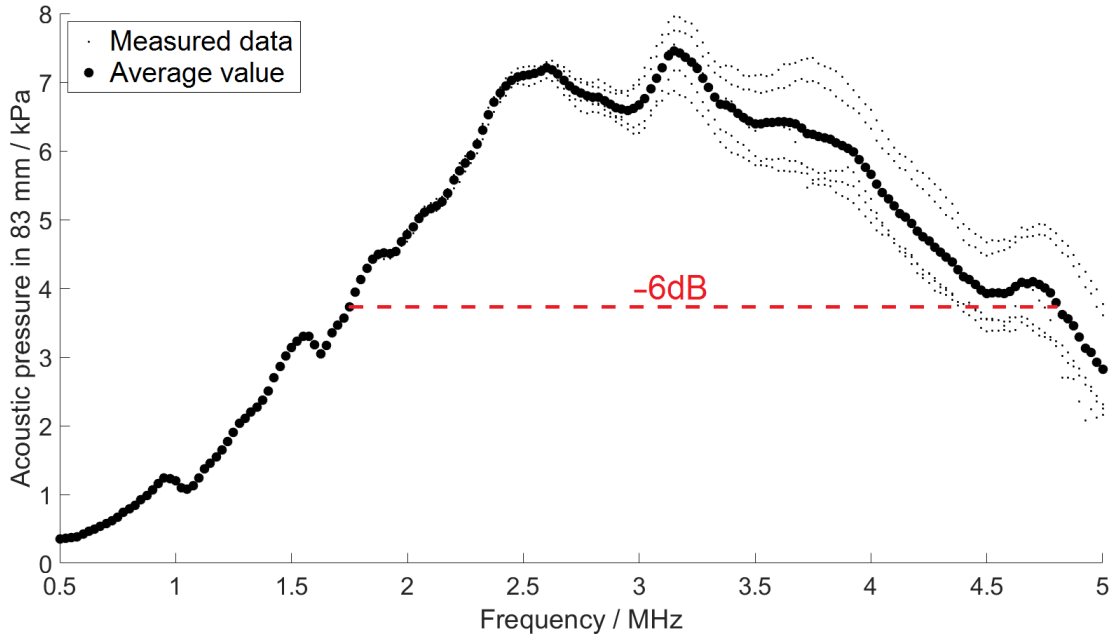
Figure 5.16: Acoustic pressure $83\,\mathrm{mm}$ in front of the CMUT surface, $60\,\mathrm{V_{DC}}$, $10\,\mathrm{V_{AC}}$, Fluorinert FC-72.

signals of the 3416 cells operated in parallel.

In summary, it can be stated that the planned resonance frequency could not be realized due to imperfections of the manufacturing process. However, since this work is mainly about the effects of different encapsulations of CMUTs for the use in medical implants, the exact frequency of the uncoated CMUTs was not in the focus of this work.

5.3 Effects of different compositions of DC and AC voltage

When operating CMUTs in conventional (non-collapse) mode, the applied voltage is limited by the pull-in voltage (U_{PI}) of the cells. The sum of applied bias and AC voltage must not exceed this limit.

$$U_{PI} > U_{tot} = U_{AC} + U_{DC} \tag{5.1}$$

While Equation (5.1) gives an upper limit for the total voltage, it is not giving any information about the proportion of the individual components. E.g. a total voltage of $10\,\mathrm{V}$ could be achieved by $(10\,\mathrm{V_{AC}} + 0\,\mathrm{V_{DC}})$ or $(0\,\mathrm{V_{AC}} + 10\,\mathrm{V_{DC}})$ or anything in between. The DIN VDE 0100-410 standard gives a limit for the planned application. However, it is of scientific interest to investigate the influence of different fractions of alternating

voltage on the total voltage. This was done in simulation and experiment. The corresponding results are presented in this chapter.

As explained in Section 2.2.2, the membrane deflection depends on the square of the applied voltage. If there is no direct voltage component, the membrane oscillation is dominated by twice the excitation frequency. For excitation with a 500 kHz continuous wave signal, the membrane would consequently oscillate at 1 MHz in the case of 10 V_{AC} and 0 V_{DC}. In this part of the work, it was investigated how different compositions of AC and DC voltage of the same total voltage affect the amplitude of oscillation and the generated sound pressure. These amplitudes correspond to the amplitude of the received voltage signal. The study was performed using CMUT chips of design LA5. For a description of the design, see Section 4.2. For this simulation study, two sinusoidal cycles were used for excitation.

In theory, the spring-softening effect has to be considered in this study. This effect causes the resonance frequency to decrease with increasing bias voltage (see Section 2.2.2). Consequently, excitation of a CMUT with the same frequency could be in or off resonance depending on the bias voltage. As a result the change in the amplitude of the simulated membrane displacement due to differing bias voltages could be distorted by the spring-softening effect as resonant excitation results in larger displacements. To eliminate this problem, the simulation study was repeated in a second run using different excitation frequencies, each corresponding to the resonance frequency found in the first run for the respective bias voltage. The determined small shift of the resonance frequency due to the spring-softening effect was found to have no significant influence on the results, so that the following presentation is limited to the results with an excitation at 1 MHz.

5.3.1 Simulation results

Simulations were performed with a sine burst (count = 2) with a frequency of $f_R = 1$ MHz. For a total voltage of 120 V the bias fraction was varied from 10 V_{DC} to 110 V_{DC} (corresponding to 8 to 92 percent of the total voltage). Figure 5.17 shows a selection of the simulated membrane oscillations for some of the examined voltage combinations.

It can be seen that the influence of the doubled frequency decreases with an increasing fraction of the bias voltage on the total voltage. It is also observable that the membrane oscillates symmetrically around its biased steady state when 100 V_{DC} and 20 V_{AC} are applied. In contrast, the blue curve (10 V_{DC}, 110 V_{AC}) shows that the membrane is almost exclusively deflected downward from the biased steady state. The simulation confirms that for the membrane displacement to be linear and for the membrane to vibrate at the excitation frequency, the bias voltage must clearly exceed the value of the signal voltage. In addition to considering the oscillation behavior of the membrane, the amplitude of the generated acoustic pressure directly in front of the CMUT membrane was determined and the respective root mean square (RMS) value is presented in Figure 5.18.
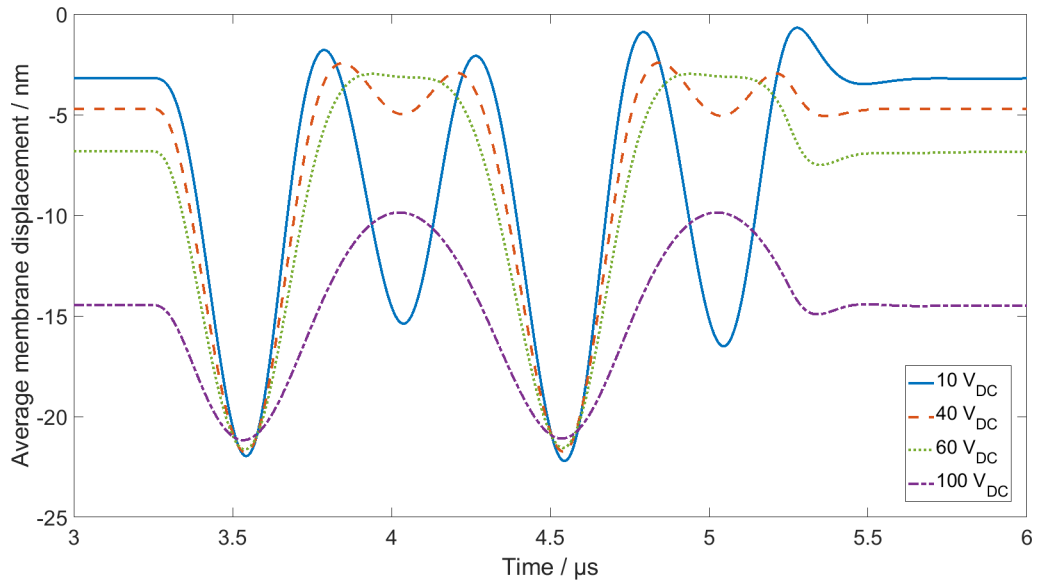
Figure 5.17: Simulated membrane displacement. CMUT design LA5,
$U_{DC}+U_{AC} = 120\,V$, $f = 1\,MHz$, burst count $= 2$.

It can be seen that the highest pressure is achieved when no bias voltage is applied and the CMUT is driven only by an AC voltage.
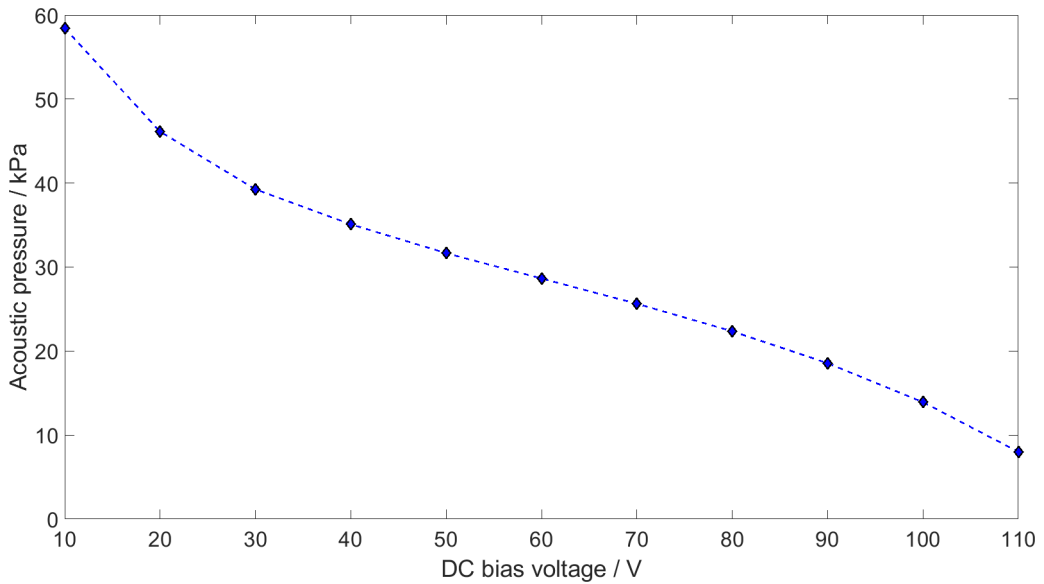
Figure 5.18: Simulated RMS amplitude of the acoustic pressure right in front of the membrane, CMUT design LA5, $U_{DC}+U_{AC} = 120\,V$, $f = 1\,MHz$, burst count 2.

5.3.2 Experimental results

The simulation results obtained in Section 5.3.1 were subsequently verified experimentally. For this purpose, a CMUT chip of design LA5 was used as transmitter and a hydrophone (type s, RP acoustics, Leutenbach, Germany) at a distance of 9.8 mm was used as receiver. The measurement was performed in Fluorinert FC-72. Again, for a total voltage of 120 V, the fraction of bias voltage was varied. Figure 5.19 shows, analogous to Figure 5.17, the measured received voltages at the hydrophone for bias voltages of 10 V, 40 V, 60 V and 100 V. It can be seen that the influence of the doubled frequency decreases with increasing bias voltage.

The amplitudes of the first and the third maximum decrease for larger bias voltages. Finally, for a bias voltage of $100\,V_{DC}$ they vanish completely and the frequency of the received signal is 1 MHz. Parallel to the amplitude of the first and the third maximum, the total amplitude of the received signal decreases with increasing bias voltage.
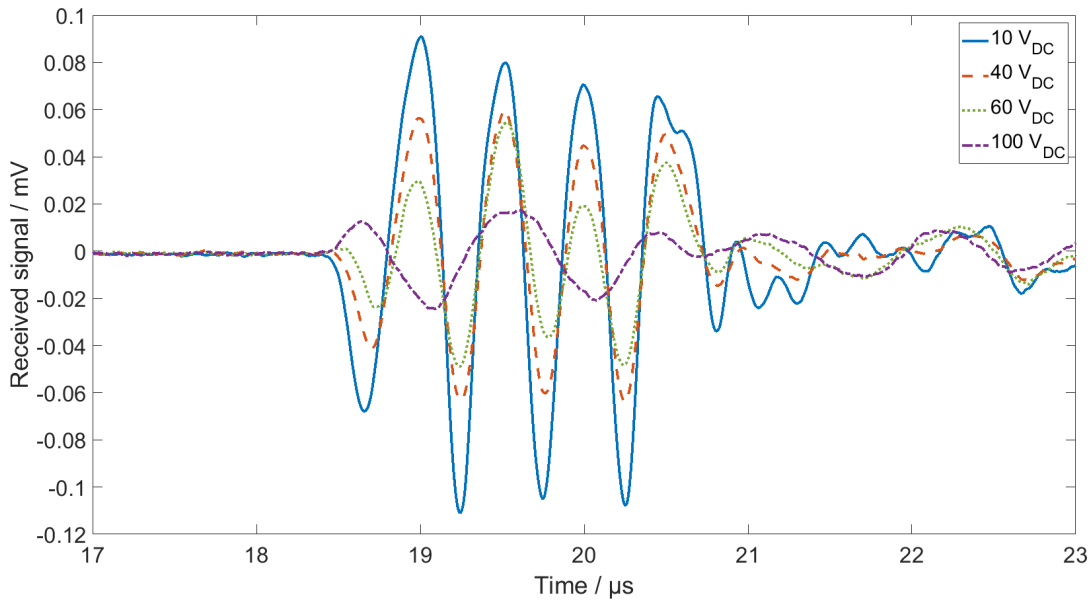
Figure 5.19: Experiment: Received voltage signal for different fractions of $U_{DC}+U_{AC} = 120$ V. CMUT for transmit, hydrophone for receive, distance 9.8 mm, f = 1 MHz, burst count 2.

The amplitudes of the received voltage for all investigated combinations of DC and AC voltage are shown in Figure 5.20. The experiment thus confirms the results from the simulation. Again, it can be seen that for a given total voltage, the maximum sound pressure is achieved when the AC component accounts for 100% of the total signal. According to the presented results, for this CMUT it would be beneficial in terms of oscillation amplitude in simulation and received voltage signal in experiment to apply a
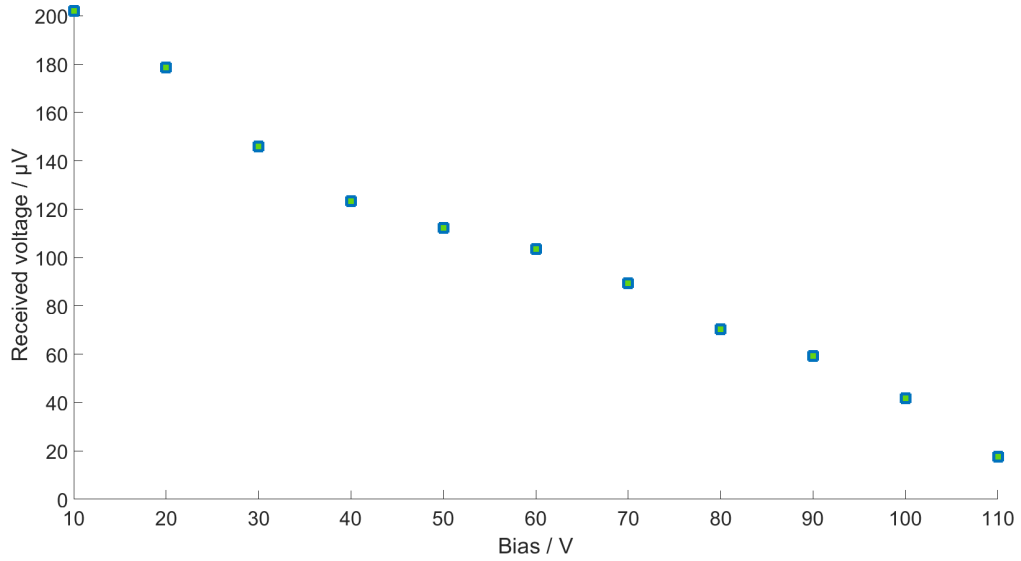
Figure 5.20: Experiment: Amplitude of the received voltage signal for different compositions of $U_{DC}+U_{AC} = 120\,V$. CMUT for transmit, hydrophone for receive. Distance $9.8\,mm$, $f = 1\,MHz$, burst count $= 2$.

total voltage signal consisting of 0% bias and 100% alternating voltage. However, since high AC voltages require additional protective measures (see Section 5.1.1), transmit operation with AC voltages above $25\,V$ is not feasible. Instead, operation was continued with $60\,V$ bias voltage (maximum permitted DC voltage without additional protective measures according to DIN VDE 0100-410) and AC signals of $10\,V$ or $15\,V$.

5.4 Investigation of additionally applied layers

Additional layers applied to a CMUT, whether functionalization layers, protective layers, or the housing of a medical implant, alter its behavior (see also Section 3.5). Depending on the material and thickness of the additionally deposited layer, effects on bandwidth, resonance frequency and sensitivity (in transmit and receive) are to be expected.
In this chapter the interaction of CMUTs with additional layers above the membrane were investigated in detail. The effects of different coating materials and coating methods were compared in simulation and experiment. The encapsulation approach, investigated in this work for the first time, consists of a foil made of PEEK or titanium, which is applied to the CMUT chip with the aid of a silicone (see also Section 4.4). The idea behind this was, on the one hand, to use a material for encapsulation that has already been shown to be suitable for encapsulation in medical implants (cf. Section 3.5). On the other hand, to realize the largest membrane oscillation possible through the additional use of a silicone to couple and to adhere the foil.

The aim was to minimize the effects of the encapsulation on the acoustic properties of the CMUT, and, in particular, on the sound pressure. As described in Section 3.5, existing encapsulations for CMUTs consist of thin layers of parylene-C or PDMS. To compare the new encapsulation method presented here with the previous standard, additional CMUT chips were encapsulated with parylene-C or a silicone.

5.4.1 Simulation study

First, simulations were performed to evaluate the effects of different combinations of silicone and foil on the oscillation behavior of the CMUTs with respect to the layer thicknesses. For this purpose, the simulation model for the CMUT design R2, presented in Section 4.2, was extended by a silicone layer and a foil (see Figure 5.21).
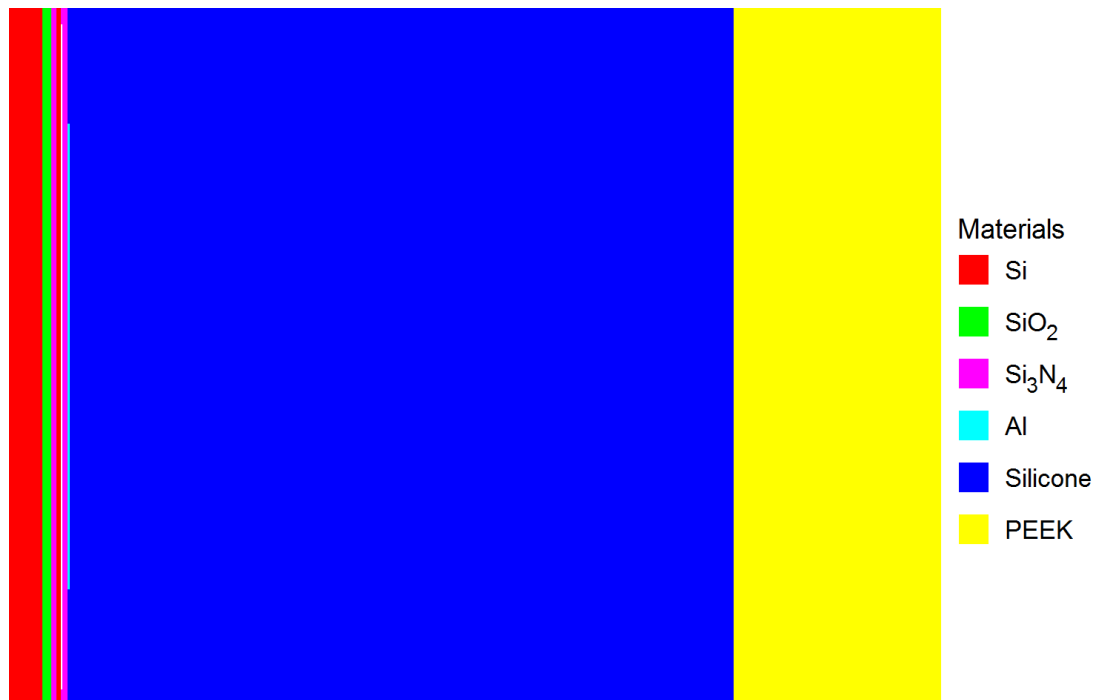
Figure 5.21: Simulation model for encapsulation study. CMUT design R2 with $80\,\mu m$ thick silicone and $25\,\mu m$ thick PEEK.

For the thickness of the foil, it was shown for both materials (PEEK and titanium) that the foil should be as thin as possible to achieve maximum deflection at the top of the foil. As an example, Figure 5.22 shows the displacements of PEEK foils of different thicknesses attached to a CMUT cell via an $80\,\mu m$ thick silicone layer. The CMUT was excited with $60\,V$ bias and a single sinusoidal burst of amplitude $15\,V$ at a frequency of $2\,MHz$.
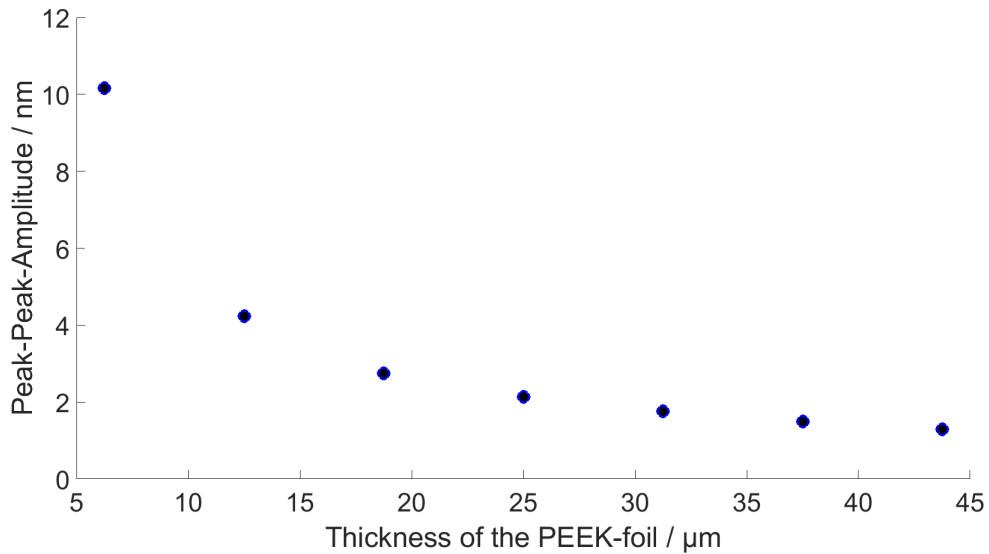
Figure 5.22: Simulated amplitude of the foil oscillation for a PEEK foil on top of 80 μm thick silicone on top of a single CMUT cell, excited with 60 V_{DC} and 15 V_{AC} at 2 MHz.

PEEK foils (OSYPKA AG, Rheinfelden, Germany) of thickness 25 μm and titanium foils (OSYPKA AG, Rheinfelden, Germany) of thickness 32 μm were the thinnest foils available. The thickness of the silicone layer was subsequently varied for these foil thicknesses. The results of this simulation study are shown for both foil materials in Figure 5.23. In each case, the amplitude of the displacement at the upper surface of the foil, averaged over the entire width of a CMUT cell, is shown there. For both materials, an optimum silicone layer thickness exists. The maximum displacement of the foil occurs for the PEEK foil at a silicone layer thickness of 60 μm and for the titanium foil at a silicone layer thickness of 85 μm.

The layer thicknesses are thus well below the usual thickness for matching layers of $\lambda/4$ for piezoelectric ultrasonic transducers. For the silicone used, $\lambda/4$ at 2 MHz is 125 μm. Therefore, the encapsulated CMUT can be assumed as composite transducer.

The oscillation amplitudes resulting from the excitation using 60 V_{DC} and 15 V_{AC} are only very small with 2.22 nm (PEEK) and 0.052 nm (titanium), respectively. This is the result of three different effects. The first reason is the excitation with only a single sinusoidal burst. A bigger amount of sine cycles used for excitation would result in larger foil displacements. Additionally, the average displacement over the entire width of the foil is plotted which is much smaller than the peak displacement. Finally, larger displacements are to be expected in the experiment because the foil is not only driven by a single cell but by a large number of cells.
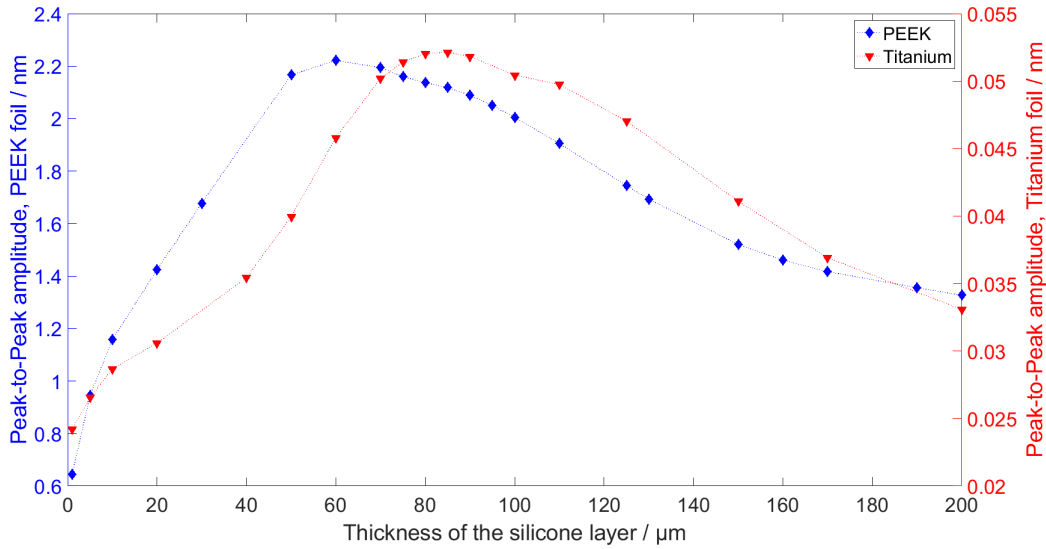
Figure 5.23: Simulated amplitude of the foil displacement for PEEK (left y-axis, blue) and titanium (right y-axis, red) for different silicone thicknesses. Excitation: $60\,\mathrm{V_{DC}}$, $15\,\mathrm{V_{AC}}$, $2\,\mathrm{MHz}$.

The significantly (about 42 times) larger displacements of the PEEK foil compared to the titanium foil are due to the greater stiffness of the titanium foil, which results both from the material itself and from the bigger thickness of the titanium foil (t=$32\,\mu$m) compared to the PEEK foil (t=$25\,\mu$m).

5.4.2 Verification and experimental evaluation

To verify the simulation results shown in Figure 5.23, CMUT chips were coated with silicone and PEEK or silicone and titanium. Due to limitations in the achievable accuracy with the chosen approach for coating the CMUT chips with silicone and foil (see Section 4.4) as well as the limited number of CMUT chips available, the target silicone layer thicknesses of $60\,\mu$m or $85\,\mu$m for the setup including a PEEK or titanium foil could not be realized. Instead, silicone layer thicknesses of $50\,\mu$m $\pm$ $5\,\mu$m were realized for both foils.
The CMUT chips coated in this way were characterized with the laser Doppler vibrometer in air and in the transmission setup in Fluorinert FC-72 and water.

Laser vibrometry in air

To examine the effects of encapsulation on the oscillation behavior of the CMUTs, measurements were made in air using the laser Doppler vibrometer. For a bias voltage of $60\,\mathrm{V_{DC}}$ and an AC signal of $15\,\mathrm{V_{AC}}$, which consisted of a single sinusoidal cycle at different frequencies, FFT scans were performed, providing directly the frequency spectrum.

75

Figure 5.24 shows the results normalized to their respective maximum when excited with a single sine burst of frequency 10 MHz. In case of the silicone-coated CMUT chip (yellow curve), the surface is very rough. As a consequence, an accurate focusing of the laser beam is not possible and the resulting output is very noisy. For excitation with 10 MHz, the noise is more pronounced than the resonances, so that these are not visible in the spectrum. Therefore, the result for an excitation with 4 MHz is shown for this chip. Consequently, the lower frequencies are excited more strongly, so that the resonances are more pronounced. Above 6 MHz, the noise increases so much that this region is hidden in the plot. Before plotting the spectra, they were each corrected for the frequency spectrum of the excitation signal. This is the reason why the curves shown in Figure 5.24 increase for frequencies below 1.0 MHz.
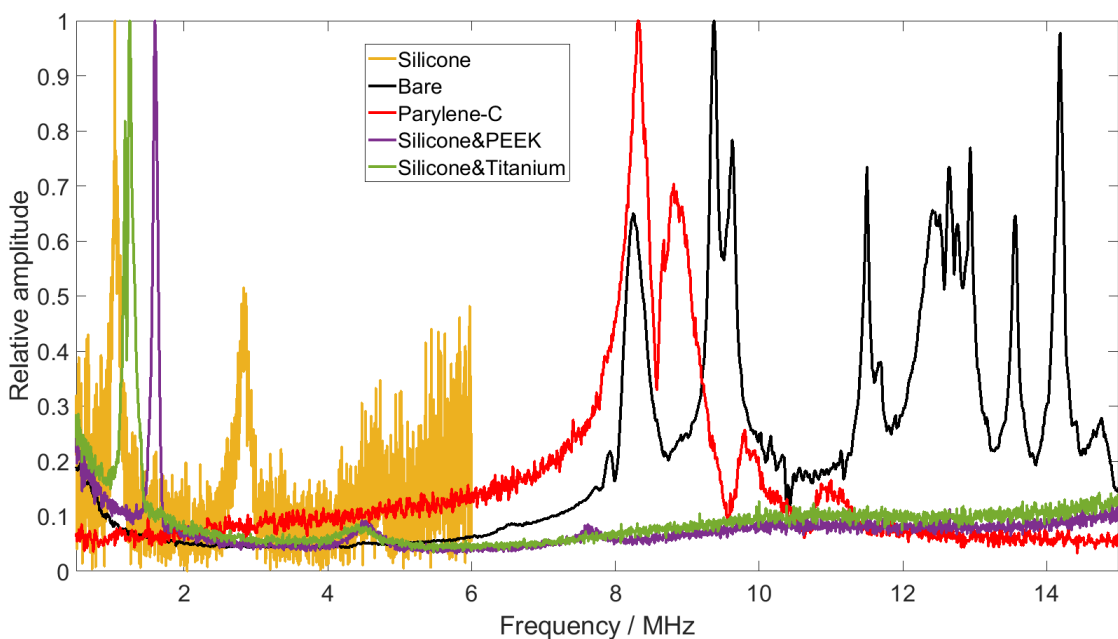
Figure 5.24: Vibrometry FFT-scan in air for CMUT chips with different encapsulations. Bias: $60 \, V_{DC}$, signal: single sine cycle with $15 \, V_{AC}$ at 10 MHz.

As described in Section 5.2.1, the resonances of the uncoated CMUT chip are in the frequency range above 8 MHz. The parylene-C coated chip (red curve) shows a similar frequency behavior with maxima at 8.3 MHz, 8.8 MHz, and 9.8 MHz. The deviation between the resonances of the chip before encapsulation and the chip coated with parylene-C are within the order of magnitude of the deviations between different cells of the chip before encapsulation. Thus, the effects of the parylene-C coating can be considered negligible with respect to the oscillation behavior in air.

The silicone-coated CMUT chip shows resonance peaks at 1.04 MHz and 2.83 MHz. In contrast to the thin parylene-C coating, the coating with 150 µm silicone thus leads to

a significantly changed oscillation behavior of the CMUT chip in air.
This is mainly due to the fact that the membrane can no longer oscillate freely but has to work against increased resistance, so that the resonance frequency is reduced.

The same applies to the two other encapsulation strategies with thin silicone layer and PEEK foil (purple, maxima at 1.59 MHz and 4.53 MHz) as well as thin silicone layer and titanium foil (green, maxima at 1.24 MHz and 4.43 MHz). In contrast to the pure silicone coating, a defined surface is present here due to the subsequently applied foil, so that the focusing of the laser beam of the vibrometer is facilitated and, as a consequence, the noise decreases. The fact that in particular the main resonance of the chip coated with silicone and titanium is reduced by approx. 0.35 MHz is due to the higher mass of the titanium foil compared with the PEEK foil.

Transmit experiments in Fluorinert FC-72

After characterizing the oscillation behavior of the encapsulated CMUT chips in air using the laser Doppler vibrometer, the next step was to investigate the transmission behavior in Fluorinert FC-72. For this purpose, a calibrated hydrophone (RP acoustics, Leutenbach, Germany, type s) was positioned at a distance of 83 mm from the CMUT chip and the received voltage was recorded. The measurements were done with a bias voltage of $60\,V_{DC}$ and an AC signal of twenty sine cycles of amplitude $10\,V_{AC}$ for frequencies between 500 kHz and 5 MHz (see also Section 4.3.4).
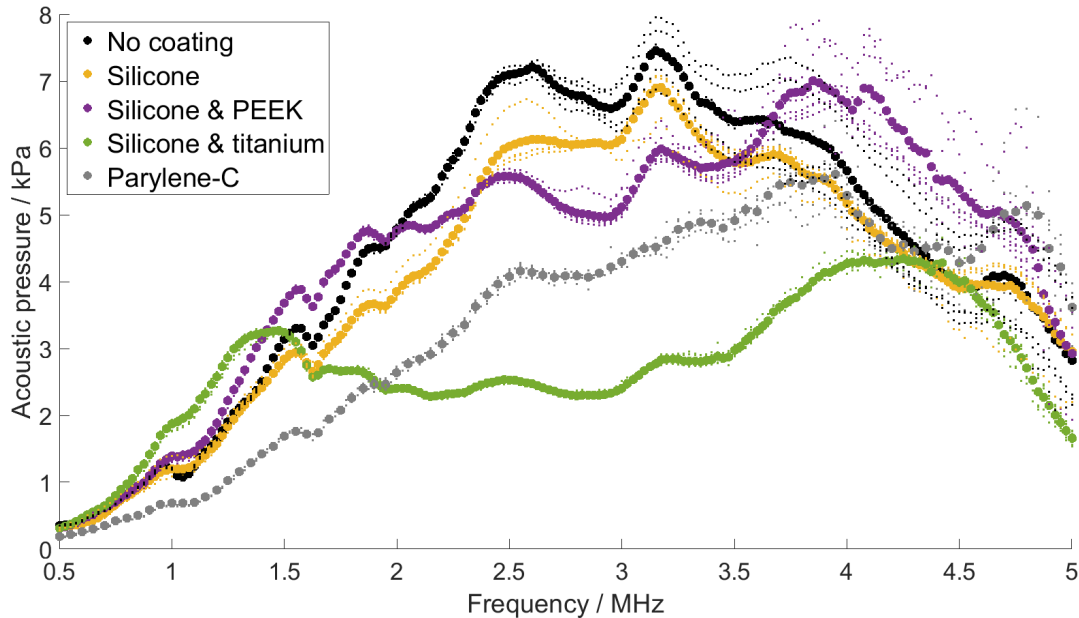
Figure 5.25: Acoustic pressure 83 mm in front of the CMUT. Setup: $60\,V_{DC}$, $10\,V_{AC}$, 20 sinusoidal cycles, Fluorinert FC-72.

Using the calibration curve of the hydrophone, the receiving voltages of the hydrophone determined in this way could then be converted into acoustic pressure (cf. Section 4.3.4). The result of these conversions is shown in Figure 5.25 for the five setups investigated (uncoated, pure silicone, silicone and PEEK, silicone and titanium, and parylene-C). The big dots represent the average value over all measurements of the respective chip, the small dots correspond to the data points on which this average value is based.

The results of the chip encapsulated with silicone are shown in yellow, and the results of the chip encapsulated with parylene-C are shown in gray. The purple dots belong to the chip encapsulated with silicone and PEEK foil and the green dots to the encapsulation with silicone and titanium foil. The main characteristics of the five variants studied are listed in Table 5.2.

Table 5.2: Characteristic acoustic parameters derived from transmit experiment in Fluorinert FC-72. Setup: $60\,V_{DC}$, $10\,V_{AC}$, 20 sinusoidal cycles, distance between CMUT aperture and hydrophone: $83\,mm$.

Encapsulation	Max. pres. at	Max. pressure	Center freq.	FWHM
Without	3.15 MHz	7.46 kPa	3.28 MHz	93%
Silicone	3.18 MHz	6.90 kPa	3.34 MHz	92%
Silicone & PEEK	3.85 MHz	7.00 kPa	3.20 MHz	108%
Silicone & Titanium	4.25 MHz	4.34 kPa	3.01 MHz	125%
Parylene-C	3.95 MHz	5.61 kPa	3.78 MHz	91%

The yellow curve, corresponding to the measurements of the CMUT chip coated only with silicone, shows a shape very similar to the black curve (chip without encapsulation). The silicone coating leads to slightly less acoustic pressure overall, but does not change the basic shape of the frequency spectrum.

The soft silicone leads to a small additional attenuation which is not frequency dependent. If the CMUT chip is encapsulated with a parylene-C layer instead, the hard parylene-C (in comparison to the silicone) leads to a frequency shift towards higher frequencies. In the frequency range up to $4\,MHz$, the generated pressure of the chip after coating with parylene-C is continuously below the values of the uncoated chip as well as those of the silicone-coated chip. The positions of the local maxima also change. The two main maxima of the curve related to the CMUT chip coated with parylene-C are located at $3.95\,MHz$ and $4.8\,MHz$.

After an encapsulation with silicone and PEEK, the CMUT chip shows a slightly different frequency response with local maxima at $1.58\,MHz$, $1.88\,MHz$, $2.48\,MHz$, $3.18\,MHz$, $3.85\,MHz$, $4.08\,MHz$ and $4.68\,MHz$. For frequencies below $2\,MHz$ and above $3.6\,MHz$, the acoustic pressures registered with the hydrophone are larger than those for the plain CMUT chip.

The combination of silicone and PEEK foil results in a slight shift of the CMUT toward higher frequencies.

The effects of an encapsulation with silicone and titanium foil are significantly larger than those of the other coatings. In addition to weakly pronounced local maxima at 1.70 MHz, 2.48 MHz, and 3.23 MHz, there are two main maxima at 1.48 MHz and 4.25 MHz. Since the drop between these two maxima is smaller than −6 dB, the largest bandwidth (125%) is obtained for this encapsulation. The strongly deviating frequency behavior of this chip can be explained by the composite of soft silicone and comparatively hard titanium foil on it.

The results of the transmission measurements in Fluorinert FC-72 have shown that the acoustic properties of the CMUT chip are only changed insignificantly by the coating with silicone. The further measurements are to take place in water, since it is much closer to the properties of human tissue.

Transmit experiments in water

The sound velocity of water ($c_{water} = 1500$ m/s) is significantly higher than the one in Fluorinert FC-72 ($c_{Fluorinert} = 512$ m/s). This results in a decrease of the near-field length (distance from the transducer surface to the last maximum on the acoustic axis) of the CMUT chips, so the distance between the CMUT chip and the hydrophone can also be decreased. Measurements in water were performed at a distance of 35 mm. The length of the excitation signal was shortened to 10 sine cycles. The other parameters (bias: 60 V_{DC}, signal: 10 V_{AC}) remained unchanged.
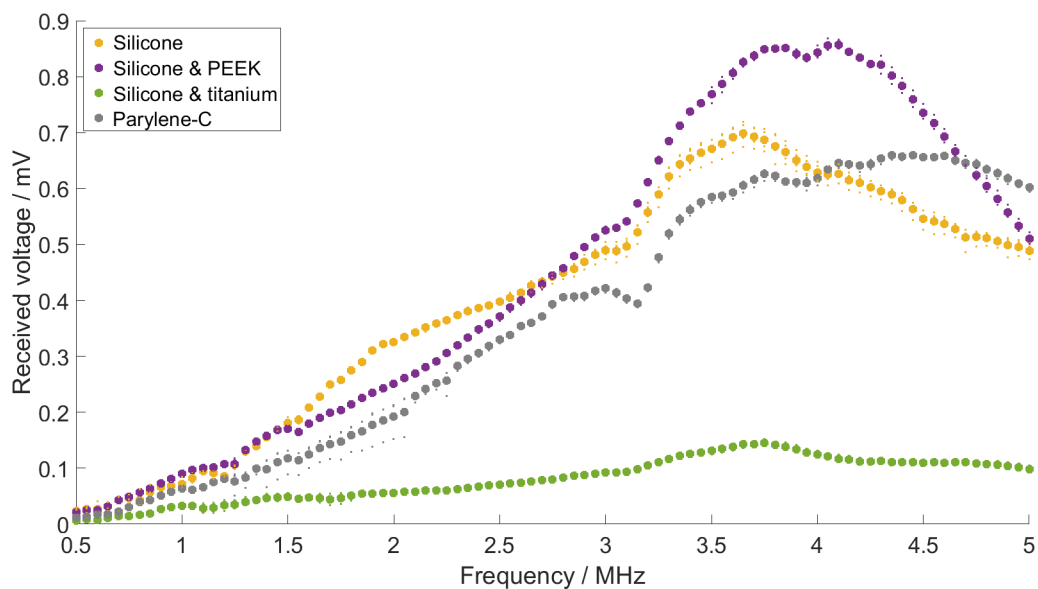
Figure 5.26: Amplitude of the received voltage in water for transmitting CMUTs with different encapsulations. Bias: 60 V_{DC}, signal: 10 V_{AC}, distance: 35 mm.

Figure 5.26 shows the amplitude of the received voltage measured with the hydrophone for the different encapsulated chips. The chip encapsulated with silicone and titanium (green dots) generates the lowest values. Compared to the measurement in Fluorinert FC-72, the other three curves are shifted towards higher frequencies. All curves have in common that they show less local maxima than in Fluorinert FC-72. This could be a consequence of the overall increased signals.

The respective main maximum is at 3.65 MHz for the chip encapsulated with silicone and at 4.45 MHz for the chip encapsulated with parylene-C. An encapsulation with silicone and PEEK foil leads to a main maximum at 4.10 MHz, while an encapsulation with silicone and titanium results in a main maximum at 3.75 MHz.

The received voltages shown in Figure 5.26 must be corrected by the calibration curve of the hydrophone. Taking into account the varying sensitivity of the hydrophone for the different frequencies (see Figure 4.16) results in the spectra shown in Figure 5.27.
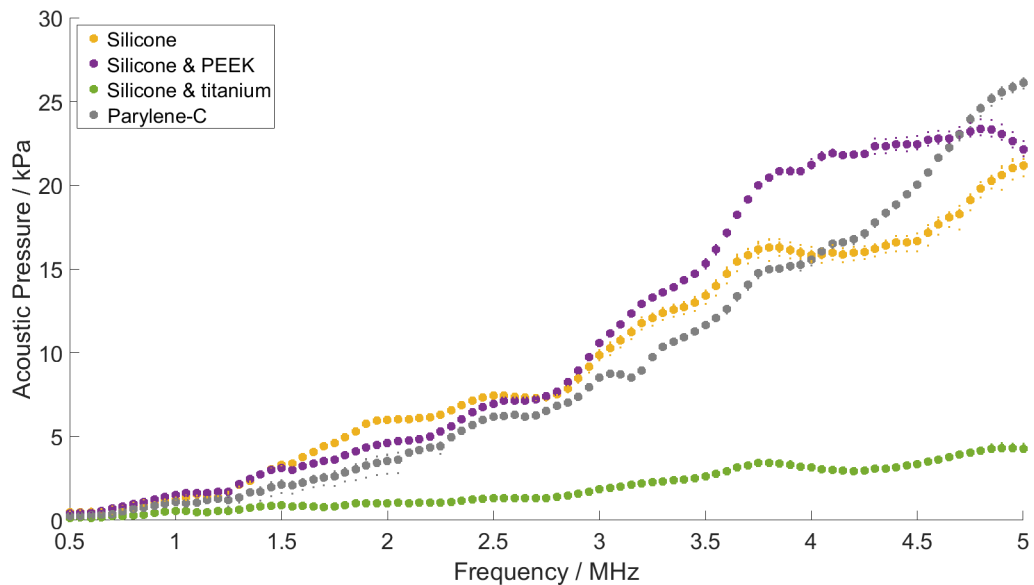
Figure 5.27: Acoustic pressure in water, 35 mm in front of the CMUT. Excitation: 60 V_{DC}, 10 V_{AC}, 10 sinusoidal cycles.

Since the sensitivity of the hydrophone for frequencies above 3.5 MHz decreases significantly (Section 5.2.3), the values at high frequencies of the investigated frequency range are raised accordingly by the correction resulting in all four chips having their maximum above 4.5 MHz. The spectra of the chips encapsulated with silicone and PEEK (purple dots) or silicone and titanium (green dots) decrease after a maximum at 4.8 MHz respect-

ively 4.9 MHz. In contrast, the maxima of the frequency spectra of the chips coated with silicone or with parylene-C are at 5 MHz. Thus, it can be assumed that the resonance frequencies of these chips are above 5 MHz. However, an increased frequency results in an increased damping of the ultrasonic wave, which is especially crucial for other media but water. Brandner *et al.* report an attenuation coefficient of $0.57\,\mathrm{dB}/(\mathrm{cm}\cdot\mathrm{MHz})$ for muscle tissue [100]. For the targeted transmission distance of 6 cm, this results in an attenuation of the ultrasonic signal by 6.8 dB at 2 MHz compared to 17.1 dB at 5 MHz. The frequency range above 5 MHz is therefore not suitable for the application being addressed in this thesis and was not investigated here. In contrast to the situation in human tissue, Brandner *et al.* report the attenuation coefficient of water as only $0.002\,\mathrm{dB}/(\mathrm{cm}\cdot\mathrm{MHz}^2)$ [100]. This corresponds to an attenuation of 0.03 dB at 2 MHz and of 0.18 dB at 5 MHz for the distance of 35 mm used in the experiments presented here. Consequently, the higher frequencies are overemphasized here compared to the situation when transmitting the human body.

Another set of measurements was made for which the distance was increased to 6 cm. The result of these measurements is shown in Figure 5.28.
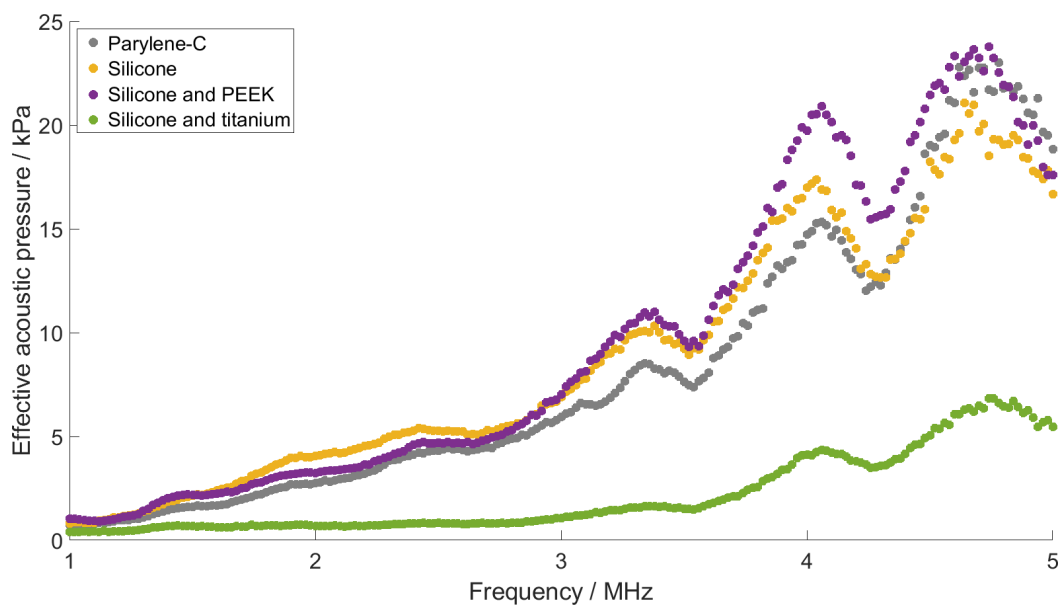
Figure 5.28: Acoustic pressure in water, 6 cm in front of the CMUT. Excitation: $60\,\mathrm{V_{DC}}$, $10\,\mathrm{V_{AC}}$, 15 sinusoidal cycles.

The measurements at a distance of 6 cm confirm the result of the measurements at 35 mm depth. Both measurements show increasingly noisy measurement results above a frequency of approx. 4.5 MHz. This is due to the low sensitivity of the available hydrophone in this frequency range. This is also a reason for the increase at frequencies above 4.5 MHz, which is consequently due to compensation artifacts when compensating

the calibration curve of the hydrophone. Taking this into account, the two curves shown indicate that the CMUT chips encapsulated with silicone and foil reach their respective maxima at 4.68 MHz (PEEK foil) respectively 4.76 MHz (titanium foil).

The slight frequency shift compared to the measurement at a distance of 35 mm is within the measurement accuracy.

Receive characteristics

Once the transmit sensitivity of the encapsulated chips in water had been characterized, the receive sensitivity of the CMUT chips was investigated. For this purpose, the silicone-coated CMUT chip was used as a transmitter and the CMUT chips with the three other encapsulations were used for reception. The distance between the two CMUTs is 35 mm, the bias voltage is $60 \, V_{DC}$, the excitation signal consists of 10 sinusoidal cycles of amplitude $10 \, V_{AC}$ with a frequency that is varied from 500 kHz to 5 MHz during the experiment.
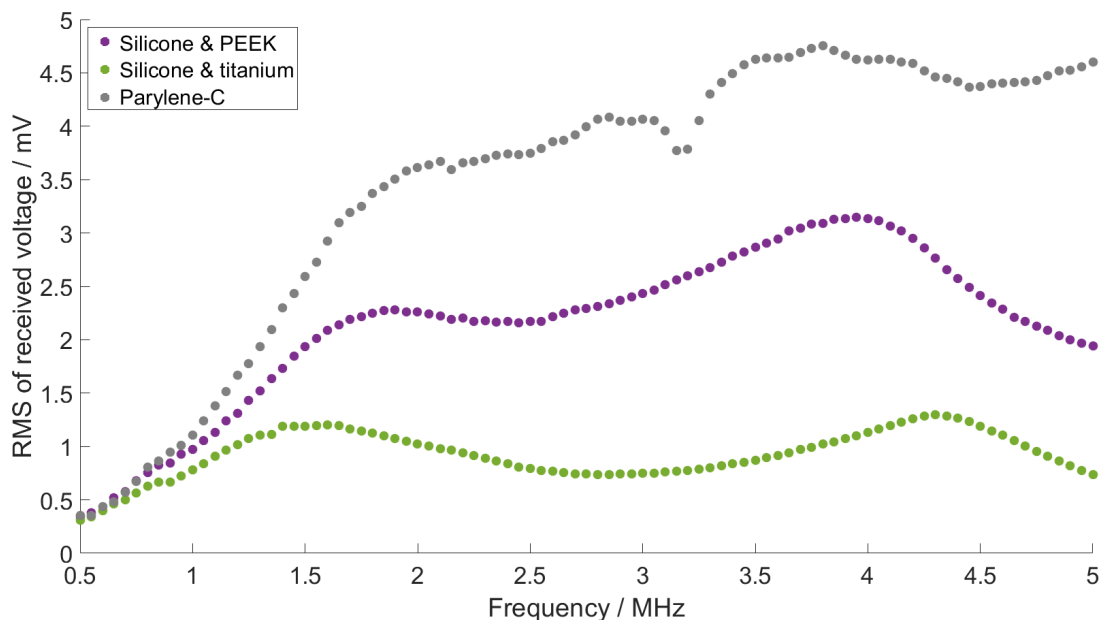
Figure 5.29: Mean RMS amplitude of received voltage in water. Transmitter: Silicone covered CMUT chip. Receiver: Encapsulated CMUT chips according to legend. Distance: 35 mm, excitation: $60 \, V_{DC}$, $10 \, V_{AC}$, 10 sinusoidal cycles.

The amplitude of the received signals in the frequency range investigated is shown in Figure 5.29 for the three encapsulations. The maximum received voltage is detected by the chip encapsulated with parylene-C (gray dots) at a frequency of 3.8 MHz. The chip encapsulated with silicone and PEEK foil (purple dots) shows lower received signals overall and has maxima at 1.9 MHz and 3.95 MHz.

The received signals measured with the chip encapsulated with silicone and titanium foil (green dots) were lower than for the other two chips. This spectrum also shows two maxima which are located at 1.6 MHz and 4.30 MHz.

Consistent with the transmit mode, the receive mode consequently shows a higher sensitivity of the silicone and PEEK encapsulated chip compared to the one encapsulated with silicone and titanium. However, while the chip encapsulated with silicone and PEEK generates larger pressures than the chip encapsulated with parylene-C in the transmit case for all frequencies below 4.7 MHz, the receive sensitivity of the latter is larger for all frequencies above 800 kHz. The reason for this can be found in losses during the transition of the acoustic waves from the water via the comparatively hard foil and the comparatively softer silicone layer to the CMUT membrane.

Finally, the determined amplitudes of the receiving signals were corrected by the excitation spectrum of the silicone-coated chip. Figure 5.30 shows the received sensitivities obtained in this way for the three encapsulation approaches investigated here. Since the transmit sensitivity of the CMUT chip used as transmitter (silicone encapsulation) was very noisy in the frequency range below 1.25 MHz, this subsequently also applies to the receive sensitivities shown in Figure 5.30. In summary, it can be seen that for all three encapsulation approaches, the receive sensitivity increases towards low frequencies.
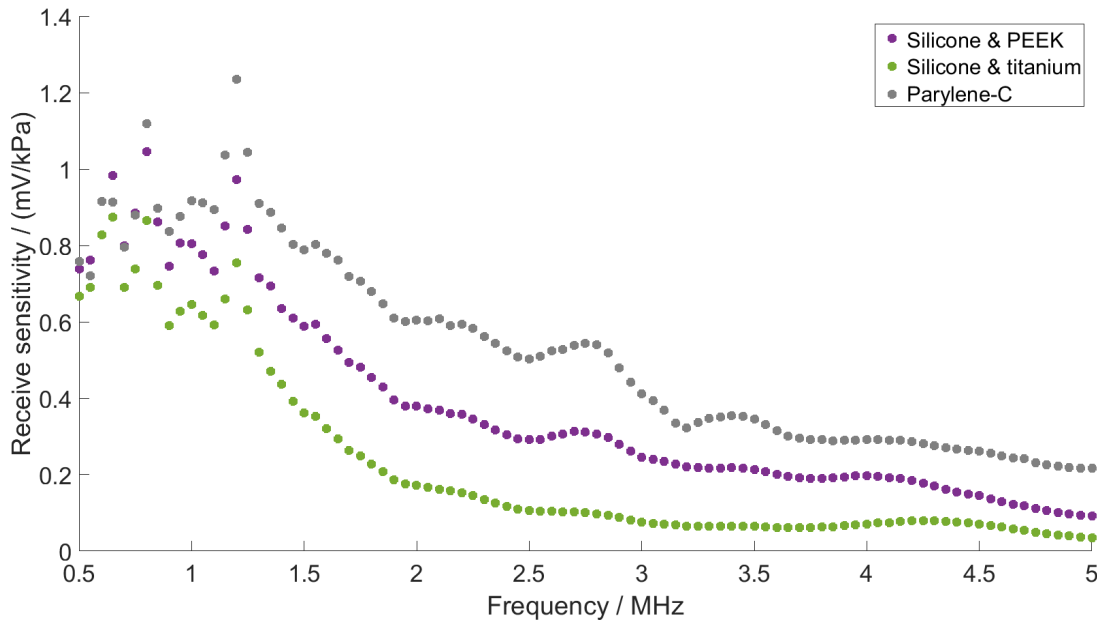
Figure 5.30: Receive sensitivity of encapsulated CMUT chips in water. Transmitter: Silicone covered CMUT chip. Receiver: Encapsulated CMUT chip according to legend. Distance: 35 mm, excitation: $60\,V_{DC}$, $10\,V_{AC}$, 10 sinusoidal cycles.

5.4.3 Soundfield in water

In addition to the frequency response, sound fields were recorded in water for the two novel encapsulations (silicone and foil). XZ and YZ scans were performed for a bias voltage of $60\,\text{V}_{\text{DC}}$ and an AC signal of 50 sine cycles at $10\,\text{V}_{\text{AC}}$. With a spatial resolution of $\delta x = \delta y = \delta z = 0.5\,\text{mm}$, planes with a width of $1\,\text{cm}$ and a length of $5\,\text{cm}$ were recorded. The excitation signal was applied at a frequency of $4.68\,\text{MHz}$ for the chip encapsulated with silicone and PEEK foil and of $4.76\,\text{MHz}$ for the chip encapsulated with silicone and titanium foil (resonance frequencies found in Section 5.4.2).

Table 5.3: Sound field characteristics for CMUT chips with different encapsulations in water.

Encapsulation	$-6\,\text{dB}$ lateral	$-6\,\text{dB}$ axial	Focus depth
Silicone & PEEK	$3\,\text{mm}$	$64\,\text{mm}$	$20\,\text{mm}$
Silicone & Titanium	$3\,\text{mm}$	$33\,\text{mm}$	$14\,\text{mm}$

The measured sound fields were dB-normalized to their respective maximum and are shown in Figures 5.32 to 5.35. Characteristic sound field parameters can be found in Table 5.3. For a better understanding of the measured sound fields, Figure 5.31 shows the sound field of an aperture of $5\,\text{mm} \times 5\,\text{mm}$ at a frequency of $4.68\,\text{MHz}$. It can be seen that the deviation between simulation and measurement is significantly smaller for the encapsulation with silicone and PEEK than for the encapsulation with silicone and titanium. When looking at the measured planes of the CMUT chip encapsulated with silicone and titanium, it is noticeable that no sound pressures are visible in the first $30\,\text{mm}$. This is due to electrical cross-talk between CMUT and hydrophone, which has disturbed the receive signal. Only from a distance of $30\,\text{mm}$ from the transducer surface electric interference and acoustic signal could be separated, so that only from here the correct values were recorded and subsequently plotted in Figures 5.34 and 5.35.
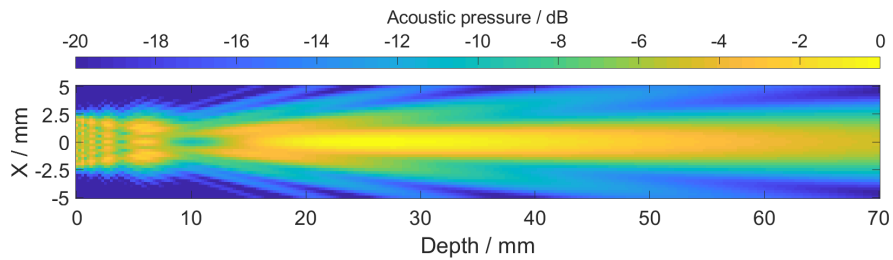
Figure 5.31: Simulated XZ-scan of an aperture with edge lengths of $5\,mm \times 5\,mm$ at $4.68\,\text{MHz}$ using Scalp.
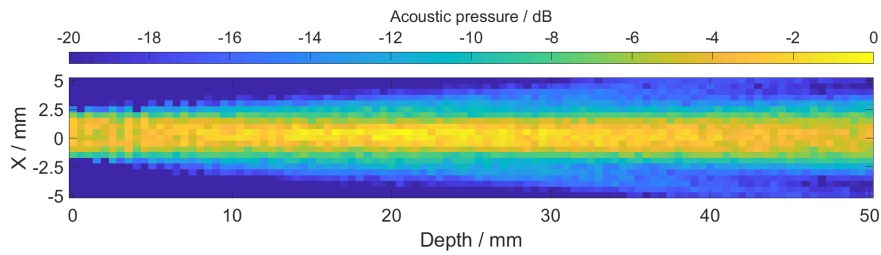
Figure 5.32: XZ-scan of a CMUT chip covered with silicone and PEEK-foil.
Excitation: $60\,\mathrm{V_{DC}}$, $10\,\mathrm{V_{AC}}$, f $= 4.68\,\mathrm{MHz}$, 50 sinusoidal cycles.
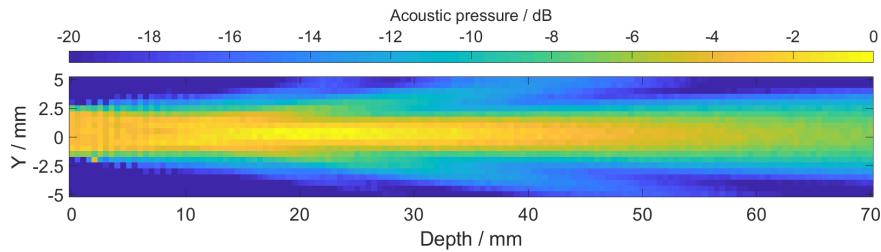
Figure 5.33: YZ-scan of a CMUT chip covered with silicone and PEEK-foil.
Excitation: $60\,\mathrm{V_{DC}}$, $10\,\mathrm{V_{AC}}$, f $= 4.68\,\mathrm{MHz}$, 50 sinusoidal cycles.
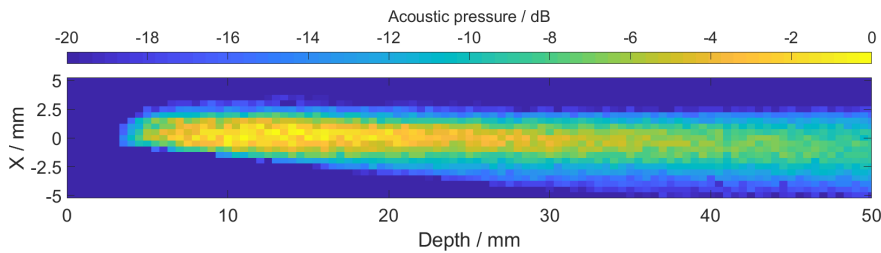
Figure 5.34: XZ-scan of a CMUT chip covered with silicone and titanium-foil.
Excitation: $60\,\mathrm{V_{DC}}$, $10\,\mathrm{V_{AC}}$, f $= 4.76\,\mathrm{MHz}$, 50 sinusoidal cycles.
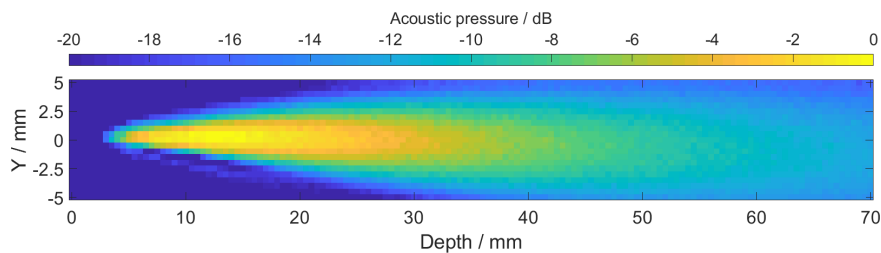
Figure 5.35: YZ-scan of a CMUT chip covered with silicone and titanium-foil.
Excitation: $60\,\mathrm{V_{DC}}$, $10\,\mathrm{V_{AC}}$, f $= 4.76\,\mathrm{MHz}$, 50 sinusoidal cycles.

85

The width of the region in which the sound pressure does not decrease by more than $-6\,\mathrm{dB}$ is for both chips similar with $3\,\mathrm{mm}$. Encapsulation with silicone and PEEK results in a more symmetrical sound field and a larger focal zone. Thus, the sound pressure on the main axis does not decrease by more than $-6\,\mathrm{dB}$ in the first $6.4\,\mathrm{cm}$, while this already happens after $3.8\,\mathrm{cm}$ for the transducer encapsulated with silicone and titanium. Besides a small effect due to the slightly larger attenuation due to the higher frequency, the difference is mainly due to the encapsulation itself. The encapsulation with silicone and titanium foil causes the transducer to be more focused and shifts the focus closer to the transducer. This effect is due to the different material parameters of the two foils. As the silicone hardens, it shrinks, pulling the overlying foil downwards. Figure 5.36 shows the CMUT encapsulated with silicone and PEEK-foil. For clarity, the PEEK-foil is outlined in blue and the CMUT chip in orange. An image of a CMUT encapsulated with silicone and titanium is shown in Figure 5.37.

To investigate the effects of the shrinkage on the alignment of the foil in detail, the surfaces of the two foils were measured after shrinkage using an optical surface measurement system (nanofocus μsurf, Oberhausen, Germany). The elevation profile was measured along the green line in Figure 5.36 from bottom to top and is shown in Figure 5.38.
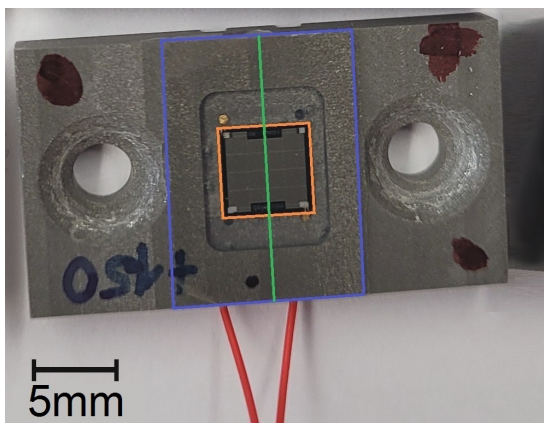
Figure 5.36: CMUT chip (orange frame) encapsulated with silicone and PEEK (blue frame).
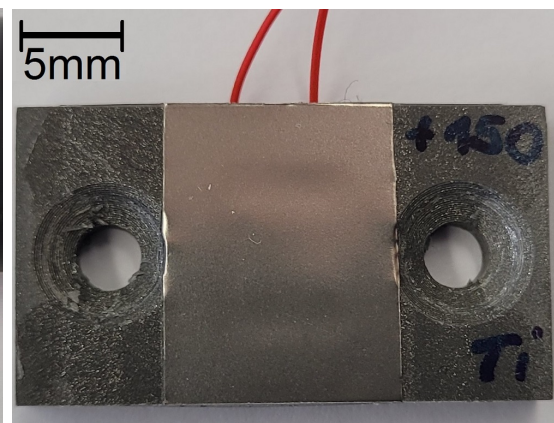
Figure 5.37: CMUT chip encapsulated with silicone and a titanium foil.

Both curves in Figure 5.38 show that the foil sags in the area adjacent to the CMUT chip. As expected, the foil is pulled down the most where the silicone layer is thickest (next to the chip). The PEEK-foil, which is softer than the titanium foil, is bent downwards to a slightly greater extent ($37\,\mu$m) than the titanium foil ($30\,\mu$m). The fact that the blue curve (PEEK-foil) shows values $20\,\mu$m higher at the right edge ($x = 13\,mm$) than at the left edge ($x = 0\,$mm) is partly due to inaccurate alignment during measurement and partly due to the foil actually being at a higher level.
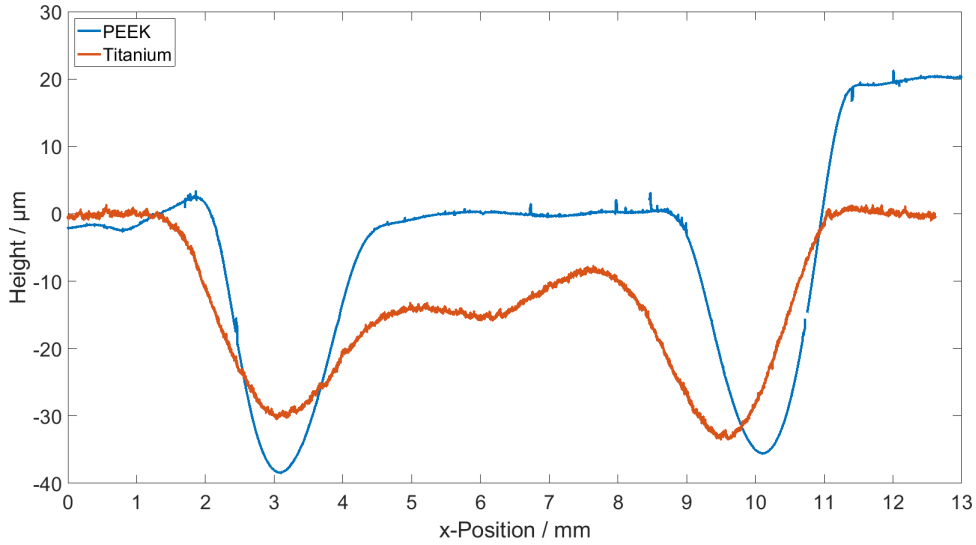
Figure 5.38: Elevation profile of the foil on a CMUT chip after shrinking of the silicone. Measured along the green line in Figure 5.36 using nanofocus μsurf.

When looking at the section above the CMUT chip (approx. from $x = 4\,\mathrm{mm}$ to $x = 9\,\mathrm{mm}$), it is noticeable that the PEEK-foil has an almost horizontal profile, while the titanium foil has a kink at $x = 6\,\mathrm{mm}$. This leads to a focusing of this transducer.

5.4.4 Efficiency in water

In addition to the XZ and YZ planes presented above, XY planes (parallel to the transducer surface) were recorded for both encapsulations consisting of silicone and foil to determine the acoustic power and, from this, the efficiency of the encapsulated CMUT chip. For the efficiency η applies:

$$\eta = \frac{P_{acoustic}}{P_{electric}} \tag{5.2}$$

Since electrical crosstalk and acoustic signal partly overlap at shorter distances for the excitation signal used here and cannot be distinguished with certainty, the XY plane was recorded at a depth of $3\,\mathrm{cm}$ in front of the transducer. With a spatial resolution of $\Delta x = \Delta y = 0.25\,\mathrm{mm}$, a plane of $20\,\mathrm{mm} \times 20\,\mathrm{mm}$ was measured with the hydrophone. Excitation was done with $60\,\mathrm{V_{DC}}$, $10\,\mathrm{V_{AC}}$ and a burst signal of 50 sinusoidal cycles at $4.68\,\mathrm{MHz}$ (PEEK encapsulation) or $4.76\,\mathrm{MHz}$ (titanium encapsulation). The measured planes for CMUT chips with both encapsulations are shown in Figures 5.39 and 5.40. Figure 5.41 shows an XY plane simulated with Scalp at a depth of $3\,\mathrm{cm}$ at a frequency of $4.68\,\mathrm{MHz}$ for an aperture of $5\,\mathrm{mm} \times 5\,\mathrm{mm}$. The comparison between measured and simulated sound field shows that the measured pressures in the corners of the plane are measurement artifacts. For this reason, only the range from $-8\,\mathrm{mm}$ to $8\,\mathrm{mm}$ of the

measured soundfield for the silicone and PEEK encapsulated CMUT was used in both the x- and y-directions to determine the acoustic power.

Figure 5.40 shows much more measurement artifacts due to larger electrical interference. In order to prevent these from distorting the result, only the inner area of the plane (bordered in blue) was used for the calculations here. As a result, the value for the total acoustic power is underestimated because the contribution of the outer area of the plane is not included.
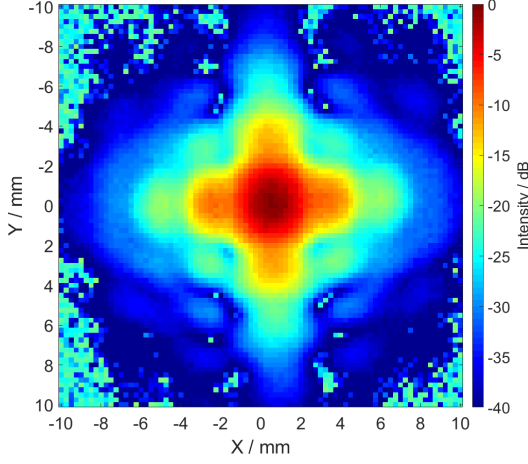
Figure 5.39: Measured XY-plane in 3 cm depth. Silicone and PEEK encapsulated CMUT chip, $60\,V_{DC}$, $10\,V_{AC}$, $4.68\,$MHz.
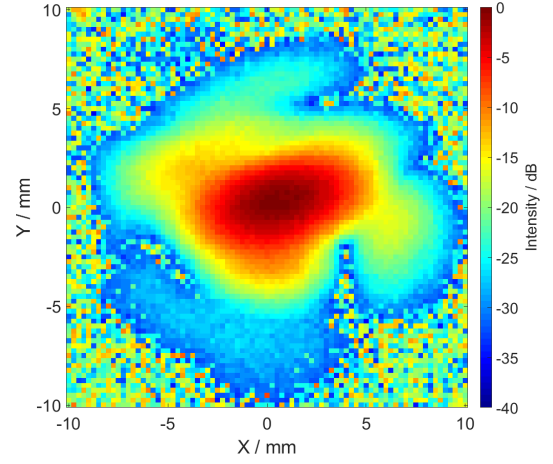
Figure 5.40: Measured XY-plane in 3 cm depth. Silicone and titanium encapsulated CMUT chip, $60\,V_{DC}$, $10\,V_{AC}$, $4.76\,$MHz.

The acoustic power P is given by:

$$P = \int_S I(x,y)\, dS \tag{5.3}$$

Here, $I(x,y)$ is the acoustic intensity at position (x,y) and S is the surface. For the given case of 81 x 81 discrete measurement points, we can convert from the integral to the sum representation and it follows:

$$P = \sum_i I_i A_i = A * \sum_i I_i \tag{5.4}$$

where $A = A_i\ \forall i$ is the area of each measurement point which can be calculated as $A = \Delta x \times \Delta y = 0.25\,mm\times 0.25\,mm= 0.0625\,$mm^2.

For the acoustic performance of the CMUT chip encapsulated with silicone and PEEK foil, this gives an acoustic power of $P_{acoustic,PEEK} = 37.37\,$mW. In contrast, the CMUT chip encapsulated with silicone and titanium has an acoustic power of only
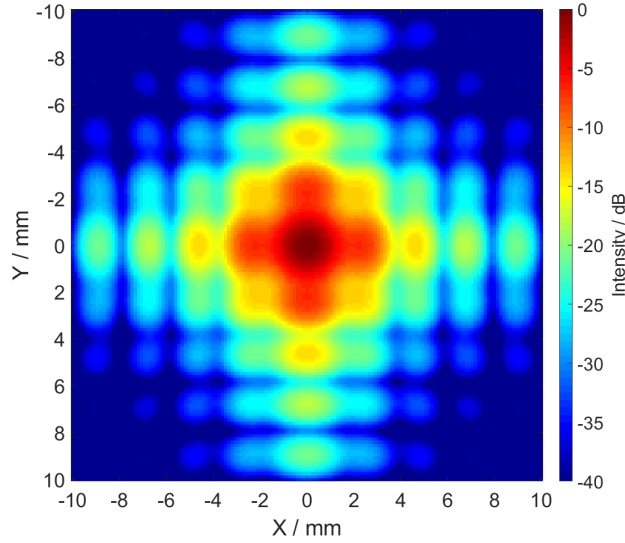
Figure 5.41: Simulated XY-plane in 3 cm depth for an aperture of 5 mm × 5 mm at a frequency of f = 4.68 MHz.

$P_{acoustic,TI} = 3.85 \, \text{mW}$.

The electric power is defined as $P_{electric} = U * I$. With the real part of the admittance Y, namely the conductance G, $Re(Y) = G = I/U$, it follows that $P = G * U^2$. Here U is the effective value of the AC voltage ($U = U_{eff} = U_{(Peak-Peak)}/\sqrt{2}$).

The conductance was determined at the impedance analyzer. Since this can only provide bias voltages of up to 40 V, the conductance was measured at the respective frequency for bias voltages of 0 V to 40 V and a value for 60 V was extrapolated from this. This value is $G_{\text{PEEK}} = 2.73 \, \text{mS}$ for the CMUT chip encapsulated with silicone and a PEEK foil at $f = 4.68 \, \text{MHz}$ and $G_{\text{Ti}} = 2.00 \, \text{mS}$ for the CMUT chip encapsulated with silicone and a titanium foil at $f = 4.76 \, \text{MHz}$. This applies to the electrical performance of the CMUT chip encapsulated with silicone and PEEK:

$$P_{electric,PEEK} = 2.73 \, \text{mS} * \left(\frac{10 \, \text{V}}{\sqrt{2}} \right)^2 = 136.5 \, \text{mW} \tag{5.5}$$

and for the chip encapsulated with silicone and titanium:

$$P_{electric,Ti} = 2.00 \, \text{mS} * \left(\frac{10 \, \text{V}}{\sqrt{2}} \right)^2 = 99.80 \, \text{mW} \tag{5.6}$$

For efficiency, this results in:

$$\eta_{PEEK,4.68 \, MHz} = \frac{P_{acoustic}}{P_{electric}} = \frac{37.37 \, \text{mW}}{136.5 \, \text{mW}} = 27.38\% \tag{5.7}$$

$$\eta_{Ti,4.76 \, MHz} = \frac{P_{acoustic}}{P_{electric}} = \frac{3.85 \, \text{mW}}{99.8 \, \text{mW}} = 3.86\% \tag{5.8}$$

5.4.5 Ex vivo experiments

After characterizing the acoustic parameters of CMUT chips with different encapsulations in water, transmission measurements were performed ex vivo for the encapsulation found to be the best, which is a combination of a silicone layer and a PEEK foil. Instead of the previously used fluids, Fluorinert FC-72 and water, chicken breast muscle was used as the transmitted medium in order to approximate the conditions in the experimental setup more closely to the later planned application in the human body. For the ex vivo experiments, CMUT chips encapsulated with silicone and PEEK foil were used for both, receiving and emitting the ultrasonic waves. Measurements were made at distances of 35 mm and 60 mm. A bias voltage of $60\,V_{DC}$ and an AC signal consisting of 25 sinusoidal cycles with an amplitude of $10\,V_{AC}$ were used for excitation. The frequency of the AC signal was varied in the frequency range between 500 kHz and 5 MHz, as in the measurements in liquid. Figure 5.42 shows a photo of the experimental setup.
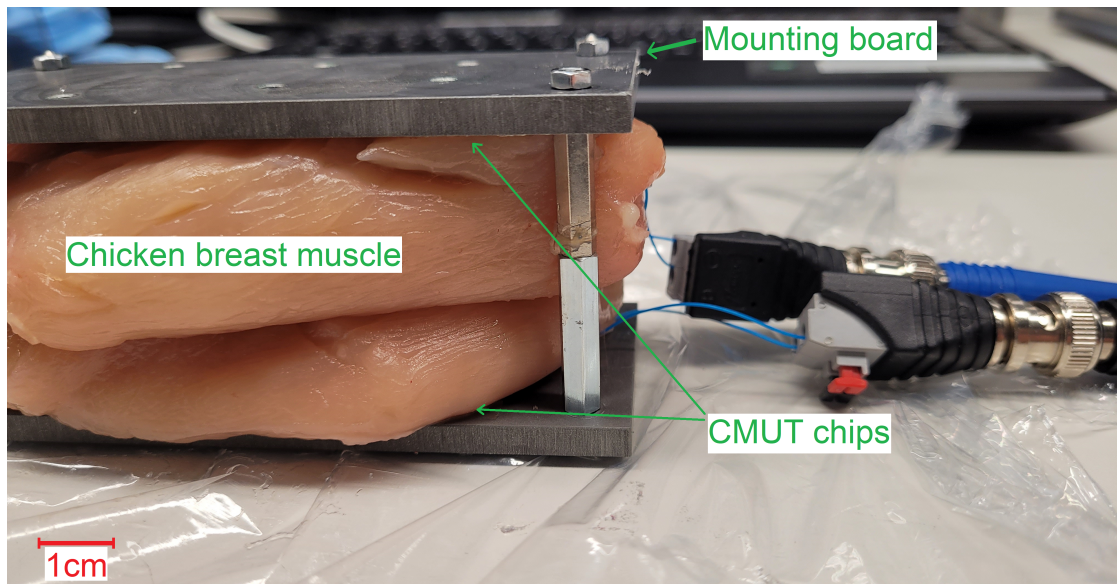
Figure 5.42: Experimental setup for ex vivo experiments with chicken breast muscle.

Note: Some of the results presented here were published in a similar form in the Sensors Journal of MDPI Publishing (see [101]).

Figure 5.43 shows the RMS amplitude of the received signal recorded for transmission distances of 35 mm and 60 mm. The attenuation of the transmitted tissue causes the amplitude of the received signal to be larger for all frequencies at a distance of 35 mm than at a distance of 60 mm. The fundamental frequency response is not changed by the change of the distance. Figure 5.43 thus shows that acoustic communication over at least 60 mm is possible with the investigated encapsulation strategy.
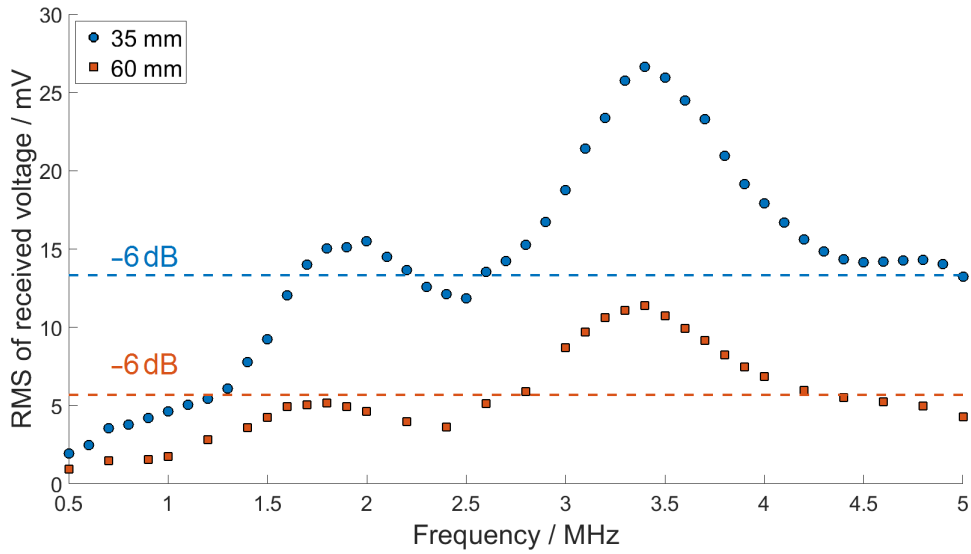
Figure 5.43: Receiving spectra of ex vivo experiments. Setup: $60\,V_{DC}$, $15\,V_{AC}$, burst count 25, silicone and PEEK covered CMUT chips for transmit and receive for distances of 35 mm and 60 mm.

Both curves show maxima at 1.9 MHz and 3.4 MHz. The cause of these maxima can be found in the experimental setup.

To ensure good coupling of the CMUT chips to the muscle tissue, the tissue was compressed by the two CMUT chips. This in return causes the muscle tissue to push on the encapsulated CMUT chips, which changes their oscillation behavior. In contrast, in the later use of the CMUT within the housing of a medical implant in a human body, no such high pressure on the surface of the CMUT chips is to be expected, so that the maxima, if they occur at all, are much weaker. Since the drop between the two maxima is bigger than $-6\,dB$, the prominence of the maxima leads to a reduction of the bandwidth, which is now 63%.

Although the goal of a bandwidth of 100% was thus not achieved, the bandwidth is still large enough to ensure efficient data transmission. Especially since the frequency behavior for the measurement at a distance of 35 mm would also allow the use of two different frequency bands (1.65 MHz to 2.2 MHz as well as 2.6 MHz to 5.0 MHz) around the two maxima.

Figure 5.44 confirms the high signal quality of the CMUT chips encapsulated with silicone and PEEK in the ex vivo experiment showing the receive signals at $f = 1.8\,MHz$ for both distances. At both distances, the CMUT chips are shown to react within three sinusoidal cycles on a change of the excitation signal. In Figure 5.44, the transient oscillation after turning on the AC signal is prominent for the first two cycles.
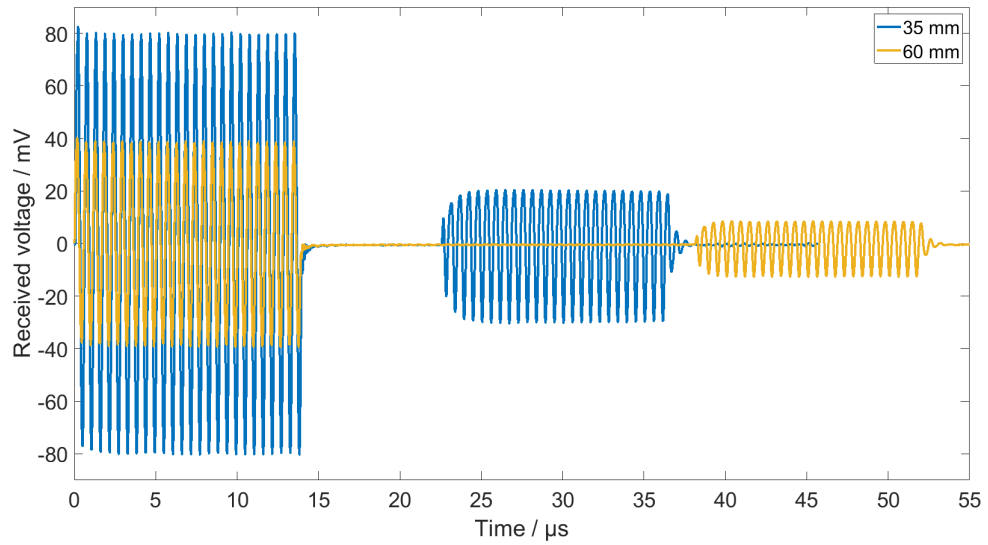
Figure 5.44: Received voltage signal ex vivo for f=1.8 MHz. CMUT chips encapsulated with silicone and PEEK for transmit and receive. Excitation: $60\,V_{DC}$, $10\,V_{AC}$, 25 sinusoidal cycles.

When the AC voltage is switched off, ringing occurs also for only two cycles.

Comparing the signal amplitudes for both depths, the attenuation coefficient can be determined from the difference in distance $(60\,\text{mm} - 35\,\text{mm} = 25\,\text{mm})$. Thus, in the experiment conducted, the attenuation coefficient of the chicken breast muscle was found to be $1.13\,\text{dB/(cm\,MHz)}$. This value agrees very well with the literature. For instance, Nassiri *et al.* give an attenuation coefficient of $1.1\,\text{dB/(cm\,MHz)}$ for beef muscle tissue normal to the fibers [102].

The received signals shown in Figure 5.44 were normalized to their respective maximum and shifted in time (Figure 5.45) to calculate the Pearson correlation coefficient. The correlation coefficient of 99.76 confirms a high signal quality (fidelity).
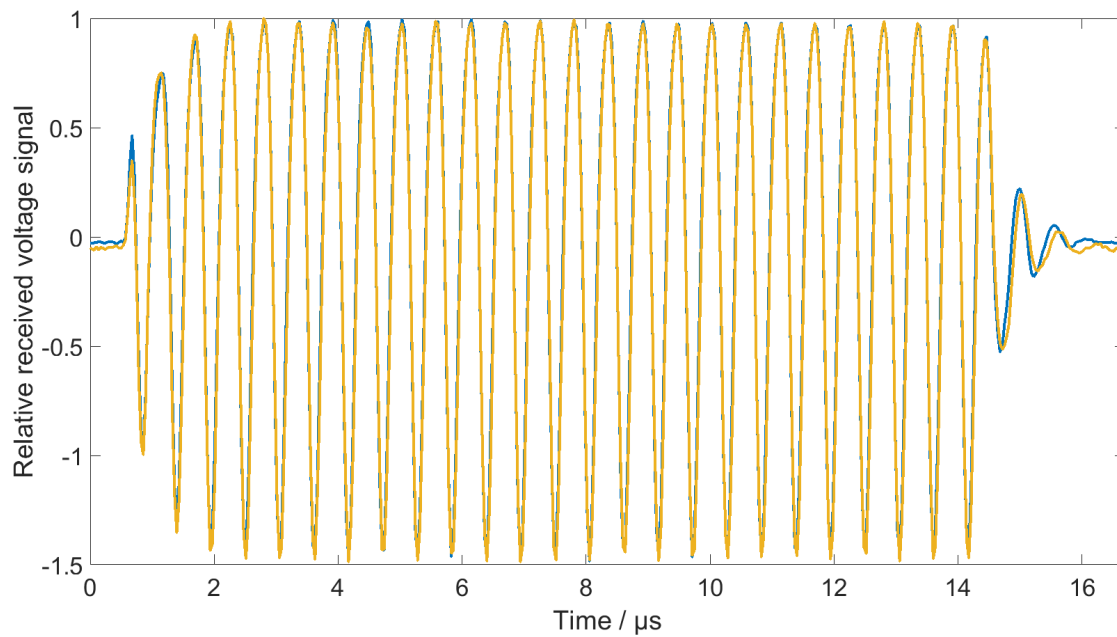
Figure 5.45: Received voltage signal ex vivo for f=1.8 MHz, normalized and shifted in time for correlation (resulting correlation coefficient: 99.76). CMUT chips encapsulated with silicone and PEEK for transmit and receive. Excitation: $60\,V_{DC}$, $10\,V_{AC}$, 25 sinusoidal cycles.

6 Discussion

The aim of this work was to examine approaches to encapsulate CMUTs to work within conventional housings of medical implants. For this, different encapsulations were examined with FEM simulations as well as with experiments. A novel encapsulation strategy based on two layers was developed. A soft silicone layer is applied directly to the CMUT membrane and supplemented by a foil made of PEEK or titanium to realize a stable and biocompatible encapsulation. Before optimizing and evaluating this new encapsulation approach, a CMUT was designed using the FEM tool PZFlex to have a center frequency of $2\,\mathrm{MHz}$ in water.

6.1 Optimization of the encapsulation approach

For the novel encapsulation strategy, the thicknesses of the surrounding layers were examined with FEM simulations. These simulations showed that the PEEK and titanium foils should be as thin as possible (see Figure 5.22). Thin PEEK and titanium foils were procured from OSYPKA AG (Rheinfelden, Germany), a medical technology company with experience in the encapsulation of implants. The thicknesses of the thinnest available foils are $t_{\mathrm{Ti}} = 32\,\mu\mathrm{m}$ and $t_{\mathrm{PEEK}} = 25\,\mu\mathrm{m}$. At sound velocities of $c_{\mathrm{Ti}} = 6100\,\mathrm{m/s}$ ([89]) and $c_{\mathrm{PEEK}} = 2536\,\mathrm{m/s}$ ([91]), wavelengths at $2\,\mathrm{MHz}$ are $\lambda_{Ti} = 3.05\,\mathrm{mm}$ and $\lambda_{PEEK} = 1.27\,\mathrm{mm}$. As the thicknesses of the foils are significantly less than the wavelengths in the material, the foils do not correspond to a $\lambda/4$-criterion. The foils should be as thin as possible to reduce their stiffness and increase the output pressure. However, the decisive factor for the thickness of the foils is to be large enough to ensure sufficient sealing for the intended application.

The thickness of the silicone layer between the CMUT membrane and the PEEK or titanium foil was optimized in FEM simulations with regard to a possibly large acoustic pressure generated by the CMUT. In contrast to the foils, the silicone layer should not be as thin as possible. While the optimal silicone thickness is $60\,\mu\mathrm{m}$ for the encapsulation with a PEEK foil, the optimal silicone thickness for the case of a titanium foil is $85\,\mu\mathrm{m}$. The experimentally determined sound velocity of the silicone was $c = 1000\,\mathrm{m/s}$. For a frequency of $2\,\mathrm{MHz}$ the wavelength within the silicone is $500\,\mu\mathrm{m}$ ($\lambda/4 = 125\,\mu\mathrm{m}$). Therefore, neither the foils nor the silicone layer correspond to a $\lambda/4$-criterion. Nevertheless, as optimal layer thicknesses could be found with regard to the pressure output, the CMUT membrane with silicone and foil can be seen as composite oscillator. This also explains the difference in the ideal silicone layer thicknesses for a PEEK and a titanium foil.

The complete oscillating system consisting of CMUT membrane, silicone layer, and foil has to be considered in the design process. Due to the small thicknesses of the encapsulating layers with respect to the wavelengths in these materials, there is no wave propagation in the single layers. A larger thickness of the silicone layer within this composite oscillator leads to an increased weight and an increased damping of the membrane. If the thickness of the silicone layer is decreased, the larger stiffness of the PEEK or titanium foil dominates the oscillation behavior, also increasing the damping. This makes it possible to find an ideal thickness of the silicone layer with respect to the acoustic pressure that is generated by the system. Titanium ($Y = 114.17\,\text{GPa}$, [89]) has a larger elastic modulus than PEEK ($Y = 4.21\,\text{GPa}$, [91]). Consequently, titanium has a larger stiffness, which is why the FEM simulations resulted in a larger optimal silicone thickness.

6.2 Laser vibrometry of uncoated CMUTs in air

Initial laser Doppler vibrometer measurements with the uncoated CMUTs in air showed that the CMUT cells exhibit a large number of different resonance peaks in the examined frequency range from $5\,\text{MHz}$ to $20\,\text{MHz}$ (see Figure 5.9). The largest peaks for each cell were found between $9.4\,\text{MHz}$ and $14.2\,\text{MHz}$. The differences to the simulation result ($f_{R,Sim} = 8.51\,\text{MHz}$) are mainly due to the insertion of layer stresses in the silicon nitride membrane during the deposition process (see Section 5.2.1). The same reason can be given for the deviation of the center frequency from cell to cell. Although the simulation did not exactly match the resonance frequency of the CMUT chip found experimentally, it is in the same order of magnitude.

6.3 Transmit experiment of uncoated CMUTs in Fluorinert FC-72

Due to the aluminum electrodes on top of the membranes of the CMUTs, measurements in water were not possible before coating. Instead, Fluorinert FC-72 was used as liquid for the first immersion experiments. The frequency spectra measured with an excitation of $60\,\text{V}_{DC}$, $10\,\text{V}_{AV}$ and 20 sinusoidal cycles revealed a center frequency of $3.28\,\text{MHz}$ for the uncoated CMUT chip. The center frequency measured in Fluorinert is above the target frequency of $2\,\text{MHz}$ aimed at in the simulation assisted adaption of the design.

However, this target frequency was not a critical threshold and achieving it is not crucial for a successful use of the CMUTs in the application. The target frequency was a compromise that resulted from the aim of the widest possible signal range (for which a low frequency is advantageous) and the aim of a possibly short pulse length and thus a large data rate. Since the increased attenuation resulting from the higher frequency allows a measured data transmission over the targeted distance of $6\,\text{cm}$, it is advantageous for

the center frequency of the CMUTs to be higher than planned, since this increases the achievable data rate.

As described in Section 5.2.3, the main objective of this work was the examination of different encapsulations of conventional CMUTs. The observed deviation of the actual resonance frequency from the simulated or targeted one had therefore only a minor relevance for this work.

The FEM model was successfully calibrated using the pre-existing cell design LA5. Here, the simulation results agreed very well with the measurements, so that the material parameters were assumed to be correctly defined in the simulation model. The development of the new cell design was based on this calibrated FEM model. Consequently, the deviation of the resonance frequency between simulation and experiment is not due to faulty material parameters. Instead, it is a result of process variables that are not known to the author as fabrication has been done by an external company.

Deviations between simulation and experiment due to residual stresses are a common problem and have been reported before by other research groups. Recently, Yu *et al.*, Zhang *et al.*, and Krenkel *et al.* found a larger resonance frequency in the experiment than estimated by simulation [98][103][104]. Krenkel *et al.* report the resonance frequency to be 18% larger in experiment than predicted by their FEM model [104]. All of them explain the deviations at least partly with the occurrence of tensile stress. Havreland *et al.* were able to show that the accuracy of their simulation model could be increased by taking into account the residual stress induced in the fabrication process [61]. Similarly, Adelegan *et al.* stated that they are considering stress stiffening effects in the design [105].

6.4 Dielectric charging of the CMUT cells

In Section 5.2.2, it was found that the CMUTs used in this work show a significant charging effect. Applying a DC voltage of 60 V leads to charge carriers accumulating in the insulation layers [98]. By that, an electrical field opposite to the one induced by the bias voltage is generated, reducing the effectively applied DC voltage. In the experiment (see Figure 5.15), this results in a decrease of the received signal by 60% within the first 100 min of continuously applying the DC voltage. After these 100 min a steady state is reached and the signal amplitude remains constant. Consequently, the CMUTs were charged for at least 120 min (including an additional safety buffer of 20 min) before starting the experiments to avoid the charging effect.

The presented measurement procedure is necessary for the characterization of the CMUT chips but not for later applications. Short signals can be used for communication between medical implants, so that the transmission duration is only a few seconds and a distortion due to the charging effect as it would occur in the transmission experiments lasting

20 min to 45 min is not to be expected. To maintain the full performance of the CMUTs in the implant, there are two possibilities. On the one hand, the bias voltage could be switched on only at times when a signal is to be transmitted or received, and on the other hand, the DC voltage could regularly be inverted (for example every minute) to counteract the accumulation of charge carriers in the insulation layers.

While these procedures are reducing the problem for the current CMUTs, the charging effect is a good starting point for future improvements of the system. Mahmud *et al.* presented the possibility to introduce insulating glass spacers into the cavities of the CMUTs to reduce the charging effect [106]. Munir *et al.* suggest optimized fabrication procedures as well as an optimized material choice for the insulation layer to reduce the charging effect [107]. A different approach to deal with the charging effect is presented by Kawasaki *et al.* who exploit this effect to enable an operation of the CMUTs without applying a DC voltage at the same time [108]. Having the same approach, Choi *et al.* published a comparison between insulation layers made of SiO_2 and Si_3N_4 [109]. They found that a layer of Si_3N_4 needs more time to discharge than a layer of SiO_2. Consequently, fabricating CMUTs with a different insulation material could also be used to reduce the charging effect.

6.5 Effects of different compositions of DC and AC voltage

In Section 5.3, the effect of different compositions of DC and AC voltage that result in the same total voltage were examined in both, FEM simulation and experiment. As a result, it could be shown that for a given total voltage, the generated acoustic pressure is maximum if no bias voltage is applied and a larger AC voltage is used instead.

In laboratory operation, but especially for the use of CMUTs in the human body, the application of large AC voltages has the disadvantage, that additional protective measures are necessary (cf. DIN VDE 0100-410 and Section 5.3). In order to avoid these protective measures and to ensure an approximately linear operation of the CMUTs [110], the following experiments were therefore carried out with the maximum permitted DC voltage of 60 V (according to DIN VDE 0100-410) and a significantly lower AC voltage of 15 V. However, the results of Section 5.3 indicate a possible way to increase the output of the CMUTs if needed.

6.6 Encapsulation results

Different encapsulations and their effect on the acoustic characteristics of CMUTs were examined in FEM simulation and experiment (see Section 5.4). CMUT encapsulations described in the literature are made of PDMS or parylene-C and are not suitable for long-term use in medical implants (see Section 3.5). Consequently, encapsulations with these materials were only used for comparison with the state of the art in this work.

Due to a limited amount of CMUT chips available as well as failures of some chips after the encapsulation, only a small number of encapsulations could be realized for experimental verification. Still, all configurations found in the simulation could be verified experimentally. In order to investigate the influence of random uncertainties in the process of encapsulation, e.g. deviations in the thickness of the cured silicone, the experiments carried out need to be repeated in future work with a larger number of identically encapsulated chips.

6.6.1 Simulation

FEM simulations of a single CMUT cell with a silicone layer and a PEEK or titanium foil on top showed that the displacement of the foil and thus the generated acoustic pressure could be significantly increased by optimizing the thickness of the silicone layer. A layer thickness of a few micrometers would be sufficient to attach the foil to the CMUT membrane. However, the displacement of the foil in response to a single sine burst of amplitude $15\,$V is substantially less in this case compared to the one of a silicone layer thickness of $60\,\mu$m (PEEK foil) or $85\,\mu$m (titanium foil). For the case of a PEEK foil, the average foil displacement increases by a factor of 2.35 if a silicone layer with an ideal thickness of $60\,\mu$m instead of $5\,\mu$m is applied. For the titanium foil, the amplitude of the foil displacement increases by a factor of 1.96 if a silicone thickness of $85\,\mu$m instead of $5\,\mu$m is used. Consequently, silicone layer thicknesses in this order of magnitude should have been realized. Due to the limited amount of CMUT chips available as well as due to limitations of the encapsulation process, the thickness of the actual silicone layer after curing could not be adjusted accurately and was $50\,\mu$m for both foil materials.

As the magnitude of the implemented layer thickness is in good agreement with the desired thickness, it is to expect that the basic characteristics of the CMUT chips encapsulated in this way correspond to those of a CMUT encapsulated with the silicone layer thickness found to be ideal in the simulations. Nevertheless, the simulation results suggest that the oscillation amplitude of the encapsulated CMUT chip, and thus the generated acoustic pressure, could be further increased in future work by using a process that allows a more precise adjustment of the thickness of the silicone layer during deposition.

6.6.2 Laser Doppler vibrometry

The oscillation behavior of CMUT chips encapsulated with different materials and encapsulation approaches was determined in Section 5.4.2. It was confirmed that an encapsulation with a thin layer of parylene-C has only minor effects on the frequency spectrum of a CMUT in air (see Figure 5.24). This is in good agreement with findings from other groups (see Section 3.5). The deviations between the frequency spectra of the uncoated chip and the chip coated with parylene-C can be explained by stress in the membrane and manufacturing tolerances of the CMUT.

All other chips are encapsulated with a silicone layer, some with an additional foil. They show a larger deviation from the frequency spectrum of the uncoated CMUT chip. In contrast to the encapsulation with a thin parylene-C layer, the silicone layer represents an additional load on the CMUT membrane. Similar to the use of CMUTs in immersion, this additional load shifts the resonance frequency toward lower frequencies as can be seen in Figure 5.24. The additional foil thus increases the resonance frequency of these three chips. By applying the foil, the CMUT chip becomes a synchronized composite oscillator. The lower resonance frequency in air for the encapsulation with a titanium foil (1.24 MHz) compared to the one with a PEEK foil (1.59 MHz) can be explained with the bigger weight of the titanium foil, which results from the combination of its higher density and larger thickness. Analogous to the decrease of the resonance frequency when changing the propagation medium from air to water, the additional load due to the titanium foil on the CMUT also results in a decrease of the resonance frequency (see Section 2.2.2).

6.6.3 Immersion experiments in Fluorinert FC-72

The results from transmit experiments in Fluorinert FC-72 (*3M*, St. Paul, USA) are described in Section 5.4.2. Using a calibrated hydrophone (RP acoustics, Leutenbach, Germany, type s), the acoustic pressure generated by the encapsulated CMUT chips was measured in the frequency range from 500 kHz to 5 MHz. In contrast to the results of the laser Doppler vibrometry measurements, the encapsulation with a silicone layer gives significantly lower deviations from the characteristics of the uncoated CMUT chip than the encapsulation with parylene-C in this experiment. Here, the additional load on the membrane due to the silicone has a similar effect as the Fluorinert FC-72. Consequently, the encapsulation results in only a minor reduction of the acoustic pressure without inducing any frequency shift. Unlike in the vibrometry measurements in air, the parylene-C encapsulation results in a frequency shift toward higher frequencies in the transmit experiments in Fluorinert. This effect can be explained by the larger thickness of the CMUT membrane including the additional parylene-C layer.

An encapsulation with silicone and a PEEK foil results in a slight shift of the frequency spectrum towards higher frequencies. A similar behavior but with additionally much lower acoustic pressures can be found for the chip encapsulated with silicone and a titanium foil. The lower acoustic pressures for the encapsulation using a titanium foil can be explained with the larger Young's modulus of the titanium, resulting in a larger stiffness of the foil. The frequency shift in both cases is caused by the formation of a composite oscillator.

Figure 5.25 shows that deviations between different measurements of the same chip are significantly larger for high frequencies than for low frequencies. This is caused by the frequency-dependence of the hydrophone sensitivity, which decreases for frequencies above 3.5 MHz so that noise becomes more prominent. The experiments in Fluorinert FC-72 show that the novel encapsulation approaches consisting of silicone and foil in-

crease the bandwidth of the CMUT (see Table 5.2).

6.6.4 Immersion experiments in water

Following the transmit experiments in Fluorinert FC-72, transmit experiments were conducted in water (see Section 5.4.2). With its sound velocity of about $1500\,m/s$, water mimics the acoustic properties of the human body much better than Fluorinert FC-72 ($512\,m/s$). Due to the electrical conductivity of water, the uncoated CMUT chip could not be used here.

Transmit characteristics

Figure 5.27 and Figure 5.28 show that all CMUT chips show a higher resonance frequency when driven in water instead of Fluorinert FC-72. This is due to the larger density of Fluorinert FC-72 ($1680\,kg/m^3$, [97]) in comparison to water ($1000\,kg/m^3$). The larger density results in a bigger load on the CMUT membrane, decreasing the resonance frequency (see Section 2.2.2).

As the sensitivity of the hydrophone used for these measurements decreases notably for frequencies above $5\,MHz$, the results for these frequencies are dominated by noise. In Figure 5.28 all CMUT chips show maxima at around $4.06\,MHz$ as well as at around $4.70\,MHz$, indicating that the different examined encapsulation approaches do not result in a large frequency shift. It can be seen that the encapsulation using silicone and a titanium foil results in significantly lower acoustic pressures. The CMUT encapsulated with silicone and a PEEK foil generates an acoustic pressure of $23.66\,kPa$ at its main resonance frequency ($4.68\,MHz$) whereas the CMUT encapsulated with silicone and a titanium foil generates an acoustic pressure of $6.83\,kPa$ (at $4.76\,MHz$). The difference regarding the output pressure can be explained by the larger stiffness of the titanium foil, making a larger force and consequently larger applied voltages necessary to produce the same output. The differences between these two chips with respect to the resonance frequency are considered as not significant.

Figure 5.27 shows that an encapsulation with silicone and a PEEK foil has comparable effects on the acoustic properties of the CMUT as the commonly used encapsulations consisting of a thin layer of parylene-C or PDMS. This demonstrates that the examined new strategy for encapsulation is able to cope with the literature standard for conventional applications. In contrast to the encapsulation approaches known from the literature, the approach presented here has the decisive advantage that titanium and PEEK are already in use in medical implants and their ability to provide biocompatible encapsulation has already been demonstrated.

Besides that, for frequencies up to $4.78\,MHz$ the encapsulation using silicone and a PEEK foil consistently gives larger pressures than the parylene-C coating.

For frequencies above 2.94 MHz, the generated acoustic pressures of the silicone and PEEK encapsulated chip are also above those of the chip encapsulated with silicone only (see Figure 5.27).

The encapsulation consisting of silicone and a titanium foil also has only a minor influence on the resulting frequency spectrum of the CMUT chip but the generated acoustic pressures are significantly lower. Thus, the encapsulation with a titanium foil is clearly inferior to an encapsulation with a PEEK foil due to larger stiffness of the titanium.

The available hydrophones suffer from low sensitivity for frequencies above 5 MHz. Consequently, the received signals are increasingly dominated by compensation artifacts after calibrating with the receive sensitivity of the hydrophone. Thus, the receive amplitudes for frequencies above 5 MHz erroneously increase so that they do not decrease below the $-6\,\mathrm{dB}$ limit and no bandwidth can be specified for the transmit mode (see Section 5.4.2).

Receive characteristics

As final step of the transmit experiments in water, the receive sensitivity of the CMUT chips encapsulated with parylene-C as well as silicone and foil was examined. The CMUT chip without coating could not be used here. For this experiment, the CMUT chip encapsulated with silicone was used as transmitter and the other three differently encapsulated chips were used as receivers.

Figure 5.29 and Figure 5.30 show that all encapsulations result in very similar frequency spectra with the parylene-C encapsulation having the best receive sensitivity. The reason for this is the significantly thicker encapsulation of the chips encapsulated with silicone and foil compared to the encapsulation with only a thin parylene-C layer. This leads to greater attenuation in receiving mode, reducing the signal amplitude. Similar to the transmit mode, an encapsulation with silicone and a PEEK foil is superior to an encapsulation with silicone and a titanium with respect to the signal amplitude. In the receiving voltage spectra (Figure 5.29), bandwidths of 4.2 MHz are found for both encapsulations consisting of silicone and foil. This corresponds to a FWHM bandwidth of 129% for the encapsulation using silicone and a PEEK foil and 149% for the encapsulation using silicone and a titanium foil. These bandwidths are very promising for an effective communication. Figure 5.29 is the most important result of the transmit experiments in immersion as it shows the voltage amplitude that can be transmitted from one encapsulated CMUT to another. Thus, this experimental setup agrees best to the use of the CMUTs in the application.

To calculate the receive sensitivity of the encapsulated CMUT chips, the transmit sensitivity of the CMUT chip encapsulated with a silicone layer needs to be taken into account. As this is noisy for frequencies below 1.2 MHz, the resulting receive sensitivities suffer from noise in this frequency range too (see Figure 5.30). In contrast to the transmit sensitivity, no clearly distinguishable local maxima can be found in the receive sensitivity of the encapsulated CMUT chips. Apart from this, the encapsulated CMUT chips

show the largest sensitivity in receiving mode for low frequencies and decrease towards higher frequencies. The receiving behavior is thus contrary to the transmit case.

It is important to notice, that neither the pure transmit sensitivity nor the pure receive sensitivity is essential for the desired application of communication between two CMUTs. In fact, the crucial aspect is the superposition of these two sensitivities, which results in frequency spectra as shown in Figure 5.29.

6.7 Fulfillment of the specifications based on the ex vivo experiments

The aim of this thesis was to develop an encapsulation strategy for the use of CMUTs in medical implants and to characterize its effect on the acoustic properties of the CMUT. The decisive factor was thereby that the CMUT should be integrated into a conventional implant housing. For this purpose, specifications were developed, that are important for a successful use of the CMUTs. To approximate the situation inside the human body for the examination of the different encapsulations, ex vivo experiments were conducted using chicken muscle tissue. As shown in the following, the fulfillment of the specifications developed at the beginning of this work could be confirmed in the essential points in the ex vivo experiments.

6.7.1 Frequency

One goal was to design a CMUT with a center frequency of 2 MHz when operating in the human body. In the final ex vivo measurements, CMUT chips coated with silicone and PEEK foil were used for both, the transmitter and the receiver. The main resonance was found to be at 3.4 MHz. In addition, a further maximum was found at 1.9 MHz (see Section 5.4.5). The center frequency of the CMUT chips encapsulated with silicone and a PEEK foil is 3.8 MHz. The target frequency of 2 MHz was not crucial but a compromise of the widest possible signal range and a possibly short pulse length (see Section 6.3). Thus, the higher center frequency of the encapsulated CMUT chips is not a problem as signal transmission over a distance of 6 cm was possible at this frequency (see Section 6.7.4).

6.7.2 Bandwidth

The objective was a FWHM bandwidth of 100%. In the ex vivo experiments, a FWHM bandwidth of 63% (2.4 MHz) was determined. This is a result of the occurrence of additional minima resulting from the pressure caused by pushing the CMUTs against the muscle tissue. With an encoding of 1 bit/Hz, this bandwidth results in a data rate of 2.4 Mbps. Assuming a more conservative encoding of three pulses per bit results in a data rate of 0.8 Mbps. The achievable data rates thus match the state of the art in

data transmission by ultrasound presented in Section 3.1. For applications that require a higher data rate, this could be significantly increased if pulse coding is used with suitable electronics. In addition to a frequency coding of the signal, the signal amplitude could also be modulated. Thus, the data rate could, e.g., be increased by a factor of eight from 0.8 Mbps to 6.4 Mbps by using 8-bit amplitude modulation. As described in Section 5.4.5, the frequency spectrum shown in Figure 5.43 additionally offers the possibility to work in a second frequency band (1.65 MHz to 2.2 MHz) to further increase the possible data rate.

Goodarzy *et al.* provided a list of data rates for widely used biomedical implants [111]. According to them, retinal implants are realized with data rates of 40 Mbps, brain-machine interfaces and wireless capsule endoscopes are used with data rates of 1 Mbps to 10 Mbps, and monitoring can be done with less than 10 Kbps. Accordingly, the data rates of 0.8 Mbps to 6.4 Mbps realized with encapsulated CMUTs in this thesis are sufficient for most applications where medical implants are used.

It can be assumed that the pressure of the surrounding tissue on the CMUT is lower for the use within a medical implant. Consequently, the higher modes that occurred in the ex vivo experiment should be less prominent and bandwidths like in the immersion experiments could be achieved.

To further increase the bandwidth of the CMUT chips before encapsulation, Liu *et al.* achieved promising results by using more than one membrane radius on a single CMUT chip and by varying the bias voltage [112]. It is to be expected that a larger initial bandwidth results in an increased bandwidth of the encapsulated CMUT chip. Consequently, larger data rates could be realized by using optimized CMUT chips.

6.7.3 Electrical excitation

In accordance with the DIN VDE 0100-410 standard, the excitation of the encapsulated CMUTs was targeted in the specifications to not exceed $25\,V_{AC}$ and $60\,V_{DC}$. As in the experiments described in this thesis a bias voltage of $60\,V_{DC}$ and an AC voltage of $10\,V_{AC}$ or $15\,V_{AC}$ were used to successfully transmit signals over a distance of 6 cm ex vivo, this specification was achieved.

The experimental results presented in this thesis were obtained with fully charged CMUTs (see Section 5.2.2). This implies that in applications, where the bias voltage is applied only for a few seconds or where it is regularly reversed in its polarity, significantly larger signal amplitudes can be expected, enabling an operation with less bias voltage. The results presented in Section 5.3 for different compositions of the total applied voltage show another possibility for reducing the bias voltage, if desired. Thus, the bias voltage could be reduced at the expense of a higher AC voltage.

6.7.4 Transmission path

A transmission distance of 6 cm was specified. It could be shown experimentally that transmission ex vivo is possible over this distance (see Section 5.4.5). At a depth of 6 cm, receive voltages of 11.4 mV (RMS) could be measured for resonant excitation (f = 3.4 MHz). For applications requiring larger signals or penetration depths, there are three possibilities to increase the signal amplitude.

First, it has to be considered that the CMUTs were used in a fully charged state (see Section 5.2.2). Due to the accumulation of charge carriers in the insulation layers of the CMUT cells, an opposing field is generated, decreasing the effective bias voltage. This phenomenon leads to the generation of significantly lower pressures in the conducted experiments. As can be seen in Figure 5.15, dielectric charging causes the received voltage in the transmission setup to decrease by 60%. If a DC voltage is only applied to the CMUTs for a short time, this charging effect is much lower, so that the amplitude of the received signal should increase by about 250% and larger distances could be covered.

Another option to increase the acoustic performance of the CMUTs is to use a larger excitation voltage. If 25 V_{AC}, the maximum AC voltage allowed regarding the DIN VDE 0100-410 standard, is used instead of only 10 V_{AC} as used in this work, a large increase of the generated pressures and thus also in the amplitude of the received signal can be expected (see Section 5.3).

Finally, the thickness of the silicone layer could be optimized. Due to limitations of the encapsulation process, the silicone layer thickness found to be ideal in FEM simulation in terms of acoustic pressure could not be realized for the prototypes. Using a different process enabling better accuracy in setting the silicone thickness could further increase the output pressure and by that the penetration depth.

6.7.5 Conclusion

The aim to develop an encapsulation strategy for the use of CMUTs within a conventional housing for medical implants was fulfilled. Immersion experiments in water and ex vivo on chicken muscle tissue demonstrated that using a silicone layer with an overlying foil of PEEK results in only minor effects on the acoustic characteristics of the CMUT. It was demonstrated in particular that this encapsulation has a positive effect on the amplitude of the transmitted signal in water as it results in larger acoustic pressures in the frequency range from 2.94 MHz to 4.82 MHz (see Figure 5.28).

6.8 Approach for further optimization

The results of this work proved that an encapsulation consisting of a silicone layer and a foil made of PEEK is well suited to integrate conventional CMUTs into conventional housings of medical implants. For a further optimization of the system, especially with

regard to the receiving properties of the encapsulated CMUT (see Figure 5.29), it would be beneficial if the oscillating membrane is brought into direct contact with the surrounding tissue to be sonicated. This idea is supported by the observation that the CMUT chip encapsulated with a parylene-C layer detected larger voltage amplitudes in the receiving mode than the chips encapsulated with silicone and foil. To realize this and thus prevent mechanical losses within the composite oscillator consisting of membrane, silicone, and foil, the CMUT membrane could be made directly from PEEK instead of the materials mainly used today, silicon and silicon nitride. By applying the top electrode on the bottom side of the PEEK membrane, the need of an additional encapsulation can be avoided. Although no research results on CMUTs fabricated using a PEEK membrane have been published so far, there are some publications presenting the successful fabrication and characterization of CMUTs with a polymer-based membrane (see Section 3.4 and reference [68]). To estimate the dimensions of a CMUT with a PEEK membrane having a resonance frequency of 2 MHz, the Young's modulus (E = 4.21 GPa, [91]) and Poisson's ratio ($\nu = 0.388$, [91]) of PEEK can be used to calculate the radius of a PEEK membrane with a given thickness. According to Equation (2.26), for a membrane thickness of 25 µm, which is the thickness of the PEEK foil used for encapsulation in this work, this results in a radius of 107.33 µm. Thus, the CMUT cells become larger than those used in this work. However, since even polymer CMUTs with membrane diameters of up to 1 mm have already been successfully fabricated, a diameter of 214 µm can be considered feasible [113].

7 Conclusion

In this thesis, encapsulation approaches for the use of conventional CMUTs within the human body were examined. First, a simulation model was developed using the FEM tool PZFlex. The model was adapted to a preexisting CMUT design, to enable an evaluation and optimization of the simulation model. The preexisting CMUT chips were characterized using laser Doppler vibrometry and impedance spectroscopy. Afterwards, the simulation model was adjusted in terms of meshing and material properties to match with the experimental results.

The verified simulation model was then used to design CMUTs for a broad bandwidth and a resonance frequency in water of $2\,\text{MHz}$. The resulting CMUT design consisted of a Si_3N_4 membrane with a thickness of $600\,\text{nm}$ and edge lengths of $80\,\mu\text{m} \times 40\,\mu\text{m}$. An aluminum electrode of thickness $250\,\text{nm}$ and edge lengths of $56\,\mu\text{m} \times 28\,\mu\text{m}$ is placed on top of the Si_3N_4 membrane. The cavity height was $200\,\text{nm}$. The fabricated CMUT chips had edge lengths of $5\,\text{mm} \times 5\,\text{mm}$. Each CMUT chip contained 3416 CMUT cells connected in parallel. The exposed aluminum top electrode prevented an evaluation of the CMUTs in water without encapsulation. Instead, the center frequency of the uncoated CMUT chips was determined in Fluorinert FC-72 and found to be $3.28\,\text{MHz}$. Due to layer stresses occurring during the fabrication process, the target frequency of $2\,\text{MHz}$ could not be realized. As the CMUT fabrication was done by an external company, no further fabrication run was possible due to limited resources. In addition to the transmit experiments in Fluorinert FC-72, laser Doppler vibrometry scans and impedance spectroscopy were performed to characterize the new CMUT design.

In addition to the characterization of the CMUTs, effects of different compositions of DC and AC voltage were examined. FEM simulations as well as transmit experiments in Fluorinert FC-72 showed that the acoustic pressure generated by a CMUT is maximum for a given total voltage if the CMUT is excited without any DC bias voltage but with 100% AC voltage. As AC voltages above $25\,\text{V}$ require additional protective measures, operation with large AC voltages is not feasible. Instead, the experiments in this work were performed with a combination of $60\,\text{V}_{\text{DC}}$ and $10\,\text{V}_{\text{AC}}$ or $15\,\text{V}_{\text{AC}}$.

In a next step, a novel approach to encapsulate these CMUTs within conventional housings of medical implants was developed and characterized using the FEM tool PZFlex. This novel encapsulation combines an inner silicone layer with an outer layer of PEEK or titanium, two materials that are widespread for medical implants. The inner silicone layer is used to attach the outer layer and to increase the output pressure. The outer layer ensures sealing of the CMUT chip.

In terms of the acoustic pressure being generated, the silicone layer was shown in simulation to have an optimal thickness of 60 µm in combination with PEEK or 85 µm in combination with titanium. Commercially available foils with a thickness of 25 µm (PEEK) or 32 µm (titanium) were used for the experiments conducted in this thesis. In the later application, the foil is to be replaced by the housing of the medical implant. The large thickness of the housing of a medical implant would decrease the sensitivity of the CMUT. Consequently, the realization of the novel approach for the encapsulation of CMUTs is based on the idea of reducing the thickness of the wall of the housing of the medical implant. This reduction should be limited to the area to be sonicated in order to increase the acoustic energy being transmitted into the body without affecting the stability of the housing. As this part of the housing enables the transmission of acoustic waves, it is called acoustic window.

Transmit experiments were conducted in Fluorinert FC-72 and water to examine both novel encapsulations and to compare the results with those of standard encapsulations for CMUTs, consisting of a thin layer of parylene-C or PDMS. It could be demonstrated that the novel encapsulation strategy results in large bandwidths of up to 149% in water and leads only to minor changes in the frequency behavior of the CMUT chips. In a depth of 60 mm, hydrophone measurements in water for a bias voltage of 60 V and a resonant excitation using 10 sine cycles of 10 V resulted in acoustic pressures of 23.66 kPa for the encapsulation with silicone and PEEK, 6.83 kPa for the encapsulation with silicone and titanium, 20.98 kPa for an encapsulation with silicone, and 22.75 kPa for an encapsulation consisting of a thin layer of parylene-C. Thus, the novel encapsulation using a silicone layer and a PEEK-foil results in acoustic output pressures that are larger than those for state of the art encapsulations of CMUTs.

In receive mode instead, the CMUT chip encapsulated with a thin layer of parylene-C provided the largest received voltage signal. Similar to the transmit mode, the encapsulation using silicone and a PEEK-foil resulted larger signals than the encapsulation using silicone and a titanium foil.

To complete the experimental part, ex vivo experiments were performed on chicken muscle tissue. These experiments proved the ability of the novel encapsulation using silicone and a PEEK foil to transfer data on a distance of 6 cm. In these experiments, a bandwidth of 63% (2.4 MHz) was demonstrated. The corresponding data rate depends on the encoding. An encoding of three pulses per bit results in a data rate of 0.8 Mbps. Strategies to increase the feasible data rates by using two frequency bands or an amplitude coding were presented in Section 6.7.2.

To conclude: The novel encapsulation approach developed in this thesis enables high sensitivities and large bandwidths. Thereby, it has the potential to become the new standard for the encapsulation of CMUTs for medical communication in particular for applications in the human body.

8 Outlook

In this work, a new encapsulation approach for the use of conventional CMUTs in the human body was presented. Whereas the feasibility of this approach has successfully been demonstrated in general, further work is required before it can be used within the human body. An important step is to determine the layer thicknesses of PEEK and titanium that are necessary to ensure a fatigue-proof long-term sealing of the housing of the medical implant. Although no defects or fatigue phenomena were found for the foils used to encapsulate the CMUT chips in this work, an evaluation of the long-term stability within the human body is pending.

The experiments within this thesis were performed using laboratory equipment. Apart from a DC voltage supply and an AC voltage supply, an oscilloscope and a computer were used to record and evaluate the received signals. To integrate CMUTs into the housing of a medical implant, a miniaturization of the electronics is needed.

Regarding the CMUT design, the aim of a resonance frequency of $2\,\mathrm{MHz}$ could not be realized. Although the ex vivo experiments proved the ability to effectively communicate over a distance of at least $6\,\mathrm{cm}$, an adaption of the CMUT design could be done in the future. Thus, the simulation model could be adapted in a further iteration to match the experimental results. Subsequently, the cell design could then be re-adapted, fabricated and evaluated.

In the experiments presented in this thesis, a charging of the dielectric layer on the ground of the cavity occurred. As a consequence, the effectively applied bias voltage is reduced, resulting in a decreased sensitivity of the CMUTs in transmit and receive operation. To reduce this effect, efforts could be made to increase the quality of the insulation layers. Alternatively, the electronics used to drive the CMUTs could be extended by the ability to regularly invert the polarity of the bias voltage. By that, the accumulation of charge carriers in the insulating layer could be reduced significantly.

Finally, the performance of the acoustic communication system could be increased by fabricating CMUTs out of PEEK instead of using conventional CMUTs. By fabricating the CMUT membrane as well as the housing of the medical implant out of PEEK, the CMUT could directly be integrated into the housing of the medical implant. Thus, with the top-electrode placed on the inner side of the membrane, no silicone layer is needed and the CMUT membranes are in direct contact with the surrounding media. The encapsulation consisting of a thin layer of parylene-C resulted in larger receive sensitivities than the novel encapsulation approaches based on silicone and a foil.

Similarly, a CMUT with a PEEK-based membrane, that does not require an additional encapsulation, is expected to have a larger receive sensitivity.

Bibliography

[1] Reinhard Lerch, Gerhard Sessler and Dietrich Wolf. *Technische Akustik: Grundlagen und Anwendungen*. Springer Berlin Heidelberg, 2009. DOI: `10.1007/978-3-540-49833-9`.

[2] *Medical implant market: Information by type, by type of material, by end user, and region - global forecast till 2027*. Tech. rep. ID: MRFR/MED/2089-CR. Market Research Future, 2021.

[3] Assefa K. Teshome, Behailu Kibret and Daniel T. H. Lai. 'A review of implant communication technology in WBAN: Progress and challenges'. In: *IEEE Reviews in Biomedical Engineering* 12 (2019), pp. 88–99. DOI: `10.1109/RBME.2018.2848228`.

[4] Paul G. Newman and Grace S. Rozycki. 'The history of ultrasound'. In: *Surgical clinics of North America* 78.2 (1998), pp. 179–195. DOI: `10.1016/S0039-6109(05)70308-X`.

[5] M. I. Haller and B. T. Khuri-Yakub. 'A surface micromachined electrostatic ultrasonic air transducer'. In: *IEEE Transactions on Ultrasonics, Ferroelectrics, and Frequency Control* 43.1 (1996), pp. 1–6. DOI: `10.1109/58.484456`.

[6] Kevin Brenner et al. 'Advances in capacitive micromachined ultrasonic transducers'. In: *Micromachines* 10.2 (2019). DOI: `10.3390/mi10020152`.

[7] Michael Möser, Gerhard Müller and H. Kuttruff, eds. *Handbook of engineering acoustics*. 2013. DOI: `10.1007/978-3-540-69460-1_21`.

[8] Dieter Guicking. *Schwingungen: Theorie und Anwendungen in Mechanik, Akustik, Elektrik und Optik*. Springer Fachmedien Wiesbaden, 2016. ISBN: 9783658141363.

[9] Gordon Stanley Kino. *Acoustic waves: Devices, imaging, and analog signal processing*. Signal processing series. Englewood Cliffs: Prentice-Hall, 1987. ISBN: 0-13-003047-3.

[10] Francis A. Duck. *Physical properties of tissue: A comprehensive reference book*. London: Acad. Press, 1990. ISBN: 0-12-222800-6.

[11] Vladimir A. Šutilov. *Physik des Ultraschalls: Grundlagen*. Vienna: Springer Vienna, 1984. ISBN: 978-3-7091-8751-7. DOI: `10.1007/978-3-7091-8750-0`.

[12] Qing Zhang et al. 'Surface-micromachined CMUT using low-temperature deposited Silicon carbide membranes for above-IC integration'. In: *Journal of Microelectromechanical Systems* 23.2 (2014), pp. 482–493. DOI: `10.1109/JMEMS.2013.2281304`.

[13] Xiao Huang, Hongliang Wang and Lijun Yu. 'Investigation on design theory and performance analysis of vacuum capacitive micromachined ultrasonic transducer'. In: *Micromachines* 12.9 (2021), p. 1127. DOI: 10.3390/mi12091127.

[14] Jose Joseph, Bo Ma and B. T. Khuri-Yakub. 'Applications of capacitive micromachined ultrasonic transducers: A comprehensive review'. In: *IEEE transactions on Ultrasonics, Ferroelectrics, and Frequency Control* (2021). DOI: 10.1109/TUFFC.2021.3112917.

[15] W. Kuhl, G.R. Schodder and F.-K. Schröder. 'Condenser transmitters and microphones with solid dielectric for airborne ultrasonics'. In: *Acta Acustica united with Acustica* 4.5 (1954), pp. 519–532.

[16] Arif S. Ergun, Goksen G. Yaralioglu and Butrus T. Khuri-Yakub. 'Capacitive micromachined ultrasonic transducers: Theory and technology'. In: *Journal of Aerospace Engineering* 16.2 (2003), pp. 76–84. DOI: 10.1061/(ASCE)0893-1321(2003)16:2(76).

[17] B. T. Khuri-Yakub and Ömer Oralkan. 'Capacitive micromachined ultrasonic transducers for medical imaging and therapy'. In: *Journal of micromechanics and microengineering: Structures, devices, and systems* 21.5 (2011), pp. 54004–54014. DOI: 10.1088/0960-1317/21/5/054004.

[18] Alessandro Caronti et al. 'Capacitive micromachined ultrasonic transducer (CMUT) arrays for medical imaging'. In: *Microelectronics Journal* 37.8 (2006), pp. 770–777. DOI: 10.1016/j.mejo.2005.10.012.

[19] Da-Chen Pang and Cheng-Min Chang. 'Development of a novel transparent flexible capacitive micromachined ultrasonic transducer'. In: *Sensors (Basel, Switzerland)* 17.6 (2017). DOI: 10.3390/s17061443.

[20] Te-I Chiu et al. 'Implementation of ultrasonic touchless interactive panel using the polymer-based CMUT array'. In: *SENSORS, 2009 IEEE*. 2009, pp. 625–630. DOI: 10.1109/ICSENS.2009.5398325.

[21] Mario Baum et al. 'An improved design for 2D arrays of capacitive micromachined ultrasound transducers: Modeling, fabrication, and characterization'. In: *2018 IEEE International Ultrasonics Symposium (IUS)*. 2018. DOI: 10.1109/ULTSYM.2018.8579656.

[22] Libo Zhao et al. 'Fabrication of capacitive micromachined ultrasonic transducers with low-temperature direct wafer-bonding technology'. In: *Sensors and Actuators A: Physical* 264 (2017), pp. 63–75. DOI: 10.1016/j.sna.2017.07.044.

[23] Yongli Huang et al. 'Fabricating capacitive micromachined ultrasonic transducers with wafer-bonding technology'. In: *Journal of Microelectromechanical Systems* 12.2 (2003), pp. 128–137. DOI: 10.1109/JMEMS.2003.809968.

[24] Ayhan Bozkurt et al. 'Theory and analysis of electrode size optimization for capacitive microfabricated ultrasonic transducers'. In: *IEEE transactions on Ultrasonics, Ferroelectrics, and Frequency Control* 46.6 (1999), pp. 1364–1374. DOI: `10.1109/58.808859`.

[25] Y. Huang et al. 'Fabrication of capacitive micromachined ultrasonic transducers (CMUTs) using wafer bonding technology for low frequency (10 kHz - 150 kHz) sonar applications'. In: *OCEANS '02 MTS/IEEE*. Vol. 4. 2002. DOI: `10.1109/OCEANS.2002.1191991`.

[26] Xuecheng Jin, I. Ladabaum and B. T. Khuri-Yakub. 'The microfabrication of capacitive ultrasonic transducers'. In: *Journal of Microelectromechanical Systems* 7.3 (1998), pp. 295–302. DOI: `10.1109/84.709646`.

[27] J. Zahorian et al. 'Monolithic CMUT-on-CMOS integration for intravascular ultrasound applications'. In: *IEEE Transactions on Ultrasonics, Ferroelectrics, and Frequency Control* 58.12 (2011), pp. 2659–2667. DOI: `10.1109/TUFFC.2011.2128`.

[28] Arif Sanli Ergun et al. 'Capacitive micromachined ultrasonic transducers: Fabrication technology'. In: *IEEE Transactions on Ultrasonics, Ferroelectrics, and Frequency Control* 52.12 (2005), pp. 2242–2258. DOI: `10.1109/TUFFC.2005.1563267`.

[29] I. Ladabaum et al. 'Surface micromachined capacitive ultrasonic transducers'. In: *IEEE transactions on Ultrasonics, Ferroelectrics, and Frequency Control* 45.3 (1998), pp. 678–690. DOI: `10.1109/58.677612`.

[30] Ira O. Wygant, Mario Kupnik and B. T. Khuri-Yakub. 'Analytically calculating membrane displacement and the equivalent circuit model of a circular CMUT cell'. In: *2008 IEEE Ultrasonics Symposium*. IEEE, 2008, pp. 2111–2114. ISBN: 978-1-4244-2428-3. DOI: `10.1109/ULTSYM.2008.0522`.

[31] Ira O. Wygant, Mario Kupnik and B. T. Khuri-Yakub. 'An analytical model for capacitive pressure transducers with circular geometry'. In: *Journal of Microelectromechanical Systems* (2018), pp. 1–9. DOI: `10.1109/JMEMS.2018.2823200`.

[32] Arthur W. Leissa. *Vibration of plates*. Columbus, Ohio: Scientific, technical information division, National Aeronautics and Space Administration, 1969.

[33] Eduard Ventsel and Theodor Krauthammer. *Thin plates and shells: Theory, analysis, and applications*. New York: Marcel Dekker, 2001. ISBN: 9780203908723.

[34] Mohamed Bellaredj et al. 'Anodic bonding using SOI wafer for fabrication of capacitive micromachined ultrasonic transducers'. In: *Journal of Micromechanics and Microengineering* 24.2 (2014). DOI: `10.1088/0960-1317/24/2/025009`.

[35] Yu Hongbin, Lou Liang and Alex Gu Yuandong. 'Capacitive micromachined ultrasonic transducer (CMUT) based micro viscosity sensor'. In: *Sensors and Actuators B: Chemical* 227 (2016), pp. 346–351. DOI: `10.1016/j.snb.2015.12.061`.

[36] P. G. Ciarlet and J. L. Lions. *Handbook of numerical analysis. Finite element methods (Part 2), numerical methods for solids (Part 2)*. Vol. 4. Handbook of numerical analysis. Amsterdam u.a.: North-Holland, 1996. ISBN: 0444817948.

[37] M. J. Turner. 'Stiffness and deflection analysis of complex structures'. In: *Journal of the Aeronautical Sciences* 23.9 (1956), pp. 805–823. DOI: 10.2514/8.3664.

[38] Josef Betten. *Finite Elemente für Ingenieure 1: Grundlagen, Matrixmethoden, Elastisches Kontinuum*. Berlin, Heidelberg: Springer Berlin Heidelberg, 2003. ISBN: 3-540-20447-4. DOI: 10.1007/978-3-642-55536-7.

[39] Najib Abboud et al. 'Finite element modeling for ultrasonic transducers'. In: *Proc.SPIE* 3341 (1998), pp. 19–42. DOI: 10.1117/12.308015.

[40] G. L. Wojcik et al. 'Electromechanical modeling using explicit time-domain finite elements'. In: *1993 Proceedings IEEE Ultrasonics Symposium*. 1993, 1107–1112 vol.2. DOI: 10.1109/ULTSYM.1993.339594.

[41] James F. Epperson. *An introduction to numerical methods and analysis, second edition*. 2nd ed. Hoboken: Wiley, 2013. ISBN: 9781118367599.

[42] Michael Jung and Ulrich Langer. *Methode der finiten Elemente für Ingenieure: Eine Einführung in die numerischen Grundlagen und Computersimulation*. 1. Aufl. Wiesbaden: Vieweg+Teubner Verlag and Teubner, 2001. ISBN: 978-3-519-02973-1. DOI: 10.1007/978-3-663-10785-9.

[43] Michael Schäfer. *Computational engineering - introduction to numerical methods*. Berlin, Heidelberg: Springer-Verlag Berlin Heidelberg, 2006. ISBN: 9783540306856. DOI: 10.1007/3-540-30686-2.

[44] Claudio Mattiussi. 'A reference discretization strategy for the numerical solution of physical field problems'. In: *Electron microscopy and holography*. Ed. by Peter W. Hawkes. Vol. 121. Advances in imaging and electron physics. Elsevier, 2002, pp. 143–279. DOI: 10.1016/S1076-5670(02)80027-1.

[45] F.D. Molina-Aiz et al. 'Comparison of finite element and finite volume methods for simulation of natural ventilation in greenhouses'. In: *Computers and Electronics in Agriculture* 72.2 (2010), pp. 69–86. DOI: 10.1016/j.compag.2010.03.002.

[46] Vinod Kumar Khanna. 'Wireless communications and powering of implants'. In: *Implantable medical electronics: Prosthetics, drug delivery, and health monitoring*. Cham: Springer International Publishing, 2016, pp. 185–207. ISBN: 978-3-319-25448-7. DOI: 10.1007/978-3-319-25448-7_10.

[47] William J. Tomlinson et al. 'Comprehensive survey of galvanic coupling and alternative intra-body communication technologies'. In: *IEEE Communications Surveys & Tutorials* 21.2 (2019), pp. 1145–1164. DOI: 10.1109/COMST.2018.2879643.

[48] Max L. Wang et al. 'Wireless data links for next-generation networked micro-implantables'. In: *2018 IEEE Custom Integrated Circuits Conference (CICC)*. IEEE, 2018, pp. 1–9. ISBN: 978-1-5386-2483-8. DOI: 10.1109/CICC.2018.8357096.

[49] Banafsaj Jaafar, Jeffrey Alan Neasham and Patrick Degenaar. 'What is ultrasound can and cannot do in the communication of biomedical implanted medical devices'. In: *IEEE Reviews in Biomedical Engineering* (2021). DOI: 10.1109/RBME.2021.3080087.

[50] Ira O. Wygant et al. '50 kHz capacitive micromachined ultrasonic transducers for generation of highly directional sound with parametric arrays'. In: *IEEE transactions on Ultrasonics, Ferroelectrics, and Frequency Control* 56.1 (2009), pp. 193–203. DOI: 10.1109/TUFFC.2009.1019.

[51] Steve Zhuang et al. 'A 50-MHz CMUT probe for medical ultrasound imaging'. In: *2018 IEEE International Ultrasonics Symposium (IUS)*. 2018, pp. 1–4. DOI: 10.1109/ULTSYM.2018.8579648.

[52] Giulia Matrone et al. 'A volumetric CMUT-based ultrasound imaging system simulator with integrated reception and mu-beamforming electronics models'. In: *IEEE Transactions on Ultrasonics, Ferroelectrics, and Frequency Control* 61.5 (2014), pp. 792–804. DOI: 10.1109/TUFFC.2014.2971.

[53] Oluwafemi Joel Adelegan et al. 'Implementing a 32 x 32 2D capacitive micromachined ultrasonic transducer (CMUT) array incorporating Silicon-Through-Glass-via (Si-TGV) interconnects'. In: *2020 IEEE International Ultrasonics Symposium (IUS)*. IEEE, 972020, pp. 1–3. ISBN: 978-1-7281-5448-0. DOI: 10.1109/IUS46767.2020.9251615.

[54] Mette Funding La Cour et al. 'Investigation of PDMS as coating on CMUTs for imaging'. In: *2014 IEEE International Ultrasonics Symposium*. IEEE, 2014, pp. 2584–2587. DOI: 10.1109/ULTSYM.2014.0645.

[55] URL: www.butterflynetwork.com/iq (visited on 10/06/2021).

[56] Martin Pekař et al. 'Preclinical testing of frequency-tunable capacitive micromachined ultrasonic transducer probe prototypes'. In: *Ultrasound in Medicine & Biology* 43.9 (2017), pp. 2079–2085. DOI: 10.1016/j.ultrasmedbio.2017.05.005.

[57] Alessandro Stuart Savoia, Giosuè Caliano and Massimo Pappalardo. 'A CMUT probe for medical ultrasonography: From microfabrication to system integration'. In: *IEEE transactions on Ultrasonics, Ferroelectrics, and Frequency Control* 59.6 (2012), pp. 1127–1138. DOI: 10.1109/tuffc.2012.2303.

[58] Mathieu Legros et al. 'Piezocomposite and CMUT arrays assessment through in vitro imaging performances'. In: *2008 IEEE Ultrasonics Symposium*. IEEE, 2008, pp. 1142–1145. ISBN: 978-1-4244-2428-3. DOI: 10.1109/ULTSYM.2008.0275.

[59] Jiujiang Wang et al. 'A review on analytical modeling for collapse mode capacitive micromachined ultrasonic transducer of the collapse voltage and the static membrane deflections'. In: *Micromachines* 12.6 (2021). DOI: 10.3390/mi12060714.

[60] Rashmi Sharma et al. 'Analytical modelling of hexagonal shaped capacitive micromachined ultrasonic transducer'. In: *International Journal of System Assurance Engineering and Management* (2021). DOI: 10.1007/s13198-020-01046-y.

[61] Andreas Spandet Havreland and Erik Vilain Thomsen. 'Analytical deflection profiles and pull-in voltage calculations of prestressed electrostatic actuated MEMS Structures'. In: *Journal of Microelectromechanical Systems* (2021), pp. 1–9. DOI: 10.1109/JMEMS.2021.3083935.

[62] Reshmi Maity, Kalpana Gogoi and N. P. Maity. 'Micro-electro-mechanical-system based capacitive ultrasonic transducer as an efficient immersion sensor'. In: *Microsystem Technologies* 2000.4 (2019), p. 939. DOI: 10.1007/s00542-019-04384-5.

[63] Mathias Engholm. *Capacitive micromachined ultrasonic transducers for 3-D imaging.* DTU Nanotech, 2018.

[64] Matthew D.C. Eames, Theodore J. Reck and John A. Hossack. 'Selectable frequency CMUT with membrane stand-off structures'. In: *2009 IEEE International Ultrasonics Symposium.* IEEE, 2009, pp. 2814–2817. ISBN: 978-1-4244-4389-5. DOI: 10.1109/ULTSYM.2009.5441596.

[65] Byung Chul Lee et al. 'High-efficiency output pressure performance using capacitive micromachined ultrasonic transducers with substrate-embedded springs'. In: *Sensors (Basel, Switzerland)* 18.8 (2018). DOI: 10.3390/s18082520.

[66] Ryan K. W. Chee et al. 'Multifrequency interlaced CMUTs for photoacoustic imaging'. In: *IEEE transactions on Ultrasonics, Ferroelectrics, and Frequency Control* 64.2 (2017), pp. 391–401. DOI: 10.1109/TUFFC.2016.2620381.

[67] Joyce Y. Liu et al. 'CMUT/CMOS-based Butterfly iQ - a portable personal sonoscope'. In: *Advanced Ultrasound in Diagnosis and Therapy* 3.3 (2019), pp. 115–118. DOI: 10.37015/AUDT.2019.190819.

[68] Carlos D. Gerardo, Edmond Cretu and Robert Rohling. 'Fabrication and testing of polymer-based capacitive micromachined ultrasound transducers for medical imaging'. In: *Microsystems & Nanoengineering* 4.1 (2018), pp. 1–12. DOI: 10.1038/s41378-018-0022-5.

[69] Mohammad Maadi, Christopher Ceroici and Roger J. Zemp. 'Dual-frequency CMUT arrays for multi-band ultrasound imaging applications'. In: *IEEE transactions on Ultrasonics, Ferroelectrics, and Frequency Control* PP (2021). DOI: 10.1109/TUFFC.2021.3062071.

[70] W. Apoutou N'Djin et al. 'Capacitive micromachined ultrasound transducers for Interstitial high-intensity ultrasound therapies'. In: *IEEE transactions on Ultrasonics, Ferroelectrics, and Frequency Control* 64.8 (2017), pp. 1245–1260. DOI: 10.1109/TUFFC.2017.2707663.

[71] Ji Hoon Jang et al. 'Dual-mode integrated circuit for imaging and HIFU with 2-D CMUT arrays'. In: *2015 IEEE International Ultrasonics Symposium (IUS).* IEEE, 2015, pp. 1–4. ISBN: 978-1-4799-8182-3. DOI: 10.1109/ULTSYM.2015.0166.

[72] Chunkyun Seok et al. 'A wearable ultrasonic neurostimulator-part II: A 2D CMUT phased array system with a flip-chip bonded ASIC'. In: *IEEE Transactions on Biomedical Circuits and Systems* 15.4 (2021), pp. 705–718. DOI: 10.1109/TBCAS.2021.3105064.

[73] Amin Nikoozadeh et al. 'An integrated ring CMUT array for endoscopic ultrasound and photoacoustic imaging'. In: *2013 IEEE International Ultrasonics Symposium (IUS)*. IEEE, 72013, pp. 1178–1181. ISBN: 978-1-4673-5686-2. DOI: 10.1109/ULTSYM.2013.0301.

[74] Azadeh Moini et al. 'Fully integrated 2D CMUT ring arrays for endoscopic ultrasound'. In: *2016 IEEE International Ultrasonics Symposium (IUS)*. IEEE, 92016, pp. 1–4. ISBN: 978-1-4673-9897-8. DOI: 10.1109/ULTSYM.2016.7728542.

[75] Fikret Yildiz, Tadao Matsunaga and Yoichi Haga. 'CMUT arrays incorporating anodically bondable LTCC for small diameter ultrasonic endoscope'. In: *2016 IEEE 11th Annual International Conference on Nano/Micro Engineered and Molecular Systems (NEMS)*. IEEE, 2016, pp. 50–53. ISBN: 978-1-5090-1947-2. DOI: 10.1109/NEMS.2016.7758198.

[76] Fikret Yildiz, Tadao Matsunaga and Yoichi Haga. 'Capacitive micromachined ultrasonic transducer arrays incorporating anodically bondable low temperature co–fired ceramic for small diameter ultrasonic endoscope'. In: *Micro & Nano Letters* 11.10 (2016), pp. 627–631. DOI: 10.1049/mnl.2016.0281.

[77] Junyi Wang et al. 'Capsule ultrasound device: Characterization and testing results'. In: *2017 IEEE International Ultrasonics Symposium (IUS), Washington, DC, USA* (2017), pp. 1–4. DOI: 10.1109/ULTSYM.2017.8092071.

[78] Hyunjoo J. Lee et al. 'Chemical vapor detection using a capacitive micromachined ultrasonic transducer'. In: *Analytical chemistry* 83.24 (2011), pp. 9314–9320. DOI: 10.1021/ac201626b.

[79] Sangjun Park et al. 'CMUT-based resonant gas sensor array for VOC detection with low operating voltage'. In: *Sensors and Actuators B: Chemical* 273 (2018), pp. 1556–1563. DOI: 10.1016/j.snb.2018.07.043.

[80] X. Zhuang et al. 'Biocompatible coatings for CMUTs in a harsh, aqueous environment'. In: *Journal of Micromechanics and Microengineering* 17.5 (2007), pp. 994–1001. DOI: 10.1088/0960-1317/17/5/020.

[81] Tzu-Hsuan Hsu et al. 'A 200-nm-gap Titanium nitride composite CMOS-MEMS CMUT for biomedical ultrasounds'. In: *2018 IEEE International Frequency Control Symposium (IFCS)*. 2018, pp. 1–3. DOI: 10.1109/FCS.2018.8597500.

[82] Changde He et al. 'Wafer-bonding fabricated CMUT device with Parylene coating'. In: *Micromachines* 12.5 (2021), p. 516. DOI: 10.3390/mi12050516.

[83] Azadeh Moini et al. 'Fabrication, packaging, and catheter assembly of 2D CMUT arrays for endoscopic ultrasound and cardiac imaging'. In: *ASME 2015 international technical conference and exhibition on packaging and integration of electronic and photonic microsystems, InterPACK 2015, collocated with the ASME 2015 13th International Conference on Nanochannels, Microchannels, and Minichannels*. American Society of Mechanical Engineers, 2015. DOI: `10.1115/IPACK2015-48611`.

[84] Ji Hoon Jang et al. 'Integration of a dual-mode catheter for ultrasound image guidance and HIFU ablation using a 2-D CMUT array'. In: *2017 IEEE International Ultrasonics Symposium (IUS)*. Piscataway, NJ: IEEE, 2017. DOI: `10.1109/ULTSYM.2017.8091627`.

[85] Amin Nikoozadeh et al. 'Forward-looking intracardiac ultrasound imaging using a 1-D CMUT array integrated with custom front-end electronics'. In: *IEEE transactions on Ultrasonics, Ferroelectrics, and Frequency Control* 55.12 (2008), pp. 2651–2660. DOI: `10.1109/TUFFC.2008.980`.

[86] Albert I-Hsiang Chen et al. 'Fabrication of a curved row–column addressed capacitive micromachined ultrasonic transducer array'. In: *Journal of Microelectromechanical Systems* 25.4 (2016), pp. 675–682. DOI: `10.1109/JMEMS.2016.2580152`.

[87] Nooshin Saeidi et al. 'Characterization of capacitive micromachined ultrasound transducer (CMUT) for targeted applications in harsh environments'. In: *2021 IEEE 34th International Conference on Micro Electro Mechanical Systems (MEMS)*. IEEE, 2021, pp. 903–906. ISBN: 978-1-6654-1912-3. DOI: `10.1109/MEMS51782.2021.9375331`.

[88] David D Zhou, Elias Greenbaum and ES Greenbaum. 'Implantable neural prostheses 2'. In: *Biological and medical physics, biomedical engineering, ch. technology advances and challenges in hermetic packaging for implantable medical devices* (2010).

[89] *PZFlex help documentation. PZFlex 2018, ver. 1.25.3.0*. OnScale Inc. 2017.

[90] Steven M. Kurtz and John N. Devine. 'PEEK biomaterials in trauma, orthopedic, and spinal implants'. In: *Biomaterials* 28.32 (2007), pp. 4845–4869. DOI: `10.1016/j.biomaterials.2007.07.013`.

[91] David A. Fitch, Brent K. Hoffmeister and Javier de Ana. 'Ultrasonic evaluation of polyether ether ketone and carbon fiber-reinforced PEEK'. In: *Journal of Materials Science* 45.14 (2010), pp. 3768–3777. DOI: `10.1007/s10853-010-4428-1`.

[92] Thomas Velten et al. 'Mikrogefertigter Wandler für die Implantat-zu-Implantat-Kommunikation per Ultraschall'. In: *Proocedings of the Mikrosystemtechnik Kongress 2019*. VDE Verlag, 2019. ISBN: 978-3-8007-5090-0.

[93] Andrew Logan and John T. W. Yeow. 'Fabricating capacitive micromachined ultrasonic transducers with a novel silicon-nitride-based wafer bonding process'. In: *IEEE transactions on Ultrasonics, Ferroelectrics, and Frequency Control* 56.5 (2009), pp. 1074–1084. DOI: 10.1109/TUFFC.2009.1141.

[94] Keysight Technologies. *Impedance measurement handbook. A guide to measurement technology and techniques.* Vol. 6th Edition. Keysight Technologies, 2016, p. 1-01.

[95] URL: www.nanofocus.com/technology/measurement-principles/usurf-technology/ (visited on 01/06/2021).

[96] Sebastian Hagemeier and Peter Lehmann. 'Multisensorisches Messsystem zur Untersuchung der Übertragungseigenschaften von Topographiesensoren'. In: *tm - Technisches Messen* 85.6 (2018), pp. 380–394. DOI: doi:10.1515/teme-2017-0138.

[97] *3M Fluorinert electronic liquid FC-72.* Technical data. 3M electronics materials solutions division, 2019. URL: https://multimedia.3m.com/mws/media/648920/3m-fluorinert-electronic-liquid-fc72-en.pdf (visited on 19/03/2020).

[98] Yuanyu Yu et al. 'Experimental characterization of an embossed capacitive micromachined ultrasonic transducer cell'. In: *Micromachines* 11.2 (2020). DOI: 10.3390/mi11020217.

[99] Abhijeet Kshirsagar et al. 'Pre-charged CMUTs with efficient low-bias voltage operation for medical applications'. In: *2013 IEEE International Ultrasonics Symposium (IUS).* IEEE, 2013, pp. 1728–1730. ISBN: 978-1-4673-5686-2. DOI: 10.1109/ULTSYM.2013.0440.

[100] Dinah Maria Brandner et al. 'Estimation of tissue attenuation from ultrasonic B-mode images-spectral-log-difference and method-of-moments algorithms compared'. In: *Sensors (Basel, Switzerland)* 21.7 (2021). DOI: 10.3390/s21072548.

[101] Jorge Oevermann, Peter Weber and Steffen H. Tretbar. 'Encapsulation of capacitive micromachined ultrasonic transducers (CMUTs) for the acoustic communication between medical implants'. In: *Sensors (Basel, Switzerland)* 21.2 (2021). DOI: 10.3390/s21020421.

[102] D.K. Nassiri, D. Nicholas and C.R. Hill. 'Attenuation of ultrasound in skeletal muscle'. In: *Ultrasonics* 17.5 (1979), pp. 230–232. DOI: 10.1016/0041-624X(79)90054-4.

[103] Xiaoli Zhang, Hui Zhang and Dachao Li. 'Design of a hexagonal air-coupled capacitive micromachined ultrasonic transducer for air parametric array'. In: *Nanotechnology and Precision Engineering* 4.1 (2021), p. 013004. DOI: 10.1063/10.0003504.

[104] Marcel Krenkel et al. 'CMUT with mechanically coupled plate actuators for low frequencies'. In: *Journal of Micromechanics and Microengineering* 29.4 (2019), p. 044001. DOI: 10.1088/1361-6439/ab035d.

[105] Oluwafemi J. Adelegan et al. 'Design and fabrication of wideband air-coupled capacitive micromachined ultrasonic transducers with varying width annular-ring and spiral cell structures'. In: *IEEE transactions on Ultrasonics, Ferroelectrics, and Frequency Control* PP (2021). DOI: 10.1109/TUFFC.2021.3076143.

[106] Marzana Mantasha Mahmud et al. 'An improved CMUT structure enabling release and collapse of the plate in the same Tx/Rx cycle for dual-frequency acoustic angiography'. In: *IEEE transactions on Ultrasonics, Ferroelectrics, and Frequency Control* 67.11 (2020), pp. 2291–2302. DOI: 10.1109/TUFFC.2020.3001221.

[107] Junaid Munir, Quratul Ain and Hyunjoo Jenny Lee. 'Reliability issue related to dielectric charging in capacitive micromachined ultrasonic transducers: A review'. In: *Microelectronics Reliability* 92 (2019), pp. 155–167. DOI: 10.1016/j.microrel.2018.12.005.

[108] Shinnosuke Kawasaki et al. 'Pre-charged collapse-mode capacitive micromachined ultrasonic transducer (CMUT) for broadband ultrasound power transfer'. In: *2021 IEEE Wireless Power Transfer Conference (WPTC)*. IEEE, 2021, pp. 1–4. ISBN: 978-1-7281-9633-6. DOI: 10.1109/WPTC51349.2021.9458104.

[109] Won Young Choi et al. 'Comparison of Si3N4-SiO2 and SiO2 insulation layer for zero-bias CMUT operation using dielectric charging effects'. In: *IEEE transactions on Ultrasonics, Ferroelectrics, and Frequency Control* 67.4 (2020), pp. 879–882. DOI: 10.1109/TUFFC.2019.2950902.

[110] Andreas Spandet Havreland et al. 'CMUT electrode resistance design: Modelling and experimental verification by a row-column array'. In: *IEEE transactions on Ultrasonics, Ferroelectrics, and Frequency Control* (2019). DOI: 10.1109/TUFFC.2019.2906795.

[111] Farhad Goodarzy, Efstratios Stan Skafidas and Simone Gambini. 'Feasibility of energy-autonomous wireless microsensors for biomedical applications: Powering and communication'. In: *IEEE Reviews in Biomedical Engineering* 8 (2015), pp. 17–29. DOI: 10.1109/RBME.2014.2346487.

[112] Zichen Liu et al. 'Design and simulation of a wide-bandwidth CMUTs array with dual-mixed radii and multi operating modes'. In: *2021 IEEE 16th International Conference on Nano/Micro Engineered and Molecular Systems (NEMS)*. IEEE, 2021, pp. 299–302. ISBN: 978-1-6654-1941-3. DOI: 10.1109/NEMS51815.2021.9451374.

[113] Richard L O'Leary and Gerald Harvey. 'Polymeric capacitive transducers and arrays for gas coupled operation'. In: *2014 IEEE International Ultrasonics Symposium*. IEEE, 92014, pp. 177–180. ISBN: 978-1-4799-7049-0. DOI: 10.1109/ULTSYM.2014.0045.

List of Figures

122

List of Tables

Acknowledgements

Material parameters

The following material parameters were used for the FEM simulations in this thesis. Material data sets not cited separately were taken from the PZFlex database [89]. The material parameters for silicone (Wacker Elastosil E43) were determined experimentally.

Table 8.1: Material properties.

Material	Density	v_{long}	v_{trans}
Silicon	$2350\,\text{kg/m}^3$	$8120\,\text{m/s}$	$5200\,\text{m/s}$
SiO$_2$	$2650\,\text{kg/m}^3$	$5750\,\text{m/s}$	$2200\,\text{m/s}$
Si$_3$N$_4$	$3270\,\text{kg/m}^3$	$11\,000\,\text{m/s}$	$6250\,\text{m/s}$
Aluminum	$2690\,\text{kg/m}^3$	$6306\,\text{m/s}$	$3114\,\text{m/s}$
Silicone	$1142\,\text{kg/m}^3$	$1000\,\text{m/s}$	$167\,\text{m/s}$
PEEK [91]	$1285\,\text{kg/m}^3$	$2536\,\text{m/s}$	$1086\,\text{m/s}$
Titanium	$4480\,\text{kg/m}^3$	$6100\,\text{m/s}$	$3100\,\text{m/s}$
Air	$1.24\,\text{kg/m}^3$	$343\,\text{m/s}$	-
Water	$1000\,\text{kg/m}^3$	$1496\,\text{m/s}$	-
Fluorinert FC-72 [97]	$1680\,\text{kg/m}^3$	$512\,\text{m/s}$	-

Publications

J. Oevermann, P. Weber and S. H. Tretbar. 'Encapsulation of capacitive micromachined ultrasonic transducers (CMUTs) for the acoustic communication between medical implants'. In: *Sensors (Basel, Switzerland)* 21.2 (2021). DOI: 10.3390/s21020421.

T. Velten, T. Knoll, A. Sossalla, J. Oevermann et al. 'Mikrogefertigter Wandler für die Implantat-zu-Implantat-Kommunikation per Ultraschall'. In: *MikroSystemTechnik Kongress 2019, Berlin*, pp. 215-218, ISBN: 978-3-8007-5090-0

J. Oevermann et al. 'Capacitive micromachined ultrasonic transducers for intracorporeal applications'. Presentation at: *BMT 2020, 54th Annual Conference of the German Society for Biomedical Engineering.*

J. Oevermann et al. 'Design of CMUTs for intracorporeal communication'. Presentation at: *18th International Workshop on Micromachined Ultrasonic Transducers MUT 2019, Grenoble, France*

J. Oevermann. 'FEM-Design of miniaturized ultrasonic transducers (CMUTs)'. Poster contribution at: *Doktorandentag der Fakultät NT der Universität des Saarlandes, 2018*